This is an open access article published under a Creative Commons Attribution (CC-BY) License, which permits unrestricted use, distribution and reproduction in any medium, provided the author and source are cited.

CHEMICAL REVIEWS

Review

Cite This: *Chem. Rev.* 2018, 118, 5201−5241

pubs.acs.org/CR

Mimicking Natural Photosynthesis: Solar to Renewable H_2 Fuel Synthesis by Z-Scheme Water Splitting Systems

Yiou Wang,[†] Hajime Suzuki,[‡] Jijia Xie,[†] Osamu Tomita,[‡] David James Martin,[§] Masanobu Higashi,[‡] Dan Kong,[†] Ryu Abe,*[,‡] and Junwang Tang*[,†]

[†]Department of Chemical Engineering, University College London, Torrington Place, London WC1E 7JE, U.K.

[‡]Graduate School of Engineering, Kyoto University, Katsura, Kyoto 615-8510, Japan

[§]Van't Hoff Institute for Molecular Sciences, University of Amsterdam, P.O. Box 94720, 1090 GS Amsterdam, The Netherlands

ABSTRACT: Visible light-driven water splitting using cheap and robust photocatalysts is one of the most exciting ways to produce clean and renewable energy for future generations. Cutting edge research within the field focuses on so-called "Z-scheme" systems, which are inspired by the photosystem II−photosystem I (PSII/PSI) coupling from natural photosynthesis. A Z-scheme system comprises two photocatalysts and generates two sets of charge carriers, splitting water into its constituent parts, hydrogen and oxygen, at separate locations. This is not only more efficient than using a single photocatalyst, but practically it could also be safer. Researchers within the field are constantly aiming to bring systems toward industrial level efficiencies by maximizing light absorption of the materials, engineering more stable redox couples, and also searching for new hydrogen and oxygen evolution cocatalysts. This review provides an in-depth survey of relevant Z-schemes from past to present, with particular focus on mechanistic breakthroughs, and highlights current state of the art systems which are at the forefront of the field.

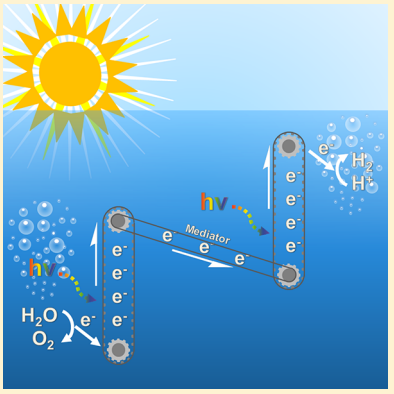

CONTENTS

Received: May 20, 2017
Published: April 20, 2018

© 2018 American Chemical Society

DOI: 10.1021/acs.chemrev.7b00286
Chem. Rev. 2018, 118, 5201−5241

1. INTRODUCTION

Solar irradiation hitting the Earth amounts to over 120 000 terawatts of power per year, while human energy consumption will be no more than 30 terawatts per year by 2050 according to nonconservative estimates.[1,2] Understandably then, solar hydrogen fuel synthesis has attracted substantial interest over the past half century as it has the potential to meet the growing global energy demand, mitigate greenhouse gas emission, and provide a solution to the concerns about sustainable energy supplies. Furthermore, both sunlight and water are abundant and essentially inexhaustible, hence there is an opportunity to achieve solar-driven hydrogen synthesis on a large scale via photocatalytic water splitting under solar irradiation.[3] Recently, interest has peaked in renewable solar hydrogen production from water via a robust two photocatalyst system, in which the two half reactions, proton reduction and water oxidation, should both be efficient. However, crucial technological advances are required in order to achieve this potential. Most importantly, large scale hydrogen fuel production demands a solar-to-hydrogen (STH) efficiency exceeding 10%, and considering almost half of the sunlight on the earth's surface lies in the visible region (400−700 nm), harvesting visible light photons efficiently is among the most crucial of all challenges.[1,4−6]

The earliest demonstration of photoassisted water splitting dates back to 1921, reported by Baur and Rebmann, using UV light and a AgCl/TlCl system in pure water.[7] Since the discovery of Honda−Fujishima effect in 1972, many efforts have been made in search for a single photocatalyst, where both proton reduction and water oxidation reactions should take place concurrently at different sites.[8,9] Such a single photocatalyst system is shown in Scheme 1, where a semiconductor

Scheme 1. A Typical Model of a Single Photocatalyst System for Water Splitting

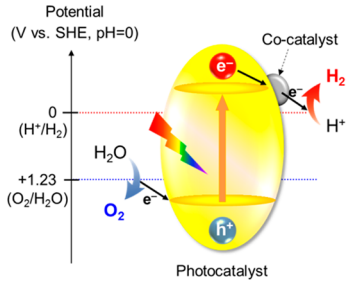

material can absorb photons with energy greater or equal to the band gap, thus exciting electrons from the valence band (VB) into the conduction band (CB), leaving positively charged holes in the valence band. The overall water splitting process requires a positive Gibbs free energy ($H_2O \rightarrow H_2 + 0.5\ O_2$, $\Delta G^0 = 237.13$ kJ/mol) and thus cannot occur spontaneously. Photogenerated electrons and holes can have strong reduction and oxidation potentials and can be used for catalytic surface redox reactions.[3] Water splitting requires two electrons or four holes to evolve one molecule of H_2 or O_2, respectively. Hence, the suitable size of band gaps and the positions of conduction band minimum (CBM) and valence band maximum (VBM) are the most important aspects for overall water splitting. The CBM of semiconductors must be more negative than the reduction potential of H^+/H_2 (0 V vs standard hydrogen electrode (SHE) at pH = 0), and the VBM must be more positive than the oxidation potential of O_2/H_2O (+1.23 V vs SHE at pH = 0). Therefore, the theoretical minimum requirement of photon energy is 1.23 eV, which corresponds to a wavelength in the range of approximately 1000 nm and is in the near-infrared range. However, activation energy (overpotential) is necessary to overcome the energy barrier of redox reactions between charge carriers and water molecules. Therefore, the band gap of a photocatalyst should be larger than the minimum requirement of 1.23 eV. In terms of the solar spectrum, 52−55% sunlight at Earth's surface is infrared light (above 700 nm), 42−43% visible light (400−700 nm), and 3−5% ultraviolet light (below 400 nm).[10] Thus, to achieve a reasonable efficiency of the overall water splitting reaction, the band gap of photocatalysts should be narrower than 3.1 eV to utilize more visible light from the solar spectrum but also possess a large enough overpotential. As for some sulfides and nitrides with suitable band gap potentials for overall water splitting, many of them are not stable in an overall water splitting reaction due to self-oxidation.[11,12] For example, most (oxy)nitrides with the introduction of N 2p orbital in the VB formation, undergo self-oxidative deactivation to some degree, in which photogenerated holes oxidize N^{3-} to N_2 ($2N^{3-} + 6h^+ \rightarrow N_2$). Self-oxidative deactivation proceeds competitively, and in some cases even when appropriate cocatalysts are used, the water splitting rate will gradually decrease as the compound decomposes.

As for some materials with narrower band gaps, such as the ground-breaking example of GaN-ZnO solid solution (2.5 eV), that could split water into H_2 and O_2 under visible light, the

DOI: 10.1021/acs.chemrev.7b00286
Chem. Rev. 2018, 118, 5201−5241

efficiency was still unsatisfactory (average quantum yield of 0.14% in the range of 300−480 nm).[13] Up to now, only a few examples of overall water splitting by a single photocatalyst system under visible light irradiation exist in literature, such as GaN:ZnO solid solutions,[13] nitrides,[14] sulfides,[5] and g-C_3N_4.[15]

The majority of reported visible light-driven photocatalysts are only efficient for half reactions of either proton reduction or water oxidation, as the combination of both band gap magnitude and positioning are difficult to engineer.[16,17]

Rather than split water using a single photocatalyst, nature uses a two-stage, double-excitation process (known as a "Z-scheme") in PSI and PSII.[18] Inspired by natural photosynthesis of green plants, inorganic analogues have been continually researched over the past 20 years. Artificial photosynthesis is achieved by coupling two narrow band gap semiconductors: an oxygen evolution photocatalyst (OEP) and a hydrogen evolution photocatalyst (HEP), connected via an electron mediator.[19−21] Briefly, photoexcited electrons in the CB of a HEP reduce protons while the holes in the VB of the OEP oxidize water, evolving H_2 and O_2, respectively, on separate photocatalysts. The CB electrons of the OEP pass through a relay/shuttle to combine with photoholes in the VB of the HEP, thus completing the cycle and maintaining charge neutrality. Overall water splitting based on the Z-scheme mechanism requires three conditions: (a) an OEP which can inject electrons to hole acceptors, (b) a HEP that can accept electrons from donors, and, crucially, (c) an electron relay system with suitable potentials where subsequent back/side reactions are suppressed. In such a dual photocatalyst system, both OEP and HEP can be driven by visible light because the band gap conditions for overall water splitting are less stringent, theoretically enabling a maximum solar energy conversion efficiency of 40% compared with a ca. 30% maximum solar conversion efficiency on a single photocatalyst.[22] For this reason, this review only focuses on *visible driven Z-scheme water splitting systems* and the main factors influencing performance, which are hereby divided into the following sections:

- Mimicking natural photosynthesis: rationale and mechanism
- Photocatalyst development for Z-scheme water splitting
- Redox couples in Z-scheme water splitting systems
- Strategies for improving efficiency of Z-scheme systems
- Conclusions and future outlook

2. MIMICKING NATURAL PHOTOSYNTHESIS: RATIONALE AND MECHANISM

Scheme 2 shows the double excitation system in natural photosynthesis along with the electron cascade steps. At certain wavelengths, this system can operate at a quantum yield over 95%.[23,24] Reaction center chlorophylls in photosystem II (PSII) absorb photons ($\lambda \leq 680$ nm), leading to the generation of electron−hole pairs. The photoinduced holes oxidize water to produce oxygen, protons, and electrons. The electrons are transferred via the electron transport chain, whereas the protons released are accumulated in one side of the membrane to build an electronic potential to support the conversion of ADP (adenosine diphosphate) into ATP (adenosine triphosphate). In photosystem I (PS I), electrons are excited by photons ($\lambda \leq 700$ nm), however, now the holes are quenched by the electrons produced by PSII, simultaneously elongating the electron lifetime so more reduction reactions can occur. The electrons from PSI are finally used to reduce $NADP^+$

Scheme 2. A Schematic Diagram of a Double Excitation Process on P680 and P700 in Natural Photosynthesis

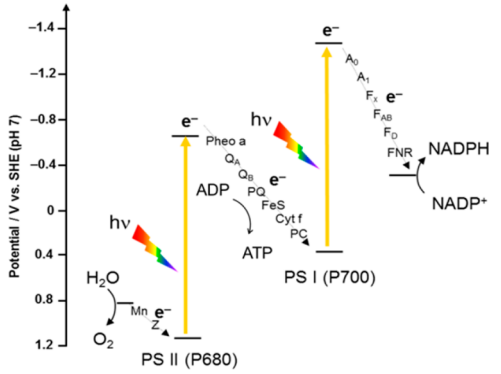

(nicotinamide adenine dinucleotide phosphate) to NADPH, which, together with ATP, provides the reduction power and energy for the conversion of CO_2 to sugars.[11]

Inspired by natural photosynthesis, an inorganic double excitation system as shown in Scheme 3 was proposed first by

Scheme 3. A Double Excitation System Based on a HEP and an OEP with a Shuttle of Ox, oxidant, and Red, reductant, molecules[a]

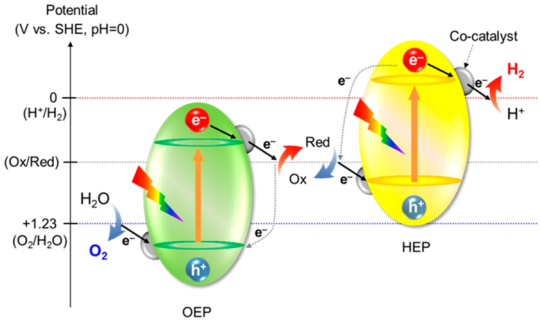

[a]Two dotted curves indicate the back reactions which should be suppressed.

Sayama and Abe et al.[19] In such a system, the water-splitting reaction is separated into two reactions: O_2 evolution and H_2 evolution. When photons are absorbed by an OEP, electrons in the VB will be excited to CB, leaving holes to oxidize water to O_2. The electrons on the CB first reduce the corresponding electron acceptors (i.e., oxidant, Ox) to form the electron donors (i.e., reductant, Red). Then, the electron donors (Red) are converted back to its oxidized form (Ox) by the oxidation of photoholes on the surface of a HEP. Hence, the electrons are transferred between two photocatalysts by the appropriate shuttle redox couple in solution continuously. Meanwhile, protons are reduced to hydrogen by the photoexcited electrons on the CB of a HEP. As such, the overall water splitting reaction is complete, with regeneration of redox mediators (ions or molecules) and light being the only energy input. However, Red can be oxidized by holes from the VB of OEP, and similarly the electrons on the CB of HEP can react with Ox, i.e., back reactions take place. Thus, for an efficient Z-scheme system, back reactions should be inhibited (dotted curves shown in Scheme 3).

A Z-scheme system can utilize visible light more efficiently than a single photocatalyst water splitting system (Scheme 1) due to the lower energy requirement to drive each half reaction

DOI: 10.1021/acs.chemrev.7b00286
Chem. Rev. 2018, 118, 5201−5241

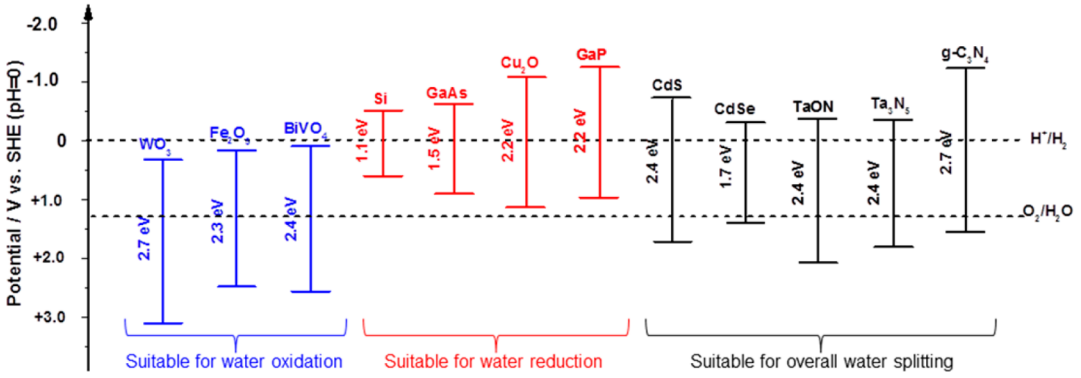

Figure 1. Band edge positions of typical semiconductors for visible driven water splitting.

in comparison to the higher energy requirement to drive an overall water splitting reaction using one photocatalyst. For instance, visible-light-responsive oxides such as WO_3 can carry out O_2 evolution if a mediator Ox can be reduced to a Red. Similarly, non-oxide photocatalysts such as, sulphides, nitrides, and dyes can be applied in H_2 evolution if they are able to oxidize mediator Red to Ox. Therefore, much more semiconductor materials can be applied in the Z-scheme system even if they are not suitable for the harsh requirements for overall water splitting as a single photocatalyst.

3. PHOTOCATALYST DEVELOPMENT FOR Z-SCHEME WATER SPLITTING

Several well-known photocatalysts for half reactions are listed in Figure 1. In constructing a Z-scheme system, photocatalysts are first examined in half (sacrificial) reactions to test their activity before coupling with a counterpart. As a test for the oxygen evolving half reaction under irradiation of visible light, the photoexcited electrons in a suitable photocatalyst CB would move to react with the sacrificial reagents which are easily reduced, such as Ag^+, leaving the photogenerated holes in VB to oxidize water to O_2. For the H_2 production reaction, the photogenerated holes on the photocatalysts are consumed by a hole scavenger such as methanol or triethanolamine, hence the remaining photoexcited electrons could be used in water reduction efficiently.[3,25] There are much more visible driven photocatalysts working for half reactions (especially with sacrificial reagents) than those so far reported in overall water splitting using Z-scheme, and the construction of Z-scheme systems based on these visible driven photocatalysts for half reactions is one of the targets of solar energy to hydrogen fuel development.[26] The reported Z-scheme systems are listed below in Table 1.

There are a few reasons why certain photocatalysts are either unsuitable or less efficient for the process, including incorrect band positions of the photocatalysts, insufficient efficiency, and incompatible redox charge mediator choice. These factors will be addressed in detail later in the review. In some cases, redox activity can take place at the solid interface of two photocatalysts and thus an aqueous mediator is not required. These cases are detailed in section 3.3. The majority of the reported Z-scheme systems use dissolved ions as redox mediators, which will be reviewed immediately in sections 3.1 and 3.2.

3.1. Oxidation Photocatalyst Dominated Systems with Dissolved Ions as Redox Mediators

The O_2/H_2O potential lies at +1.23 V (vs SHE at pH = 0). However, due to the overpotential to the chemical reaction, it usually requires a more positive VBM position (vs SHE at pH = 0) to achieve gaseous oxygen production.[27] Oxygen generation from water splitting is a relatively slow procedure because it requires four holes to form one molecule of O_2 by water oxidation, while per H_2 production only needs two electrons. Furthermore, electrons transfer much faster than holes in most oxide photocatalysts which are n-type semiconductors, so the process is much more facile.[28] Hence, a large driving force has to be provided by a deep VBM of a semiconductor. A consequence of this deep lying VBM, a problem in the majority of metal oxides, is that this makes the band gap very large, so a large portion of the visible spectrum from sunlight cannot not be sufficiently harvested.[29] Only a few metal oxides have been reported to work under visible irradiation for efficient half reactions (O_2 evolution), for example monoclinic $BiVO_4$ (~2.4 eV),[30] WO_3 (~2.7 eV),[25] and Ag_3PO_4 (2.6 eV).[31]

3.1.1. WO_3. Tungsten oxide (WO_3) is a well-documented photocatalyst in water oxidation, which has an appreciably more positive CBM than water reduction potential and a much more positive position of VBM than the water oxidation potential.[32] The band gap energy of WO_3 is around 2.7−2.8 eV with relatively positive CBM of +0.5 V and VBM of +3.2 V (vs SHE at pH = 0). The redox potentials of the two most commonly used mediator pairs, Fe^{3+}/Fe^{2+} and IO_3^-/I^-, are around +0.77 V and +1.09 V (vs SHE at pH = 0), respectively, which are thermodynamically able to be reduced by CB electrons in WO_3.[33] With decent stability under low pH and suitable band positions, WO_3 samples are widely used with Fe^{3+}/Fe^{2+} redox couples under acidic conditions. WO_3 is among the most widely used oxygen production photocatalyst in half reactions.

WO_3 was the first material utilized in an UV-driven Z-scheme water splitting system as a water oxidation photocatalyst to achieve a stoichiometric H_2 and O_2 gas generation by Sayama et al. in 1997.[19] In a Fe^{3+}/Fe^{2+} mediated solution, WO_3 loaded with RuO_2 produced O_2 along with the other half reaction of proton reduction by Fe^{2+}. The activity was promoted by RuO_2 loaded on WO_3 as a cocatalyst, which is crucial to reduce the overpotential needed for oxidation.[34] The pathway is accessible because the Fe^{3+}/Fe^{2+} potential is +0.77 V (vs SHE at pH = 0), which is positive enough for the CB electrons of WO_3 (+0.5 V vs SHE at pH = 0) to reduce.

DOI: 10.1021/acs.chemrev.7b00286
Chem. Rev. 2018, 118, 5201−5241

WO_3 has been widely reported for water oxidation in Z-Scheme system coupled with either inorganic semiconductors such as doped $SrTiO_3$ or polymeric photocatalyst g-C_3N_4 and so on as the counter HEP.[35−38] Still, tailoring cocatalysts and electron mediator conditions is just as important as photocatalyst selection. Interestingly, it is found that IO_3^-/I^- is the most suitable redox shuttle in the WO_3 related systems. This is probably due to the suitable pH of the mediator solution (between pH 7−10), as some papers claim[39] that the acidic media (pH < 4) would change the WO_3 to H_xWO_y because WO_3 is not stable in very acidic (pH < 3) or basic (pH > 9) conditions. Admittedly, some reports studied WO_3 in acidic media where stability is less studied.

WO_3 is also the first semiconductor applied in visible-driven Z-scheme water splitting system by Sayama and Abe et al.[37] (Pt/$SrTiO_3$:Cr,Ta)−(IO_3^-/I^-)−(PtO_x/WO_3) system was the first example of visible light-driven overall water splitting reported in 2002, and an apparent quantum yield (AQY) of 1% was achieved at 420 nm under optimized conditions in 2005 (Figure 2).[37,40] For the first time, selective O_2 evolution was

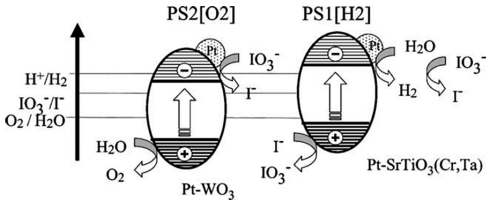

Figure 2. Speculated reaction mechanism using IO_3^-/I^- redox mediator (pH = 7). Reprinted with permission from ref 37. Copyright 2002 Elsevier.

achieved on PtO_x/WO_3 even in the presence of a considerable amount of I^- which was thermodynamically more favorable to be oxidized by holes. This is the key property for the construction of a Z-scheme; the adsorption of IO_3^- anions, instead of I^-, to the photocatalyst surface is thermodynamically preferable under pH of 7, thus ensuring a close contact between shuttle species and charges. H_2 and O_2 could be generated at a ratio of 2:1 when the two half reactions were combined. In this work, the pH of the solution was also important. Alkaline conditions were shown to be more favorable for water splitting because acidic conditions generate side products such as I_3^- which can be reduced to I^- in place of IO_3^-, breaking the redox cycle. The pH value was also optimized to avoid the formation of an oxyanionic tungstate compound or a hydrogen tungstate ion.

WO_3 was also involved in the first visible light-driven organic photocatalyst based Z-scheme system. It was via both (Pt/g-C_3N_4)−(IO_3^-/I^-)−(Pt/WO_3) and (Pt/g-C_3N_4)−(Fe^{3+}/Fe^{2+})−($BiVO_4$) systems recently reported by Martin et al, and the former one containing WO_3 achieved the most efficient performance of H_2 and O_2 evolution at rates of 2.12 and 1.10 μmol h^{-1}, respectively, from water for over 24 h.[35] The organic-derived g-C_3N_4 was synthesized from a facile and extremely cheap precursor, urea. In this work, the optimum pH of 8.3 pointed out not only the inefficiency due to the formation I_3^- at lower pH but also the instability in alkaline media (pH > 9). The mass ratio of WO_3 to g-C_3N_4 was also shown to be significant, as the difference of light absorption between the two photocatalysts influences the overall water splitting rate. Pt species act as an electron trap for photogenerated electrons in WO_3 so that the mediator could accept them efficiently and also elongate electron−hole lifetimes. IrO_2−Pt-coloaded WO_3 for O_2 evolution was also successfully coupled with a coumarin dye sensitized Pt intercalated $H_2K_2Nb_6O_{17}$ for H_2 evolution in the presence of I_3^-/I^- redox couple.[41]

3.1.2. $BiVO_4$ and Bi_2MoO_6. As a polymorphic compound with various crystal structures including, tetragonal zircon, monoclinic scheelite, and tetragonal scheelite phases, the monoclinic scheelite phase of $BiVO_4$ is one of the most efficient visible light-driven water oxidation photocatalysts (Figure 3I).[42] Monoclinic $BiVO_4$ has a band gap of ca. 2.4 eV, with CBM locating at +0.46 V (vs SHE at pH = 0) and VBM at +2.86 V (vs SHE at pH = 0).[43] The more negative VBM of $BiVO_4$ than those of conventional oxides is basically attributed to the hybridization between the O 2p and Bi 6s orbitals.[30] In the presence of sacrificial agent Ag^+, the performance of $BiVO_4$ outperforms WO_3. The narrower band gap of $BiVO_4$ facilitates a larger range of light absorption in comparison to WO_3, and the more negative band position allows more mediators with different redox potentials to be used. Other Bi-based materials such as Bi_2MoO_6 also come into sight, while the major attention has been paid on $BiVO_4$ probably due to a higher quantum yield achieved on it.[36]

The first $BiVO_4$ based Z-scheme water splitting system was reported in 2004 in a (Pt/$SrTiO_3$:Rh)−(Fe^{3+}/Fe^{2+})−($BiVO_4$ or Bi_2MoO_6) system (Figure 3II).[36] Using Fe^{3+} ($FeCl_3$) as an electron scavenger, $BiVO_4$ could evolve oxygen steadily, while separately, Fe^{2+} ($FeCl_2$) was found to be sufficient as a hole scavenger for hydrogen evolution over Pt/$SrTiO_3$:Rh. Combining the two sides, H_2 and O_2 from overall water splitting were observed steadily even after 158 h. This system worked under wavelengths of up to 530 nm, consistent with the absorption

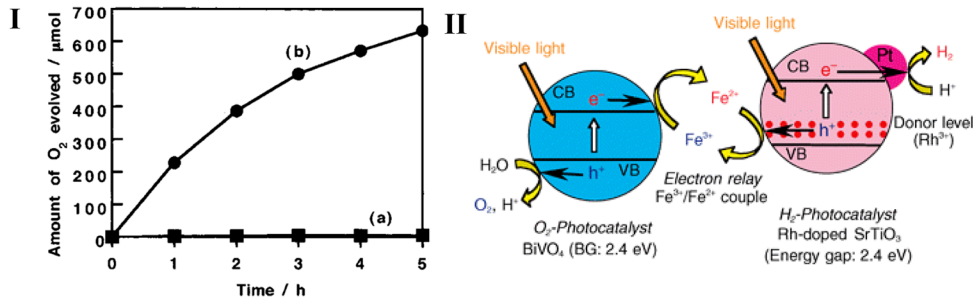

Figure 3. (I) Photocatalytic O_2 evolution from aqueous $AgNO_3$ solutions (0.05 mol/L, 320 mL) under visible light irradiation (λ > 420 nm) on (a) $BiVO_4$ (s−t) and (b) $BiVO_4$ (s−m). (II) The working diagram of Z-scheme water splitting based on $BiVO_4$. Reprinted with permission from refs 44 and 36. Copyright 2001 American Chemical Society and 2004 The Chemical Society of Japan.

DOI: 10.1021/acs.chemrev.7b00286
Chem. Rev. 2018, 118, 5201−5241

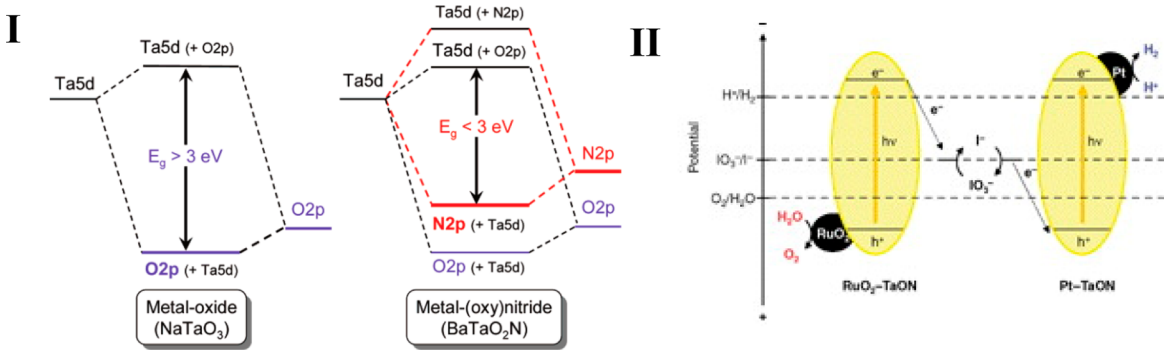

Figure 4. (I) Schematic band structures of a metal oxide ($NaTaO_3$) and metal (oxy)nitride ($BaTaO_2N$). (II) The working diagram of Z-scheme water splitting based on TaON. Reproduced with permission from refs 5 and 48. Copyright 2007 American Chemical Society and 2008 The Chemical Society of Japan.

onsets of Pt/$SrTiO_3$:Rh and $BiVO_4$. The AQY of (Pt/$SrTiO_3$:Rh)−(Fe^{3+}/Fe^{2+})−($BiVO_4$) is 0.3% at 440 nm, which is higher than both (Pt/$SrTiO_3$:Rh)−(Fe^{3+}/Fe^{2+})−(Bi_2MoO_6) and (Pt/$SrTiO_3$:Rh)−(Fe^{3+}/Fe^{2+})−(WO_3) (0.2%). But the WO_3 based system showed a higher AQY of 0.5% than 0.4% of the $BiVO_4$ system at 420 nm.[36]

Co complex electron mediators such as $[Co(bpy)_3]^{3+/2+}$ and $[Co(phen)_3]^{3+/2+}$ (bpy = 2,2′-bipyridine, phen = 1,10-phenanthroline) redox couples are also suitable for use in Ru/$SrTiO_3$:Rh and $BiVO_4$ systems for visible light-driven water splitting. The maximum AQY was 2.1% at 420 nm. It is suggested by the authors that the doped Rh species in $SrTiO_3$ was very important because Rh not only assisted long wavelength photon absorption but also acted as active sites for the oxidation of these mediator ions. A lack of Rh as active oxidation sites on other photocatalysts failed to form oxidation product of Co^{3+}, hence resulting in low activity.[45] The choice of OEP is also crucial in achieving stable and stoichiometric water splitting using these complexes. The use of other oxides, such as TiO_2 and WO_3, failed to evolve O_2 at a stable rate in the presence of such a Co complex, suggesting the occurrence of undesirable decomposition of such Co complexes. The moderate oxidation potentials of holes generated in the VB of $BiVO_4$, which is more negative than those oxides due to significant contribution of Bi 6s orbitals, is probably crucial to suppress such undesirable decomposition. This system also emphasizes the influence of pH of the reactant solution on water splitting. The optimum pH was 7 because under acidic conditions, the oxidation of Co(II) complex ions on $BiVO_4$ suppressed oxygen evolution. Conversely, the reduction of the Co(III) complex was not influenced dramatically by pH and remained unchanged. Further discussion will be presented later in section 4.

3.1.3. Oxynitrides. Oxynitrides of early transition metals with d^0 electronic configurations have been utilized in visible light induced water splitting systems due to properties of suitable band structure, good stability, and facile synthesis.[5] Oxynitrides can be synthesized by annealing the corresponding metal oxide powder under an ammonia atmosphere at temperatures of ca. 1123−1273 K.[5] Due to the more negative potential of the N 2p orbital in comparison to O 2p, the partially or fully replacement of O 2p orbitals could lead the VBM of the oxynitrides to shift upward without affecting the CBM, thus tuning the material's band gap to respond to visible light (Figure 4I). Oxynitrides could be partially decomposed to N_2 by photogenerated holes ($2N^{3-} + 6h^+ \rightarrow 3N_2$), and this could be suppressed as the reaction processes.[5] Tantalum oxynitride (TaON) is a typical photocatalyst herein and its CBM is −0.3 V (vs SHE at pH = 0) and the VBM is +2.1 V (vs SHE at pH = 0), thus the band gap is 2.4 eV corresponding to 520 nm.[46] When suitable cocatalysts were loaded on TaON, H_2 or O_2 could be evolved depending on the nature of the cocatalyst. For an oxygen evolution reaction in the presence of Ag^+ as an electron scavenger, the initial quantum yield of TaON was nearly 34% ($\lambda \sim 420$ nm).[47]

The first example of an oxynitride-based water splitting system was demonstrated in 2008. Although unmodified TaON could not generate O_2 from IO_3^- aq, loading of either IrO_2 or RuO_2 cocatalyst afforded appreciable O_2 evolution. It was reported that (Pt/TaON)−(IO_3^-/I^-)−(RuO_2/TaON) was an efficient system which produced H_2 and O_2 with an AQY of 0.1−0.2% ($\lambda \sim 420$ nm). This pioneering work then led to the discovery of a plethora of oxynitride materials as H_2/O_2 evolution photocatalysts in Z-schemes (Figure 4II).[48] By focusing on different cocatalysts on the photocatalyst, this study demonstrated the effective role in controlling the selectivity of mediators and the flexibility of the system.[49]

The most effective oxynitride-based Z-scheme system was found to be Pt/ZrO_2/TaON for H_2 and RuO_2/TaON for O_2 evolution.[50] RuO_2 was found to promote the IO_3^- reduction as well as the water oxidation, which was supported by the cathodic response in an absence and presence of IO_3^-. The enhancement of gas evolution rate was observed when the loading amount of RuO_2 was increased from 0 to 0.5 wt % due to the increased density of active sites. However, an excess amount of Ru loading also overcovered the TaON surface so that light absorption decreased along with activity. The concentration of I^- ions was also an important factor which will be discussed in next section.[50] The shortcomings in this work were mainly on the back reaction of water splitting on RuO_2 and TaON as proved by cathodic photocurrent due to O_2 reduction on both RuO_2/TaON and TaON in a PEC setup. The intrinsic property of the back reaction on RuO_2/TaON and the competitive oxidation of I^- were the main reasons for a lower performance.[50]

TaON is an intermediate phase between Ta_2O_5 and Ta_3N_5. Ta_3N_5 has a longer absorption edge than TaON (active to 591 nm, CBM at −0.4 V and a VBM at +1.7 V), therefore Ta_3N_5 has been applied in visible driven Z-scheme overall water splitting as an O_2 evolution photocatalyst as well in the presence of cocatalysts such as Ru, Rh, and Ir.[51] The half reaction of Ta_3N_5 showed a high AQY of 10% for O_2 evolution

DOI: 10.1021/acs.chemrev.7b00286
Chem. Rev. 2018, 118, 5201−5241

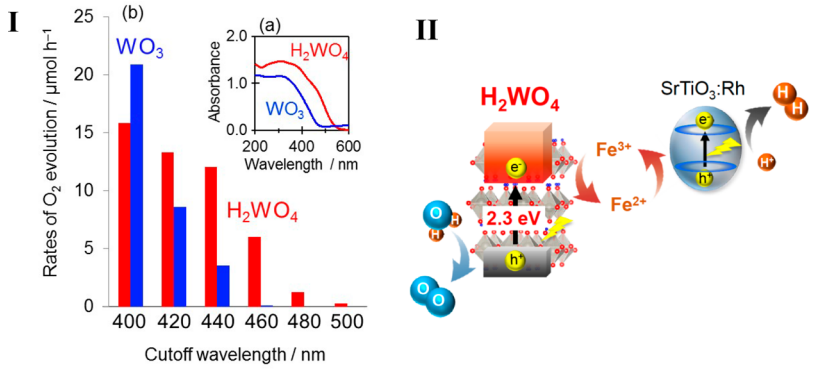

Figure 5. (I) (a) Diffuse reflectance spectra of H_2WO_4 and WO_3. (b) Rates of O_2 evolution over H_2WO_4 and WO_3 in $Fe(ClO_4)_3$ aqueous solution (5 mM, pH 2.3) under visible light irradiation (Xe lamp, cut off filter: L-42, Y-44, Y-46, Y-48 ,Y-50, O-52). (II) The working diagram of Z-scheme water splitting based on H_2WO_4. Reproduced with permission from ref 55. Copyright 2017 The Royal Society of Chemistry.

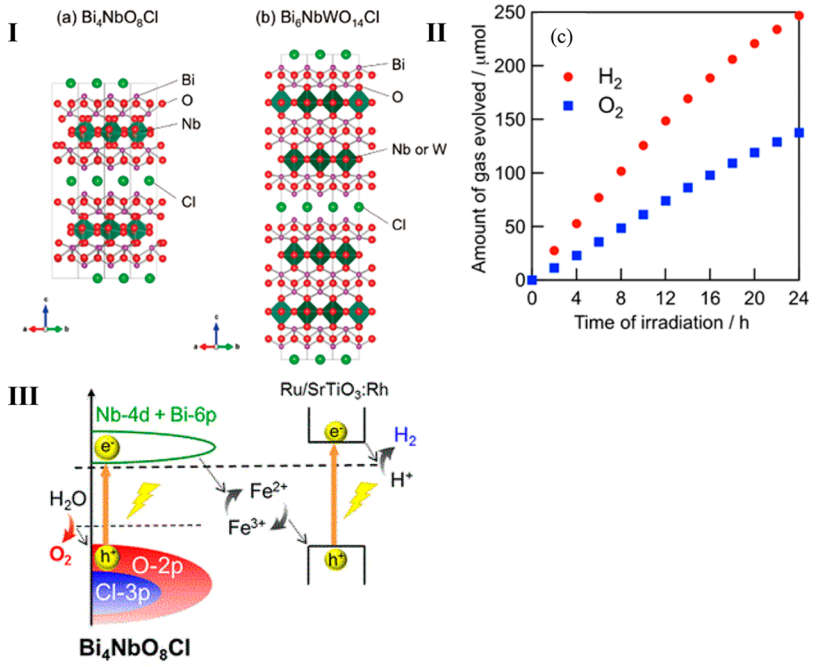

Figure 6. (I) Crystal structure of (a) Sillén–Aurivillius oxychloride Bi_4NbO_8Cl and (b) its related intergrowth compound $Bi_6NbWO_{14}Cl$ proposed by Aurivillius. (II) Time course of Z-scheme water splitting coupled with $Ru/SrTiO_3$:Rh photocatalyst via Fe^{3+}/Fe^{2+} redox mediator. (III) The working diagram of Z-scheme water splitting based on Bi_4NbO_8Cl. Reproduced with permission from ref 56. Copyright 2016 American Chemical Society.

in the existence of Ag^+, then a Z-scheme system was constructed by $(Pt/ZrO_2/TaON)-(IO_3^-/I^-)-(Ir/R\text{-}TiO_2/Ta_3N_5)$ (anatase and rutile TiO_2 noted as A- and R-TiO_2).[52,53] Ir loaded on the surface acted as active sites, while R-TiO_2 effectively controlled the IO_3^-/I^- adsorbed on the surface, thus suppressing the backward reaction. As mentioned before, competitive reactions in a Z-scheme are often observed and must be taken into consideration. R-TiO_2 selectively adsorbed IO_3^- and hindered adsorption of I^-, which is needed for O_2 evolution. It is reasonable that A-TiO_2 did not perform as well as R-TiO_2 due to the lack of unique adsorption properties. TiO_2 loading increased the activity 10-fold by the enhanced absorbance, which indicates that the suitable surface modification should not be neglected.

Oxynitrides, as mentioned above, were reported to undergo self-oxidative reaction where holes competitively oxidize nitrogen anions ($2N^{3-} + 6h^+ = N_2$) during water oxidation, causing the deactivation to the system. To solve this issue, cocatalysts including IrO_x and CoO_x nanoparticles were developed to scavenge holes and thus act as active sites for water oxidation. Considering the short diffusion lengths of photoholes in bulk n-type semiconductors, the dispersion of such cocatalysts should be as homogeneous and high as possible without compromising light harvesting ability.[54]

3.1.4. Tungstic Acids. Recently, Suzuki et al. demonstrated that tungstic acid monohydrate (H_2WO_4) functioned as a stable OEP in Z-scheme water splitting with an Fe^{3+}/Fe^{2+} redox by harvesting visible light up to 500 nm, which is beyond the absorption edge of WO_3.[55] Figure 5I shows the initial rate of O_2 evolution from $Fe(ClO_4)_3$ aqueous solution over H_2WO_4 and WO_3 under the irradiation conditions with different cutoff filters, along with their UV–vis absorption spectra. It should be noted that the H_2WO_4 sample showed appreciable activity for O_2 generation under the irradiation longer than 460 nm, where the WO_3 photocatalyst showed almost no activity. H_2WO_4 is often used as a precursor of WO_3; there has been no report on

DOI: 10.1021/acs.chemrev.7b00286
Chem. Rev. 2018, 118, 5201–5241

its application to photocatalytic water splitting. One of the reasons why the H_2WO_4 so far received little attention as an OEP is the lack of O_2 evolution ability of H_2WO_4 with Ag^+ electron acceptor, which is generally used for the first test of O_2 evolution ability of photocatalysts. Thus, this result implies that careful attention should be paid to electron acceptor choice when searching for new photocatalytic materials for water splitting. The working diagram of H_2WO_4 based Z-scheme is shown in Figure 5II.

3.1.5. Oxyhalides and Nitrogen-Doped TiO_2 as Potential OEPs. Abe, Kageyama et al. recently demonstrated that an oxychloride Bi_4NbO_8Cl could stably and efficiently oxidize water to O_2 under visible light even without any surface modifications, thereby enabling stable Z-scheme water splitting when it was coupled with $Ru/SrTiO_3$:Rh in the presence of Fe^{3+}/Fe^{2+} redox.[56] Bi_4NbO_8Cl belongs to an $n = 1$ member of Sillén−Aurivillius perovskite family $[(Bi_2O_2)_2X]^{3+}[A_{n-1}B_nO_{3n+1}]^{3-}$, which is composed of perovskite $[A_{n-1}B_nO_{3n+1}]$ layers sandwiched by a $[(Bi_2O_2)_2X]^{3+}$ Sillén block (see Figure 6I-a). It was revealed that the VBM of Bi_4NbO_8Cl consisting of mainly O 2p orbitals (not Cl 3p) is much more negative (~2.2 V vs SHE) than those of conventional oxides (~3.0 V vs SHE in most cases) or oxychlorides (e.g., BiOCl, ~3.0 V vs SHE). Consequently, Bi_4NbO_8Cl possesses both a narrow bandgap (~2.4 eV) for visible light absorption and a more negative CBM than the water reduction potential (Figure 6III). It was presumed that the photogenerated holes populated on O^{2-} anions near VBM (or O^- ions) were rather stable and just brought about O_2 evolution, instead of oxidative decomposition, which often occurred in conventional anion-doped narrow band gap materials such as (oxy)nitrides. The authors also demonstrated that a Sillén−Aurivillius related oxychloride $Bi_6NbWO_{14}Cl$ (see Figure 6I-b) worked as a stable OEP in the Z-scheme water splitting system. These findings would provide new strategies for developing durable photocatalytic materials for water splitting under visible light by manipulating the perovskite block as well as the $(Bi_2O_2)_2Cl$ block in the Sillén−Aurivillius phases, with a general formula of $[(Bi_2O_2)_2X]^{3+}[A_{n-1}B_nO_{3n+1}]^{3-}$ (X = halogens, n = 1, 2, 3,...).

Maeda et al. recently demonstrated that a rutile TiO_2 powder doped with tantalum and nitrogen (TiO_2:Ta/N) could function as a stable OEP for Z-scheme water splitting with both Fe^{3+}/Fe^{2+} and IO_3^-/I^- redox couples under visible light. The preintroduction of Ta cations into TiO_2 precursor via microwave-assisted solvothermal synthesis was found to suppress the production of Ti^{3+} and/or anionic vacancies during nitridation process with NH_3 stream. The decreased formation of such unfavorable sites that enhance charge recombination probably afford TiO_2:Ta/N to oxidize water in a stable manor. Although the formation of such reduced cation species (e.g., Ti^{3+}, Nb^{4+}), as well as anion defects, during nitriding has so far limited the active oxynitride photocatalyst to Ta-based one (e.g., TaON), the present new strategy probably enables us to develop new oxynitride (or nitrogen-dope) materials as stable OEPs with high photocatalytic activity in Z-scheme water splitting systems.

3.2. Reduction Photocatalyst Dominated Systems with Dissolved Redox Mediators

As mentioned above, the development of the other half reaction (H_2 evolution) is naturally indispensable for an efficient Z-scheme system. The up to date visible light-driven HEP are next discussed.

3.2.1. Cation Doped $SrTiO_3$. Doped $SrTiO_3$ is one of the most well documented H_2 production photocatalysts used in the construction of Z-schemes. Non-doped $SrTiO_3$ has a relatively large band gap (3.1 eV), which prohibits its use in visible light driven water splitting system.[37] Hence, cationic doping of $SrTiO_3$ has often been used to introduce a new energy level above the original VB to act as an electron donor level, which allows visible light absorption. However, besides the electron donor level, the dopant can also act as a recombination center for charge carriers so the activity can decrease in certain circumstances. Therefore, the dopant must be selected carefully to ensure it is efficient for H_2 evolution in overall water splitting, striking a balance between light absorption, redox functionality, and electron trapping capabilities.

The visible light response of Rh-doped $SrTiO_3$ is thought to be due to a new donor level induced by Rh (Figure 7). Pt/

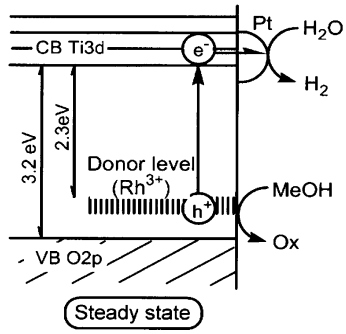

Figure 7. Proposed band structure and visible light response of Rh-doped $SrTiO_3$ photocatalyst. Reproduced with permission from ref 16. Copyright 2004 American Chemical Society.

$SrTiO_3$:Rh can achieve a quantum yield of 5.2% at 420 nm for the H_2 evolution half reaction in an aqueous methanol solution.[16] There are two onsets of the absorption band of $SrTiO_3$:Rh including a shoulder one at 420 nm and a band from 580 to 1000 nm due to the oxidation state of the rhodium. Rh dopants existed in two forms, Rh^{3+} and another higher oxidation state (e.g., Rh^{4+}), according to the diffuse reflectance spectrum. The Rh^{4+} could be easily reduced to Rh^{3+} by electrons excited by photons. The photogenerated electrons from the donor level formed with Rh^{3+} were transferred to the CB of $SrTiO_3$ to reduce protons, while the holes (positive charge) left on the electron donor level oxidized methanol. This Pt/$SrTiO_3$:Rh system was also examined for the O_2 generation, but was relatively inefficient, likely due to the discrete Rh^{3+} sites. It appears that such discrete oxidation site of Rh^{3+} cannot catalyze water oxidation efficiently because it requires four-electron abstraction while it can catalyze one or two-electron oxidation processes (e.g., methanol or Fe^{2+}).

As mentioned above, Sayama, Abe et al. combined Pt/$SrTiO_3$:Cr,Ta with PtO_x/WO_3 in the presence of an IO_3^-/I^- mediator in an aqueous solution and first reported visible responsive overall water splitting system via a Z-scheme (Figure 2).[37] With the extremely low overpotential for H_2 production in water electrolysis, Pt was selected as the cocatalyst for proton reduction to hydrogen. It is worth noting that Pt/$SrTiO_3$ worked well for O_2 evolution with IO_3^- as the electron scavenger. However, after doping of Cr and Ta, O_2 could hardly

DOI: 10.1021/acs.chemrev.7b00286
Chem. Rev. 2018, 118, 5201−5241

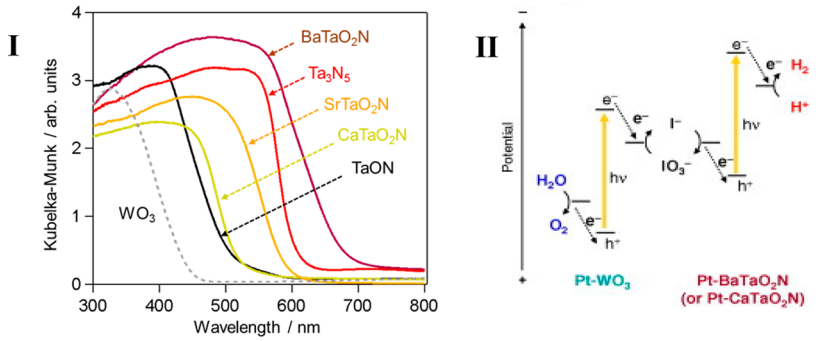

Figure 8. (I) UV−vis diffuse reflectace (DR) spectra of $ATaO_2N$ (A = Ca, Sr, Ba), TaON, Ta_3N_5, and WO_3. (II) The working diagram of Z-scheme water splitting based on $ATaO_2N$. Reproduced with permission from refs 11 and 60. Copyright 2011 The Chemical Society of Japan and 2008 Elsevier.

be detected under the same conditions, therefore encouraging active site selectivity which is favorable to construct a Z-scheme system. This work pointed out only oxide semiconductors containing Cr^{3+} such as doped $SrTiO_3$ (Cr−Ta-doped), doped $CaTiO_3$ (Cr−Ta-doped), and $CrTaO_4$ showed H_2 production activities if loaded by Pt as a cocatalyst, notably Pt/$SrTiO_3$:Cr,Ta exhibited the highest H_2 production rate. Considering similar ionic radii of Cr^{3+} and Ta^{5+} in comparison to Ti^{4+}, it was more likely that the dopants substituted the titanium ions in the lattice. The codoping of Ta and Cr makes the photocatalyst more efficient than that doped by Cr only for water splitting due to the neutralized total charge on the lattice, which likely decreased the probability of charge recombination and also increased stability for the reaction.

3.2.2. Oxynitrides. As mentioned above, TaON was investigated as both OEP and HEP. Pt-loaded TaON as a HEP was coupled with PtO_x/WO_3 in an IO_3^-/I^- aqueous solution to construct a Z-scheme system.[57] H_2 could be produced in the presence of NaI as hole scavenger on Pt/TaON, and the evolution rate decreased due to the accumulation of IO_3^- ions, which were competitively reduced back to I^- in place of water reduction. Additionally, TaON was shown to be resistant to photocorrosion in this half reaction process, as no O_2 or N_2 was detected (by gas chromatography), probably due to efficient scavenge of holes by I^- adsorbed on the TaON surface.[57] To some extent, O_2 was also evolved, which was due to a thin Ta-oxide overlayer on TaON because the surface of TaON was oxidized under visible light irradiation as confirmed by the in situ multiple internal reflection IR (MIR-IR) results.[58] Overall water splitting was achieved when PtO_x/WO_3 was combined and stably produced the stoichiometric H_2 and O_2 for 60 h at the pH of 5.3, reaching 0.5% of AQY at 420 nm.[59]

Mixed tantalum oxynitride perovskites of $ATaO_2N$ (A = Ca, Sr, Ba) have shown to be active for visible light driven H_2 evolution.[60,61] These materials were synthesized by annealing amorphous $A_2Ta_2O_7$ under NH_3. The absorption edges of $ATaO_2N$ (A = Ca, Sr, Ba) were at 520, 600, and 660 nm, respectively, showing a cationic effect that absorption increased along with the ionic radii (Figure 8I). The highest H_2 evolution rate among them was from $BaTaO_2N$ (50 μ mol/h), followed by $SrTaO_2N$ (42 μ mol/h) and then $CaTaO_2N$ (24 μ mol/h). It was speculated that Ta_3N_5 might exist in these materials, but Pt/Ta_3N_5 yielded a nondetectable amount of H_2 in the presence of I^-, therefore it could be confirmed that the activity came from the unique perovskite−oxynitride crystal structure.[47]

The first Z-scheme for an overall water splitting system was reported to respond to wavelengths longer than 600 nm using the $(Pt/BaTaO_2N)-(IO_3^-/I^-)-(PtO_x/WO_3)$ system in 2008 by Higashi et al. (Figure 8II).[60] The quantum yield (based on Pt/$BaTaO_2N$) for overall water splitting was determined to be 0.1% at 420−440 nm. Crucially, self-oxidative photocorrosion was not significantly detected in this system. However, as for Pt/$SrTaO_2N$, self-oxidative photocorrosion was detected in the form of gaseous N_2, and ultimately the system failed to work with PtO_x/WO_3. The reason why only Pt/$SrTaO_2N$ suffered from that was not clear yet but could likely be due to the formation of strontium iodate/iodide. However, photocorrosion could be decreased if calcination temperature was increased, suggesting that a higher crystallinity helped anchor the strontium ions in place. It was noticed though, that the rate of gas evolution eventually decreased in this system due to I_3^- formation. An accumulation of I_3^- ions that could not be reduced by PtO_x/WO_3 effectively could be avoided by increasing pH of solution. Unfortunately, WO_3 is not stable in alkaline solution with pH over 9. Therefore, other visible light-driven photocatalysts with satisfying stability in high pH are still needed in order to be coupled with $ATaO_2N$.

The modification of a TaON surface with ZrO_2 was reported to be useful as a passivation layer.[47] In the $(Pt/ZrO_2/TaON)-(IO_3^-/I^-)-(PtO_x/WO_3)$ system, 6.3% AQY at 420 nm was achieved. When annealed in ammonia, the formation of reduced species (Ta^{3+} or Ta^{4+}) along with anion defects that act as recombination sites are basically inevitable. However, the formations of such unexpected reduced species and defects were effectively suppressed by ZrO_2 modification, resulting in higher efficiency. Various zirconium precursors were also investigated, with the best precursor being $ZrO(NO_3)_2{\cdot}H_2O$, which dispersed well and could modify the anionic vacancies during the nitridation process, leaving fewer impurities and reducing the recombination sites.

So far, the highest AQY of a Z-scheme in the presence of a dissolved mediator for overall water splitting was achieved using a $(MgTa_2O_{6-x}N_y/TaON)-(IO_3^-/I^-)-(PtO_x/WO_3)$ system.[47] The AQY of 6.8% at 420 nm under optimum conditions has been reported in 2015. The band locations ensured an absorption of visible light up to 570 nm as a type II heterojunction structure.[47] As expected, electron transfer occurs from the CB of $MgTa_2O_{6-x}N_y$ to the CB of TaON, and holes transfer from the VB of TaON to the VB of $MgTa_2O_{6-x}N_y$, thus the recombination of charge carriers was effectively suppressed by the heterostructure, as confirmed by the prolonged charges' lifetime from time-resolved infrared spectra

DOI: 10.1021/acs.chemrev.7b00286
Chem. Rev. 2018, 118, 5201−5241

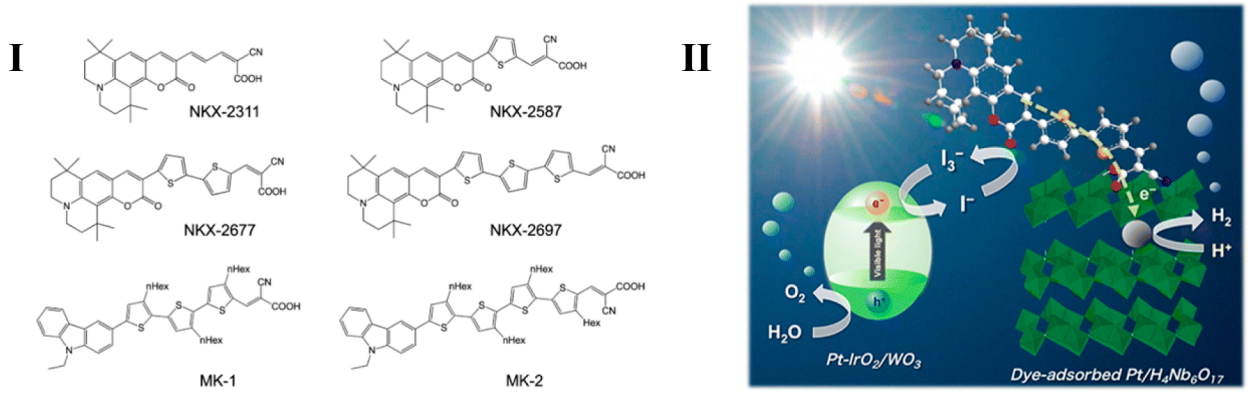

Figure 9. (I) Molecular structures of dyes. (II) The working diagram of Z-scheme water splitting based on dye-adsorbed Pt/$H_4Nb_6O_{17}$ and IrO_2–Pt/WO_3. Reproduced with permission from ref 62. Copyright 2013 American Chemical Society.

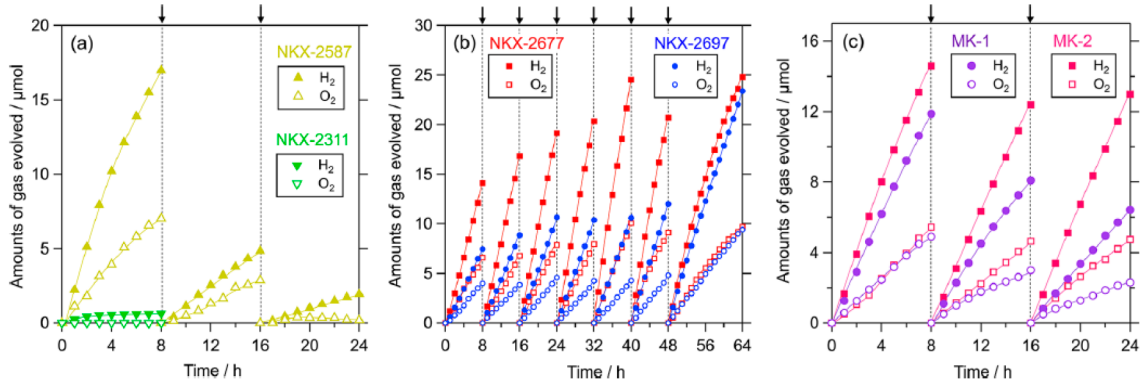

Figure 10. Time courses of photocatalytic evolution of H_2 (closed) and O_2 (open) using a mixture of dye-adsorbed [(a) NKX-2311 and NKX-2587, (b) NKX-2677 and NKX-2697, and (c) MK-1 and MK-2] Pt/$H_4Nb_6O_{17}$ (50 mg) and IrO_2–Pt/WO_3 (100 mg) suspended in 5 mM KI aqueous solution (pH ∼ 4.5, without adjustment) under visible light. Arrows indicate evacuation of gas phase. Reproduced with permission from ref 62. Copyright 2013 American Chemical Society.

(TRIR). When irradiated by light with wavelength above 520 nm, the junction still produced H_2 while TaON alone did not. The gas evolution rate was even higher than that of Pt/$MgTa_2O_{6-x}N_y$ only with wavelength >420 nm, revealing a spatially separated charge transfer mechanism that was responsible for the enhancement of photocatalytic activity at longer wavelength. Pt metal was observed to be photoreduced on the surface of TaON instead of $MgTa_2O_{6-x}N_y$, which confirmed photoexcited electrons were transferred from $MgTa_2O_{6-x}N_y$ to TaON. The one-pot synthesis method of ammonia treating $MgTa_2O_6/Ta_2O_5$ provided a more intimate interfacial contact and fewer defects than a simple mechanical mixture of $MgTa_2O_{6-x}N_y$ with TaON. Although heterojunction structures were widely used in photocatalysts, this was the first time for heterojunctions to be applied as a HEP in a Z-scheme system. This work demonstrated the possibility of using heterostructured photocatalysts for half reactions in overall water splitting.

3.2.3. Dye-Sensitized Systems. Although various semiconductors, not only conventional metal oxides, have been successfully employed as HEPs in Z-scheme water splitting systems as introduced above, there are still a limited number of efficient photocatalysts. This is primarily due to the difficulty in tuning the band levels of inorganic semiconductors. On the other hand, it is much easier to tune the energy levels (HOMO and LUMO) of organic dyes, as proven in the extensive studies on dye-sensitized solar cells with redox couples such as I_3^-/I^-. Thus, using dye-sensitized n-type semiconductors as a HEP with such a redox couple appears to be one of the promising ways to achieve efficient water splitting by harvesting wide range of visible light. However, the most serious issue of such organic dyes is their instability, specifically the instability of the oxidized state (reactive radical species in most cases) of simple dye molecules in aqueous medium. Actually, there are few reliable dye-sensitized photocatalysts that are active for H_2 production using a reversible electron donor such as I^-.

Abe et al. demonstrated that the introduction of an oligothiophene moiety between the donor and acceptor parts dyes (see the structures in Figure 9) drastically improved the stability during their redox cycles in aqueous solution.[62] Both the electrochemical measurements and photocatalytic reactions indicated that the oxidized states of dyes having oligothiophene moieties possessed sufficiently long lifetimes even in aqueous solution. The long lifetime of oxidized species enabled dye regeneration by accepting an electron from the I^- anion, achieving sustained and stoichiometric production of H_2 and I_3^- under visible light irradiation when combined with a n-type semiconductor, internally platinized layered niobate (Pt(in)/$H_4Nb_6O_{17}$). Then water splitting into H_2 and O_2 under visible light was achieved using such coumarin or carbazole dye-sensitized Pt(in)/$H_4Nb_6O_{17}$ as HEP, coupled with an OEP (IrO_2–Pt-coloaded WO_3) in the presence of I_3^-/I^- redox couple (see Figure 10), while the use of dyes without

DOI: 10.1021/acs.chemrev.7b00286
Chem. Rev. 2018, 118, 5201–5241

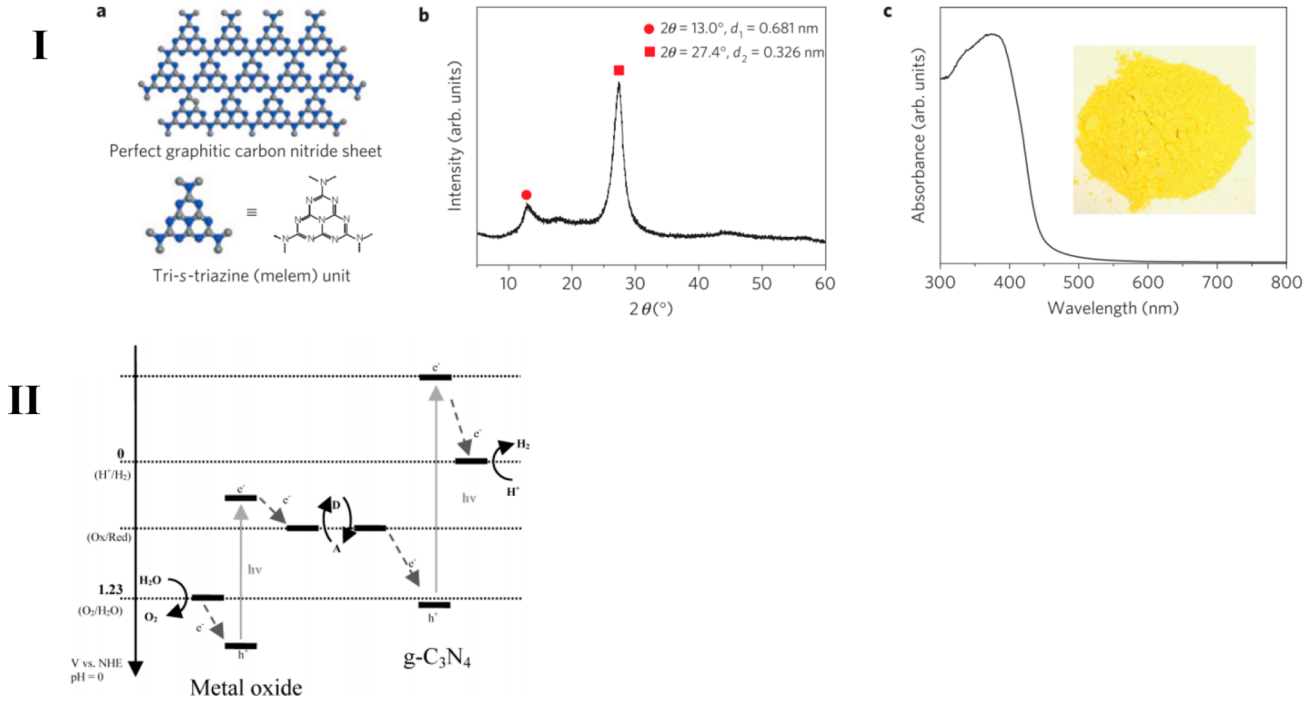

Figure 11. (I) (a) Crystal structure and optical properties of graphitic carbon nitride. Schematic diagram of a perfect graphitic carbon nitride sheet constructed from melem units. (b) Experimental XRD pattern of the polymeric carbon nitride, revealing a graphitic structure with an interplanar stacking distance of aromatic units of 0.326 nm. (c) Ultraviolet−visible diffuse reflectance spectrum of the polymeric carbon nitride. Inset: Photograph of the photocatalyst. (II) The working diagram of Z-scheme water splitting based on g-C_3N_4. Reproduced with permission from refs 63 and 35. Copyright 2009 Macmillan Publishers Limited and 2014 American Chemical Society.

oligothiophene moiety failed to split water stably due to the occurrence of oxidative decomposition of dyes.[62]

3.2.4. g-C_3N_4. Apart from crystalline inorganic semiconductors, which have been well studied since the discovery of the Fujishima−Honda effect in early 1970s, polymeric semiconductors have attracted increasing attention since graphitic carbon nitride (g-C_3N_4) was reported for visible light-driven photocatalytic hydrogen production (Figure 11I).[63,64] Composed of ordered heptazine units, g-C_3N_4 has been reported to have a relatively small band gap of 2.7−2.9 eV with a negative enough CBM position (at −1.2 V vs SHE at pH = 0) to drive electrons to reduce protons to hydrogen.[29] Composed of extremely abundant elements, graphitic carbon nitride is low-cost, robust, and nontoxic. However, as g-C_3N_4 has only been used as a photocatalyst since 2008, efficiencies are still relatively low for H_2 production and the wavelength absorption limit is only 460 nm. Consequently, many strategies have since been employed to improve the compound in terms of performance and durability. Precursors including urea, melamine, dicyandiamide, and thiourea have been found to be able to produce g-C_3N_4 by simple pyrolysis in various atmospheres, including air.[64] Elemental doping of P, B, F, I, S, O, and N was also examined.[65−72] Other methods such as nanostructure design and molecular incorporation were also applied herein to enhance the moderate performance.[73,74] However, only a few groups have succeeded in coupling the g-C_3N_4 in Z-scheme water splitting.

Liu et al. reported a route to prepare g-C_3N_4 from human waste (urea), making g-C_3N_4 extremely cheap.[75] The first g-C_3N_4 based overall water splitting system was reported by Martin and Tang et al. in 2014.[35] Further, it was found that the degree of polymerization influenced the performance of hydrogen evolution and the optimum urea-derived g-C_3N_4 showed an internal quantum yield of 26.5% under visible light (400 nm) with a TON of 641, as one of the highest efficient visible light photocatalysts for water reduction reaction.[64] For this half reaction, various other cocatalysts such as Au and Ru were also examined, yet Pt was found to be the most efficient.

In the urea-derived g-C_3N_4 based Z-scheme system, both (Pt/g-C_3N_4)−(IO_3^-/I^-)−(PtO_x/WO_3) and (Pt/g-C_3N_4)−(Fe^{3+}/Fe^{2+})−($BiVO_4$) represented splitting water continuously, with an initial gas evolution rate of H_2 and O_2 at 7.4 and 3.7, 1.5, and 0.8 μmol h^{-1}, respectively. The systems worked both under both full arc and visible, yielding reproducible H_2 and O_2 for over 24 h. The VBM of g-C_3N_4 lied as deep as +1.5 V (vs SHE at pH 0), which is suitable for the both redox couples (IO_3^-/I^-, +0.67 V at pH 7; Fe^{3+}/Fe^{2+}, +0.77 V) (Figure 11II). One thing to note was that only urea-derived g-C_3N_4 was active in these systems. Thiourea and dicyandiamide did not work here although they could photocatalytically produce H_2 from water.[35] Their unsatisfying band positions and the surface conditions could be the reason of the phenomena, but it could also be that they are simply not efficient enough to generate a detectable amount of hydrogen. As for urea-derived g-C_3N_4, the lower degree of surface protonation was more favorable for the adsorption of I^- or Fe^{2+} ions on the photocatalyst surface, thus making the cycle reaction easy to facilitate.

3.2.5. (Oxy)sulfides. (Oxy)sulfide materials have been studied as HEPs because many of them have both the narrow bandgaps for visible light absorption and very negative CBMs for water reduction, due to the contribution of S 3p orbitals to VBM formation. Zhao et al. applied an oxysulfide $Sm_2Ti_2S_2O_5$ with a band gap of ca. 2 eV as a HEP in Z-scheme water splitting coupled with rutile TiO_2 as an OEP in the presence of IO_3^-/I^- redox couple, while this system still required UV light

DOI: 10.1021/acs.chemrev.7b00286
Chem. Rev. 2018, 118, 5201−5241

for the excitation of the OEP.[76] Then, Kato et al. demonstrated for the first time a metal sulfide based Z-scheme water splitting with a $[Co(terpy)_3]^{3+/2+}$ redox in 2015 by utilizing Ru-loaded $(CuGa)_{0.8}Zn_{0.4}S_2$ as a HEP and $BiVO_4$ as an OEP.[77] The combination resulted in stable generation of H_2 and O_2 with a stoichiometric ratio under visible light irradiation ($\lambda > 420$ nm), as well as under a solar simulator, without any reduced activity. It was proposed that the predominant contribution of Cu 3d orbital to the VBM of the $(CuGa)_{1-x}Zn_{2x}S_2$ photocatalyst is crucial in achieving such stable reaction without suffering from self-oxidative deactivation (photocorrosion). This efficient molecular shuttle will be discussed in more detail in a later section (section 4.3.3).

3.3. Water Splitting with Solid Redox Mediators

As mentioned above, the redox mediator pairs existing in a Z-scheme more or less compete with reduction on the HEP and oxidation on the OEP, although these redox couples relayed electrons well in many reported systems. A simple solid electron shuttle instead of the redox pairs should be more favorable as it rules out the redox diffusion process,[48] which could also be facile and appropriate to practical use.[99] Dissolved ions redox-mediated systems are easily investigated by half reaction tests for either H_2 or O_2 with appropriate sacrificial reagent, following pure water splitting by the coupled pairs. However, in a solid shuttle system, one has to synthesis the HEP/shuttle/OEP double junction first before testing the gas evolution activities. Another obstacle to solid junctions is the charge recombination between layers.[96] The following section describes the successful examples of Z-schemes for pure water splitting using a solid mediator, which in principle should be more facile than systems that use a liquid mediator. The primary requirement for the solid mediator is high conductivity, which includes such materials as graphene oxide, gold nanoparticles, and carbon nanoparticle/dots.

3.3.1. Photoreduced Graphene Oxide. The first visible driven solid mediator Z-scheme for overall water splitting by Iwase et al. is illustrated in Figure 12, where photoreduced

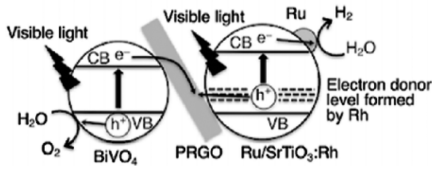

Figure 12. Mechanism of water splitting in a Z-scheme photocatalyst system consisting of $Ru/SrTiO_3$:Rh and $BiVO_4$ under visible-light irradiation using RGO as a mediator. Reproduced with permission from ref 99. Copyright 2011 American Chemical Society.

graphene oxide (PRGO) was used as the electron shuttle in a system composed of $BiVO_4$ and $Ru/SrTiO_3$:Rh. Doped $SrTiO_3$ acted as the HEP and $BiVO_4$ as the OEP, which were the most commonly used two photocatalysts in a dissolved mediate system.[99] The highest rates achieved were 11 and 5.5 μmol h^{-1} for H_2 and O_2 production, respectively, indicating pure water splitting. When irradiated by light, due to the staggering of band positions, electrons in $BiVO_4$ migrated through the PRGO layer to combine with the positive charges (i.e., Rh^{4+} species) in $SrTiO_3$:Rh. Meanwhile, the photogenerated holes in $BiVO_4$ and the photoexcited electrons in $Ru/SrTiO_3$:Rh were used to oxidize and reduce water, respectively, thus forming an overall water spitting. As a conductor, PRGO worked as the mediator. Different from other "dissolved redox mediators", PRGO was a conductor and transferred electrons freely between semiconductors, but the back pathway was suppressed because the photoexcited electrons in $BiVO_4$ cannot reduce proton and the positive charges (i.e., Rh^{4+} species) in $Ru/SrTiO_3$:Rh cannot oxidize water at the same time.[96] PRGO was photo reduced on $BiVO_4$ instead of on $Ru/SrTiO_3$:Rh, which could help electron relay. Both the reduced GO on $Ru/SrTiO_3$:Rh and hydrazine-reduced GO failed to perform overall water splitting. The reason was that in those two occasions, the hydrophobicity was so high that the powders turned to be immiscible in water. According to the authors, this phenomenon could be seen by eye and the carbon state shown in XPS confirmed the low portion of C−O bond which was favorable for good dispersion. So, to maintain the enhanced activity in the Z-scheme, the hydrophobicity at the surface had to be controlled.[99]

These authors have also applied this strategy (i.e., the use of PRGO as solid electron mediator) to metal sulfide-based Z-scheme systems, in which various Cu-based sulfides such as $CuGaS_2$, $CuInS_2$, and Cu_2ZnGeS_4 were employed as HEPs combined with rutile TiO_2 (OEP) via PRGO.[100] Although these early systems required UV light irradiation for the excitation of TiO_2, these authors later combined $CuGaS_2$ with CoO_x-loaded $BiVO_4$ to demonstrate water splitting under visible light.[100] The CoO_x cocatalyst was revealed to play a crucial role in the Z-scheme system to promote water oxidation on $BiVO_4$, thereby enhancing the electron injection from CB of $BiVO_4$ to $CuGaS_2$ through PRGO. It should be noted that there is a strong relation between the activity of present Z-scheme systems and the photoelectrochemical properties of photocatalyst materials employed. Only the combination of p-type and n-type photocatalysts for H_2 evolution and O_2 evolution, respectively, was effective at present even if the sufficient overlap between the band potentials for electron transfer was satisfied between the HEP and OEP.

3.3.2. Au and Ag. The first all-solid-state Z-scheme system reported was composed of $Au@CdS/TiO_2$ for methyl viologen reduction reaction instead of water splitting.[110] By the deposition−precipitation method, a core−shell-type nanoparticle was obtained, which was specified to be CdS-coated Au nanocrystals on TiO_2 surface. The $Au@CdS/TiO_2$ photocatalytic activity was much higher than any of two components. The reasons could be due to the higher charge-separation efficiency by Z-scheme mechanism, for electrons in CB of TiO_2 transfer to Au and then to VB of CdS, influenced by the large work function of gold.[110] Although this work was not visible light-driven Z-scheme water splitting, it opened a possible window for all-solid-state Z-scheme system development. Far from satisfactory, many efforts have been made in the past decade but the majority mainly focused on the dye degradation or half reaction of H_2 evolution, while only several systems worked for water splitting. One of the significant challenges is the interfacial contact between the solid electron mediator, HEP and OEP. Another challenge is that the system should remain stable during reaction. Thus electron mediators are limited to conductive/electron rich materials such as Au and reduced graphene oxide (RGO).[98,111]

Very recently, an efficient Z-scheme system composed of $SrTiO_3$:La,Rh/Au nanoparticle/$BiVO_4$:Mo photocatalyst sheets was reported, which could be prepared by two methods.[98,112] On the photocatalyst sheet prepared by the first method, HEP and OEP particles were physically embedded into the gold layer

DOI: 10.1021/acs.chemrev.7b00286
Chem. Rev. 2018, 118, 5201−5241

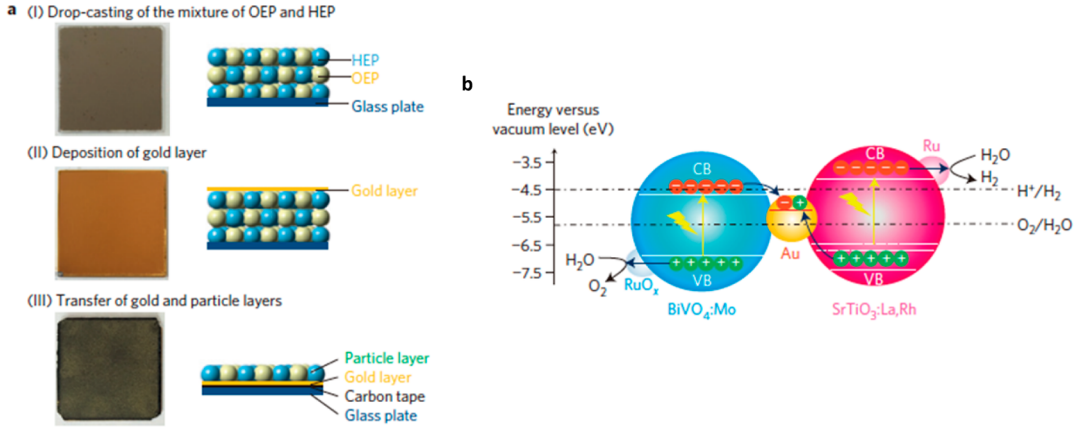

Figure 13. (a) Illustration of the preparation of the $SrTiO_3$:La,Rh/Au/$BiVO_4$:Mo sheet by the particle transfer method, and (b) schematic of overall water splitting on the Ru-modified $SrTiO_3$:La,Rh/Au/$BiVO_4$:Mo sheet. Reproduced with permission from ref 98. Copyright 2016 Macmillan Publishers Limited.

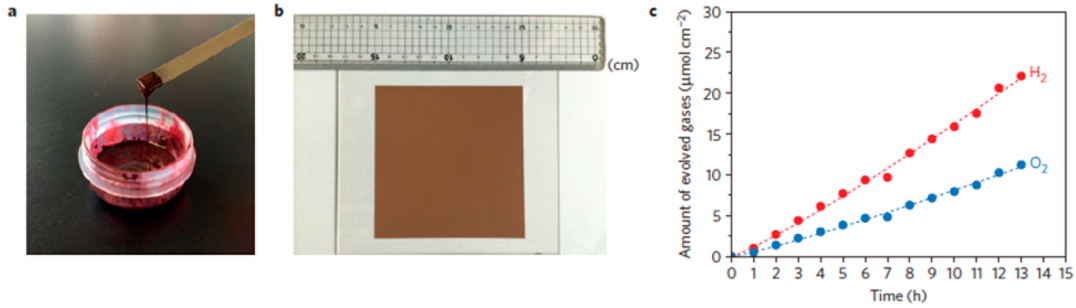

Figure 14. (a) Photograph of the ink used for screen printing the photocatalyst sheet. (b) Photograph of a 10 cm × 10 cm $SrTiO_3$:La,Rh/Au nanoparticle/$BiVO_4$:Mo printed sheet. (c) Time course of the water splitting reaction using a Ru-modified $SrTiO_3$:La,Rh/Au colloid (40 wt %)/$BiVO_4$:Mo printed sheet under simulated sunlight at 288 and 5 KPa. The sample (6.25 cm^2) was photodeposited with $RuCl_3 \cdot 3H_2O$ (0.17 μmol). Reproduced with permission from ref 98. Copyright 2016 Macmillan Publishers Limited.

(see Figure 13a). The STH energy conversions efficiency reached 1.1% with an AQY of 33% at 419 nm, which were both nearly 1 order of magnitude higher than that reported in the liquid mediator system and became a bench mark result in the Z-scheme systems.[98] Unlike PRGO used in the previous section, the underlying gold layer provided a much better charge transfer for the embedded photocatalysts via a particle transfer method. The contact resistance of a Schottky barrier, which is the most common problem in solid state Z-scheme systems and also the strongest dependency in this work, between the metallic gold layer and semiconductors, was reduced by controlling the annealing time and temperature. The extended annealing temperature and duration enhanced the contact between them, probably due to crystallinity, while too high temperature or too long durations decreased the activity considerably, which was attributed to the volatilisation of V_2O_5.[30] The back reaction, which was a crucial factor in other Z-scheme systems, was considered in this work as well, as H_2 and O_2 formed at sites in close proximity to each other. Protection layers of Cr_2O_3 and amorphous TiO_2 were applied for effectively capping the surface and suppressing back reactions.[113]

The second method was a screen-printing technology.[98] The sheet design could be screen printed by an ink, which contained photocatalysts loaded with Au. The water splitting activity of a printed sheet went up according to an increasing amount of Au in the colloid, indicating the Au nanoparticles acted as an electron conductor between particles (Figure 14). The STH in the second system was 0.1%, which was less than the first example that was due to difficulty in the appropriate thickness of cocatalyst loading. The activity was also found to decay with time, which was due to aggregation of Au that lowered electron relay between HEP and OEP particles. However, the authors showed how screen printing technology could be a viable design for facile large-scale production in the future.

Apart from Rh-doped $SrTiO_3$ as the effective HEP, an oxynitride $LaMg_{1/3}Ta_{2/3}O_2N$ was recently demonstrated to function as visible light responsive HEP in such systems. Pan et al. reported that a photocatalytic sheet consisting of $RhCrO_x$/$LaMg_{1/3}Ta_{2/3}O_2N$ (HEP) and rutile-TiO_2 (OEP) embedded in the Au layer with an amorphous TiO_2 protective layer exhibited activity for simultaneous evolution of H_2 and O_2, while this sheet required UV light.[105] The authors then demonstrated water splitting under visible light by combining the $RhCrO_x$/$LaMg_{1/3}Ta_{2/3}O_2N$ and $BiVO_4$:Mo coated with an amorphous TiO_2 layer.[98] A reduced graphene oxide (RGO) was also applied as an additional solid mediator to the conductive layer to bridge particulate photocatalysts.[106]

Other metals including Ag were also reported to work as shuttles in Z-scheme water splitting systems, such as $ZnRh_2O_4$/Ag/$Ag_{1-x}SbO_{3-y}$ by Kobayashi et al.,[108] where electrons are transferred from the CB of $Ag_{1-x}SbO_{3-y}$, via the solid-state mediator Ag, to the VB of $ZnRh_2O_4$. The size of Ag is believed to be crucial, which is still in the nanometer regime after heating to 1173 K. Such small Ag nanoparticles ensure maximum use of surface area and thus more sites for charge

DOI: 10.1021/acs.chemrev.7b00286
Chem. Rev. 2018, 118, 5201−5241

transfer. It should be noted that even without Ag, the physical mixture of $Ag_{1-x}SbO_{3-y}$ and $ZnRh_2O_4$ was also able to split water but only 33% of the activity. This also confirms the important role of silver mediator in the charge transfer of Z-scheme water splitting.

3.3.3. Conductive Carbon. As introduced above, quite efficient Z-scheme system composed of $SrTiO_3$:La,Rh/Au nanoparticle/$BiVO_4$:Mo photocatalyst sheets was reported to exhibit the highest STH (1.1%) of an artificial Z-scheme systems based on particulate photocatalysts. However, there were some issues in such a Au-mediator based system. One is the non-negligible cost of Au mediator, while it depends on the amount of use. However, the scaling up potential could be more practical if low-cost conducting media, as well as narrower bandgap semiconductors, are developed in this system. Another issue is the occurrence of backward reaction (i.e., water formation from evolved H_2 and O_2) on Au, while the rate of this reaction is much lower than that on Pt. Although the occurrence of backward reaction was considerably suppressed by the protection layer of Cr_2O_3 and amorphous TiO_2 as described above, it was still appreciable when the reactions were carried out at high background pressures. Thus, the reactions were carried out at low background pressures of 5 KPa in most cases in the report.[107]

Very recently, the same research group successfully introduced a conductive carbon as an efficient electron mediator to a particulate photocatalyst sheet. The unfavorable occurrence of backward reaction was effectively suppressed (see Figure 15), thereby affording efficient Z-scheme water splitting

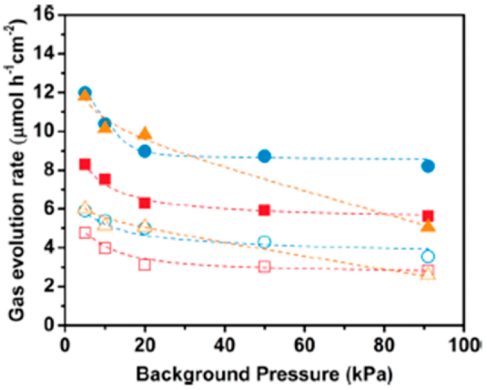

Figure 15. Squares (□), circles (○), and triangles (△) stand for Ru-loaded $SrTiO_3$:La,Rh/C/$BiVO_4$:Mo, Cr_2O_3/Ru-loaded $SrTiO_3$:La,Rh/C/$BiVO_4$:Mo, and a-TiO_2/Cr_2O_3/Ru-loaded $SrTiO_3$:La,Rh/Au/$BiVO_4$:Mo, respectively. Closed and open symbols represent hydrogen and oxygen, respectively. Photodeposition from $RuCl_3{\cdot}3H_2O$ (0.2 μmol), K_2CrO_4 (0.2 μmol), Ti peroxide (1.3 μmol), and the overall water-splitting reaction were carried out under Xe lamp (300 W) illumination (λ > 420 nm) at 288 K. The area of the photocatalyst sheets was 7.5 cm^2. Reproduced with permission from ref 107. Copyright 2017 American Chemical Society.

even at ambient pressure.[107] The $SrTiO_3$:La,Rh/C/$BiVO_4$:Mo sheet was demonstrated to split pure water (pH 6.8) with an STH energy conversion efficiency of 1.2% at 331 and 10 KPa while retaining 80% of this efficiency at 91 KPa. Importantly, the photocatalyst sheet showed higher efficiency than conventional powder suspension systems and photoelectrochemical parallel cells, mainly because of suppressed overpotential. The simple and inexpensive preparation of a carbon-based photocatalyst sheet, as well as the quite high STH efficiency, enables the possibility of large-scale application of such photocatalyst panels for the practical H_2 production from water under solar light.

3.4. Water Splitting without Mediators

Further, to simplify a Z-scheme structure for water splitting, a system based on interparticle electron transfer could be developed as mediator-free Z-scheme systems. Compared with Z-scheme containing dissolved redox mediator and solid mediator systems, mediator-free Z-scheme system is very challenging and was reported very recently, e.g., (Ru/$SrTiO_3$:Rh)−($BiVO_4$) or (Ru/$SrTiO_3$:Rh)−(Ir/CoOx/Ta_3N_5) systems as illustrated in Figure 16.[94,97]

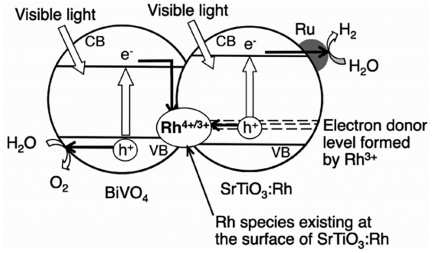

Figure 16. Scheme of photocatalytic water splitting. Reproduced with permission from ref 96. Copyright 2011 Cambridge University Press.

The reversibility of an oxidation state between Rh^{3+} and Rh^{4+} is the benefit side in this Z-scheme charge transfer process. Ru/$SrTiO_3$:Rh has two absorption onsets, one at 520 nm due to the donor level formed by Rh^{3+} to CB and the other at 580 nm assigned to the VB to acceptor level by Rh^{4+}. The 520 nm band was responsible to the H_2 evolution, while the band at 580 nm was inactive. To clarify the details of Rh oxidation reversibility, H_2 reduction under different temperatures was tested. The Rh^{3+} of $SrTiO_3$:Rh under 473 K and below was able to be reversibly oxidized, but the one reduced at 573 K was quite stable. The characterizations of the samples treated at lower temperatures were similar to the nonreduced compounds, while the high temperature appeared to significantly reduce the reversible oxidation state. It was concluded that the surface Rh ions, with reversible oxidation state, served for the electron transfer process as the role of a shuttle.[107]

In the (Ru/$SrTiO_3$:Rh)−($BiVO_4$) system, the AQY was reported to be 1.7% at 420 nm and the STH conversion efficiency reached 0.12%. To prove there was electron relay between two photocatalysts, two systems denoted as a separation system and a mixture system composed of the same materials were compared. When the two photocatalysts located at different regions in the reactor (separation system), overall water splitting was not observed because there was no physical contact or conductive/redox species in this system so that the charge transfer could not proceed through aqueous media. Water splitting only followed if the powders were mixed (mixture system), indicating the electron transfer between particles happened to realize the overall water splitting in this dual excitation system. The pH of the system influenced the activity mainly due to a zeta potential effect whereby the overall charge upon Ru/$SrTiO_3$:Rh caused aggregation, the highest degree when pH was 3.5, while $BiVO_4$ was found not to be influenced by pH value.

An (Ru/$SrTiO_3$:Rh)−(Ir/CoOx/Ta_3N_5) system applied a similar concept. Ta_3N_5 worked as an OEP and Ru/$SrTiO_3$:Rh as a HEP. Electrons from the CB of Ta_3N_5 transfer to the Rh

DOI: 10.1021/acs.chemrev.7b00286
Chem. Rev. 2018, 118, 5201−5241

Table 1. List of HEPs, OEPs, Shuttle Mediator Used for Water Splitting by a Z-Scheme Driven by Visible Light

HEP	OEP	mediators	pH	efficiency or activity	ref
$Pt/SrTiO_3$:Cr,Ta	Pt/WO_3	IO_3^-/I^-	7	AQY = 0.1% (420.7 nm)	38 (2001)
Pt/TaON	Pt/WO_3	IO_3^-/I^-	7	AQY = 0.4% (420 nm)	57 (2005)
Pt/TaON	RuO_2/TaON	IO_3^-/I^-	6	H_2: 2.8 μmol h^{-1}; O_2: 1.4 μmol h^{-1}; 300 W Xe lamp (λ > 420 nm)	48 (2008)
$Pt/ATaO_2N$ (A = Ca,Ba)	Pt/WO_3	IO_3^-/I^-	without control	AQY = 0.1% (420−440 nm)	61 (2009)
Pt/ZrO_2/TaON	Pt/WO_3	IO_3^-/I^-	5.4	AQY = 6.3% (420.5 nm)	78 (2010)
Pt/ZrO_2/TaON	Ir/TiO_2(rutile)/Ta_3N_5	IO_3^-/I^-			51 (2010)
Pt/ZrO_2/TaON	RuO_2/TaON	IO_3^-/I^-		H_2: 8 μmol h^{-1}; O_2: 3.6 μmol h^{-1} 300 W Xe lamp (λ > 420 nm)	78 (2011)
$Pt/BaZrO_3$−$BaTaO_2N$	PtO_x/WO_3	IO_3^-/I^-		STH = 0.0067%	79 (2013)
$Pt/Sm_2Ti_2S_2O_5$	TiO_2(rutile)	IO_3^-/I^-	11	H_2: 6 μmol h^{-1}; O_2: 3 μmol h^{-1} 450 W Hg lamp (λ > 300 nm)	76 (2014)
$Pt/SrTiO_3$:Cr,Ta	PtO_x/H-Cs-WO_3	IO_3^-/I^-	4	AQY = 1.5% at 420 nm	80 (2013)
$Ru/SrTiO_3$:Rh	Ru/$SrTiO_3$:Na,V	IO_3^-/I^-	without control	H_2: 0.6 μmol; O_2: 0.3 μmol for 48 h;, 300 W Xe lamp (λ > 420 nm)	81 (2012)
Pt/TiO_2(anatase):Cr,Ta	Pt/TiO_2(rutile):Cr,Ta	IO_3^-/I^-	without control	H_2: 0.38 μmol; O_2: 0.19 μmol for 180 h; LED (λ = 420 nm)	82 (2016)
NKX2677-adsorbed $Pt/H_4Nb_6O_{17}$	$IrO_2/Pt/WO_3$	I_3^-/I^-	4.5	H_2: 2.6 μmol h^{-1}; O_2: 1.3 μmol h^{-1}; 300 W Xe lamp (λ > 420 nm)	41 (2009)
MK2-adsorbed $Pt/H_4Nb_6O_{17}$	$IrO_2/Pt/WO_3$	I_3^-/I^-	4.5	H_2: 1.6 μmol h^{-1}; O_2: 0.6 μmol h^{-1}; 300 W Xe lamp (λ > 410 nm)	62 (2013)
$Pt/g\text{-}C_3N_4$	Pt/WO_3	IO_3^-/I^-	8.3	H_2: 2.1 μmol h^{-1}; O_2: 1.1 μmol h^{-1}; 300 W Xe lamp (λ > 395 nm)	35 (2014)
$Pt/MgTa_2O_{6-y}N_x$/TaON	PtO_x/WO_3	IO_3^-/I^-		AQY = 6.8% (420 nm)	83 (2015)
$Ru/SrTiO_3$:Rh	RuO_2/TiO_2:Ta,N	IO_3^-/I^-		H_2: 1.3 μmol h^{-1}; O_2: 0.5 μmol h^{-1};, 300 W Xe lamp (λ > 420 nm)	84 (2017)
$Pt/SrTiO_3$:Rh	$BiVO_4$	Fe^{3+}/Fe^{2+}	2.4	AQY = 0.3% (440 nm)	36 (2004)
$Pt/SrTiO_3$:Rh	Bi_2MoO_6	Fe^{3+}/Fe^{2+}	2.4	AQY = 0.2% (440 nm)	36 (2004)
$Pt/SrTiO_3$:Rh	WO_3	Fe^{3+}/Fe^{2+}	2.4	AQY = 0.2% (440 nm)	36 (2004)
$Ru/SrTiO_3$:Rh	$BiVO_4$	Fe^{3+}/Fe^{2+}	2.4	STH = 0.02%	85 (2008)
$Au/SrTiO_3$:Rh	WO_3	Fe^{3+}/Fe^{2+}	2.4	H_2: 140 μmol; O_2: 71 μmol for 22 h; 300 W Xe lamp (λ > 420 nm)	85 (2008)
$Ru/SrTiO_3$:Rh	WO_3	Fe^{3+}/Fe^{2+}	2.4	H_2: 416 μmol; O_2: 197 μmol for 22 h; 300 W Xe lamp (λ > 420 nm)	85 (2008)
$Ru/SrTiO_3$:Rh	$BiVO_4$	Fe^{3+}/Fe^{2+}	2.4	AQY = 4.2% (420 nm)	86 (2013)
$Ru/SrTiO_3$:Rh	$IrO_x/SrTiO_3$:Rh,Sb	Fe^{3+}/Fe^{2+}	2.4	H_2: 3 μmol h^{-1}; O_2: 1.4 μmol h^{-1}; 300 W Xe lamp (λ > 420 nm)	87 (2014)
$Pt/g\text{-}C_3N_4$	$BiVO_4$	Fe^{3+}/Fe^{2+}	3	H_2: 0.6 μmol h^{-1}; O_2: 0.3 μmol h^{-1}; 300 W Xe lamp (λ > 395 nm)	35 (2014)
$Ru/SrTiO_3$:Rh	H_2WO_4	Fe^{3+}/Fe^{2+}	2.3	H_2: 4.7 μmol h^{-1}; O_2: 2.2 μmol h^{-1}; 300 W Xe lamp (λ > 400 nm)	88 (2015)
$Ru/SrTiO_3$:Rh	Bi_4NbO_8Cl	Fe^{3+}/Fe^{2+}	2.4	H_2: 12.4 μmol h^{-1}; O_2: 6.3 μmol h^{-1}; 300 W Xe lamp (λ > 400 nm)	56 (2016)
$Ru/SrTiO_3$:Rh	$Bi_6NbWO_{14}Cl$	Fe^{3+}/Fe^{2+}	2.4	H_2: 7.0 μmol h^{-1}; O_2: 3.5 μmol h^{-1}; 300 W Xe lamp (λ > 400 nm)	89 (2016)
$Ru/SrTiO_3$:Rh	Ag(I)-substituted $Na_2W_4O_{13}$	Fe^{3+}/Fe^{2+}	2.4	H_2: 2.6 μmol h^{-1}; O_2: 1.3 μmol h^{-1}; 300 W Xe lamp (λ > 420 nm)	90 (2015)
$Ru/SrTiO_3$:Rh	WO_3	Fe^{3+}/Fe^{2+}	2.1	H_2: 5 μmol h^{-1}; O_2: 2.5 μmol h^{-1}; 300 W Xe lamp (λ > 400 nm)	91 (2016)
$Ru/SrTiO_3$:Rh	RuO_2/TiO_2:Ta,N	Fe^{3+}/Fe^{2+}	2.4	STH = 0.021%	84 (2017)
$Ru/SrTiO_3$:Rh	$BiVO_4$	$[Co(bpy)_3]^{3+/2+}$	3.8	STH = 0.06%	92 (2013)
$Ru/SrTiO_3$:Rh	$BiVO_4$	$[Co(phen)_3]^{3+/2+}$	7	H_2: 10 μmol h^{-1}; O_2: 4.8 μmol h^{-1}; 300 W Xe lamp (λ > 420 nm)	92 (2013)
$Ru/SrTiO_3$:Rh	TiO_2:Cr,Sb	$[Co(phen)_3]^{3+/2+}$	7	H_2: 1.3 μmol h^{-1}; O_2: 0.7 μmol h^{-1}; 300 W Xe lamp (λ > 420 nm)	92 (2013)

DOI: 10.1021/acs.chemrev.7b00286
Chem. Rev. 2018, 118, 5201−5241

Table 1. continued

HEP	OEP	mediators	pH	efficiency or activity	ref
$Ru/(CuGa)_{0.8}Zn_{0.4}S_2$	$BiVO_4$	$[Co(terpy)_3]^{3+/2+}$	without control	STH = 0.025%	77 (2015)
$Ru/SrTiO_3$:Rh	PtO_x/WO_3	$[SiW_{11}O_{39}Mn^{3+}(H_2O)]^{5-}$ /$[SiW_{11}O_{39}Mn^{2+}(H_2O)]^{6-}$	4.5	H_2: 1.7 μmol h^{-1}; O_2: 0.8 μmol h^{-1}; 300 W Xe lamp (λ > 400 nm)	93 (2016)
$Ru/SrTiO_3$:Rh	$BiVO_4$	none (dispersed)	3.5	AQY = 1.7% (420 nm); STH = 0.12%	94 (2009)
$Ru/SrTiO_3$:Rh	$BiVO_4$	none (composite)	7	AQY = 1.6% (420 nm)	95 (2014)
$Ru/SrTiO_3$:Rh	$AgNbO_3$	none	3.5	H_2: 1.9 μmol h^{-1}; O_2: 0.7 μmol h^{-1}; 300 W Xe lamp (λ > 420 nm)	96 (2011)
$Ru/SrTiO_3$:Rh	Bi_2MoO_6	none	3.5	H_2: 12 μmol h^{-1}; O_2: 5.2 μmol h^{-1}; 300 W Xe lamp (λ > 420 nm)	96 (2011)
$Ru/SrTiO_3$:Rh	TiO_2:Cr,Sb	none	3.5	H_2: 6.7 μmol h^{-1}; O_2: 3.3 μmol h^{-1}; 300 W Xe lamp (λ > 420 nm)	96 (2011)
$Ru/SrTiO_3$:Rh	TiO_2:Rh,Sb	none	3.5	H_2: 5.1 μmol h^{-1}; O_2: 2.2 μmol h^{-1}; 300 W Xe lamp (λ > 420 nm)	96 (2011)
$Ru/SrTiO_3$:Rh	WO_3	none	3.5	H_2: 5.7 μmol h^{-1}; O_2: 2.4 μmol h^{-1}; 300 W Xe lamp (λ > 420 nm)	96 (2011)
$Ru/SrTiO_3$:Rh	$Ir/CoO_x/Ta_3N_5$	none	3.9	STH = 0.013%	97 (2013)
$Ru/SrTiO_3$:La, Rh	$Ir/CoO_x/Ta_3N_5$	none	3.9	AQY = 1.1% (420 nm); STH = 0.037%	98 (2014)
$Ru/SrTiO_3$:Rh	$BiVO_4$	none (panel)	without control	H_2: 0.71 μmol h^{-1}; O_2: 0.27 μmol h^{-1}; 300 W Xe lamp (λ > 410 nm)	95 (2016)
$Ru/SrTiO_3$:Rh	$BiVO_4$	RGO	3.5	AQY = 1.03% (420 nm)	99 (2011)
$Pt/CuGaS_2$	TiO_2	RGO	without control	AQY = 1.3% (380 nm), STH = 0.023%	100 (2015)
$Pt/CuGaS_2$	$CoO_x/BiVO_4$	RGO	without control	H_2: 3.5 μmol h^{-1}; O_2: 1.7 μmol h^{-1}; 300 W Xe lamp (λ > 420 nm)	101 (2016)
[Rudpbpy]/$SrTiO_3$:Rh	$BiVO_4$	RGO	3.5	H_2: 8 μmol h^{-1}; O_2: 4 μmol h^{-1}; 300 W Xe lamp (λ > 420 nm)	102 (2015)
$Pt/g\text{-}C_3N_4$	WO_3	RGO	7	AQY = 0.9% (420 nm)	103 (2015)
$Pt/CuLi_{1/3}Ti_{2/3}O_2$	TiO_2	RGO	without control	STH = 0.002%	104 (2016)
$CrO_x/Ru/SrTiO_3$:La,Rh	$BiVO_4$:Mo	Au		AQY = 33% (419 nm), STH = 1.1% (288 K, 5 KPa)	98 (2016)
$RhCrO_x/LaMg_{1/3}Ta_{2/3}O_2N$	$BiVO_4$:Mo	Au		AQY = 0.07% (418 nm), STH = 0.001%	105 (2016)
$RhCrO_x/LaMg_{1/3}Ta_{2/3}O_2N$	$BiVO_4$:Mo	Au, RGO		AQY = 0.25% (418 nm), STH = 0.0035%	106 (2016)
$Ru/SrTiO_3$:La,Rh	$BiVO_4$:Mo	carbon	6.8	AQY = 26% (419 nm), STH = 1.0% (331 K, 91 KPa)	107 (2017)
$ZnRh_2O_4$	$Ag_{1-x}SbO_{3-y}$	Ag	7	AQY = 0.04% (420 nm)	108 (2014)
$Ru/SrTiO_3$:Rh	Fe−H−Cs−WO_3	VO_2^+/VO^{2+}	2.4	STH = 0.06%	109 (2017)

3d orbitals which were the donor in the HEP with the help of metallic Ir served as an electron sink. One highlight of this work lay on the CoO_x cocatalysts which suppressed the degradation of the nitride compound, thus enhancing the water oxidation activity.[97,98]

4. REDOX COUPLES IN Z-SCHEME WATER SPLITTING SYSTEMS

As reviewed in the previous sections, most Z-scheme water splitting systems rely on an effective redox couple such as IO_3^-/I^- (I_3^-/I^-) or Fe^{3+}/Fe^{2+}. Some new redox couples (e.g., metal complexes) and solid electron mediators (e.g., Au particles or reduced graphene oxides) have recently been demonstrated as well. Because of their significance in Z-scheme systems, this section concentrates on the fundamental properties of such redox couples dissolved in aqueous solution (except for the solid electron mediators), their development over the decades, and the features of Z-scheme systems associated with each redox couple. Table 1 summarizes the redox shuttles used so far in a Z-scheme system.

Redox couples used to achieve efficient Z-scheme water splitting should have the following properties: (1) an appropriate redox potential (between the reduction and oxidation potentials of water), (2) sufficient reversibility (i.e., redox cyclability) under reaction conditions (e.g., solution, pH) without deposition or precipitation, and (3) good transparency to UV and visible light. However, Z-scheme water splitting systems are difficult to construct, even if all of the intrinsic properties described above are present. This is because of the preferential occurrence of backward reactions on each photocatalyst. Reduction of Ox to Red (indicated by the broken lines in Figure 17 which is a redraw of Scheme 3 for discussion in this section), a thermodynamically advantageous backward reaction is favored over reduction of water to H_2 on a HEP. In contrast, oxidation of Red to Ox proceeds preferentially over oxidation of water to O_2 on an OEP. Furthermore, it is more

DOI: 10.1021/acs.chemrev.7b00286
Chem. Rev. 2018, 118, 5201−5241

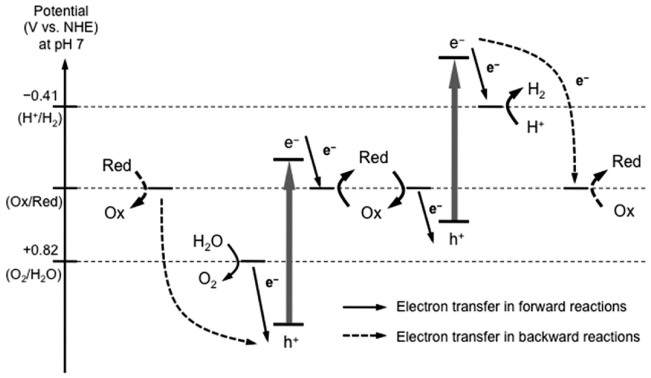

Figure 17. Forward and backward reactions in Z-scheme water splitting (potentials at pH 7).

difficult to achieve simultaneous evolution of H_2 and O_2 in Z-scheme water-splitting systems in which the two different photocatalysts coexist in an aqueous solution containing both Red and Ox because the two reactions require different ideal redox concentrations. A high concentration of Red is favorable for H_2 evolution but causes a significant backward reaction on O_2 evolution photocatalysts. These backward reactions suppress O_2 evolution. On the other hand, a high concentration of Ox, which is desirable for O_2 evolution, reduces the H_2 evolution rate. To construct a two-step water-splitting system, it is thus necessary to develop effective combination of photocatalysts and redox couples with sufficiently high selectivity for forward reactions (all solid lines in Figure 17). The key is to clarify the selectivity of redox couples based on their ad/desorption onto the relevant photocatalysts. Thus, this section will mainly discuss the adsorption properties of each redox couple on specific photocatalysts and their intrinsic properties as both are crucial to construct an efficient Z-scheme water splitting system.

4.1. Triiodide/Iodide (I_3^-/I^-) and Iodate/Iodide (IO_3^-/I^-) Redox Systems

4.1.1. Fundamental Properties of I_3^-/I^- and IO_3^-/I^-. Although iodine can possess wide range of valences from −1 to +7, the following redox cycles can proceed stably in aqueous solution:

$$I_3^- + 2e^- \rightarrow 3I^- \qquad E^\circ = +0.54\text{V}$$

$$IO_3^- + 3H_2O + 6e^- \rightarrow I^- + 6OH^- \qquad E^\circ = +0.26\text{V}$$

The former (I_3^-/I^-) is most commonly used in dye-sensitized solar cells coupled with an organic solvent such as acetonitrile. Although another redox reaction ($I_2 + 2e^- \rightarrow 2I^-$) can also occur in such organic solvent, its contribution should be negligible in aqueous solution considering the low solubility and facile ionization ($I_2 + I^- \rightarrow I_3^-$) of I_2 in water containing a certain amount of I^-. Unfortunately, only a few Z-schemes functioned for water spitting via an I_3^-/I^- redox cycle.[41,62,80] In contrast, IO_3^-/I^- redox is commonly employed in Z-scheme water splitting systems, in which various semiconductor materials, including metal oxides, oxynitrides, oxysulfides, and carbon nitrides, have been used. However, the multielectron redox nature of IO_3^-/I^- is undoubtedly a disadvantage and generally necessitates the loading of effective cocatalysts (e.g., Pt) to accelerate the six-electron process.

The redox potential of IO_3^-/I^- shifts with the change in pH in accordance with the Nernst equation, whereas that of I_3^-/I^- is independent. If the reaction occurs at pH = 7, the redox potential of IO_3^-/I^- is +0.67 V, which is reasonably close to that of I_3^-/I^- (+0.54 V). It should be noted that disproportional reactions of I_3^- can occur under basic conditions, for example:

$$3I_3^- + 6OH^- \rightarrow 8I^- + IO_3^- + 3H_2O$$

Thus, the pH of the reaction solution has a significant influence on the redox properties and thereby on the overall efficiency of Z-scheme water splitting. It appears that the redox cycle of I_3^-/I^- dominates under acidic conditions, whereas the contribution of IO_3^-/I^- increases with the increasing pH. However, it is fundamentally difficult to distinguish between the IO_3^- directly produced from I^- via the six-electron process and that produced via disproportion of the I_3^- oxidatively generated from I^-.

I_3^- exhibits photoabsorption up to ∼500 nm, whereas neither I^- nor IO_3^- shows photoabsorption of wavelengths longer than 300 nm, as shown in Figure 18. This strong, broad absorption

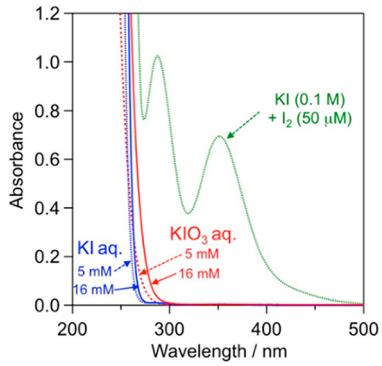

Figure 18. Absorption spectra of aqueous solutions containing I^-, IO_3^-, or I_3^- (precursors: KI, KIO_3, or I_2, without pH adjustment).

by I_3^- undoubtedly causes a significant light shielding effect that decreases the number of photons absorbed by photocatalyst particles and consequently lowers the photocatalytic efficiency. Although photochemical reactions of these anionic species rarely occur under irradiation with wavelengths longer than 300 nm, a photochemical reaction of IO_3^- can occur under irradiation with UV light with $\lambda < 300$ nm and is accompanied by O_2 release. The reaction can be expressed by the following equation:

$$IO_3^- + h\nu(\lambda < 300\text{ nm}) \rightarrow I^- + 3/2O_2$$

This reaction can occur when a combination of high-pressure Hg lamp and quartz water jacket is employed by which strong UV light centered at 254 and 265 nm is emitted. Although the quantum yield of this reaction is not high, we should use a Pyrex water jacket (or a Pyrex window cell), which blocks UV light with wavelengths shorter than 300 nm, to distinguish photocatalytic O_2 evolution from photochemical O_2 evolution.

4.1.2. Photocatalytic Water Reduction Using I^- as a Hole Acceptor. In 1996, Ohno et al. reported photocatalytic H_2 evolution using I^- as a hole scavenger on Pt-loaded TiO_2 photocatalysts.[114] As seen in Figure 19, UV irradiation ($\lambda > 300$ nm) to Pt/TiO_2 (rutile, TIO-5) suspended in an aqueous KI solution (1 M, pH 2.4) resulted in simultaneous, stoichiometric (1:1) generation of H_2 and I_3^-. The reaction was readily terminated, most likely due to a backward reaction (i.e., reduction of I_3^-). The authors also revealed that pH had a

DOI: 10.1021/acs.chemrev.7b00286
Chem. Rev. 2018, 118, 5201−5241

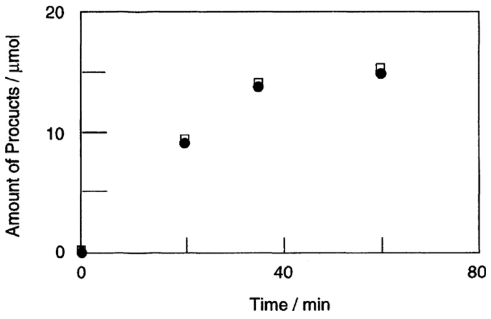

Figure 19. Time courses of the hydrogen evolution (squares) and the conversion of iodide ion into triiodide ions (circles) as the result of the photocatalytic reactions using the Pt-loaded TiO_2 (TIO-5) particles. The reaction was carried out in the cell containing the photocatalyst (200 mg) and 1.0 mol dm^{-3} aqueous solution of potassium iodide (50 mL) at pH 2.4. Reproduced with permission from ref 114. Copyright 1996 The Chemical Society of Japan.

significant influence on activity. As seen in Figure 20, the initial reaction rates decreased drastically when the pH increased to ~4.

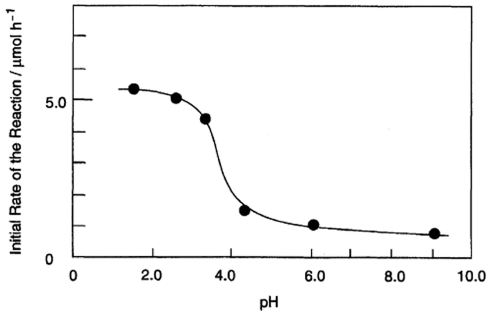

Figure 20. pH dependence of the initial rate of the photocatalytic reaction using Pt-loaded TiO_2 (Kanto Chemicals) particles as the photocatalyst. The reaction rates were determined from the amounts of triiodide ions generated during the photoirradiation for 1 h. The photocatalyst was heat-treated at 500 °C for 1 h. Reproduced with permission from ref 114. Copyright 1996 The Chemical Society of Japan.

This remarkable change in activity was explained by the change in the surface charge of TiO_2 from positive to negative near the isoelectric point (~6). Indeed, I^- adsorption on the TiO_2 surface in aqueous solutions decreased significantly due to the increased pH, undoubtedly due to electrical repulsion between the negatively charged surface and I^- anions.[114] However, the authors might underestimated the H_2 evolution activity of these Pt/TiO_2 photocatalysts under basic conditions because the activity was mainly evaluated based on I_3^- generation rather than H_2 evolution (see Figure 20).

In 2001, Abe et al. revealed that Pt-loaded TiO_2 photocatalysts efficiently produced H_2 and generate IO_3^- from basic aqueous solutions containing I^-.[38,115] IO_3^- was the dominant product at pH > 9, whereas I_3^- was the main product when the pH was below 3. Mixtures were generated when the pH was between 3 and 9. The initial H_2 evolution rates from NaI (aq) on Pt/TiO_2 were almost same regardless of the pH (3 or 11) (Figure 21). The rates decreased gradually in both cases, undoubtedly due to backward reactions (i.e., reduction of I_3^- and/or IO_3^-). Fast decrease of H_2 evolution in the basic solution strongly suggested that the IO_3^- anions were reduced

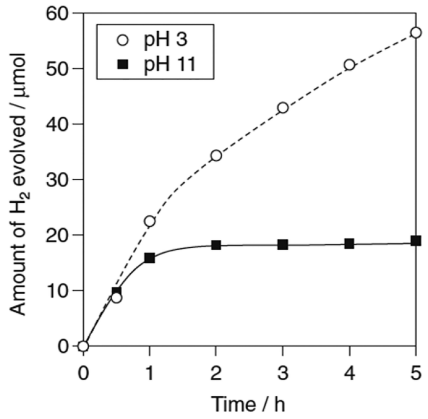

Figure 21. Time course of photocatalytic evolution of H_2 using Pt(0.5 wt %)TiO_2 (anatase, Ishihara ST-01) photocatalyst suspended in 0.1 M of NaI aqueous solution under UV light irradiation (λ > 300 nm, 400 W Hg lamp). Reproduced with permission from ref 11. Copyright 2011 The Chemical Society of Japan.

more efficiently than I_3^-, which was confirmed via ion chromatography instead of UV−vis. absorption. The amount of IO_3^- anions measured was smaller than the stoichiometric value derived from H_2 evolution amount, which was likely due to the facile adsorption of IO_3^- anions on the photocatalyst surfaces. In addition, the study showed that anatase TiO_2 particles could generate H_2 from NaI (aq) much more efficiently than rutile TiO_2 particles under basic conditions.

4.1.3. Photocatalytic Water Oxidation Using IO_3^- as an Electron Acceptor. The construction of Z-scheme water splitting systems using I_3^-/I^- redox reactions has likely been disrupted by the low reactivity of I_3^- as an electron acceptor on conventional OEP. In contrast, IO_3^- as an electron acceptor enabled efficient and selective O_2 evolution on some photocatalysts such as rutile TiO_2.[11,115] Figure 22 shows, for example,

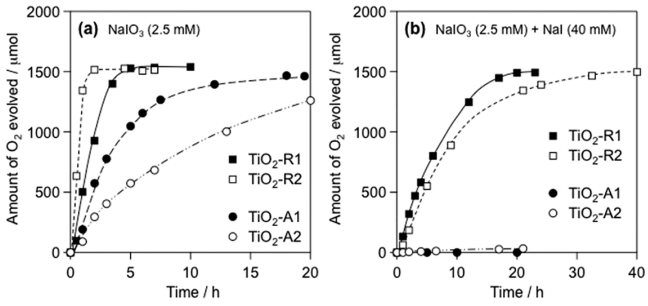

Figure 22. Time course of photocatalytic O_2 evolution over TiO_2 photocatalysts suspended in aqueous solution (400 mL, pH 11 adjusted by NaOH) containing (a)1 mmol of $NaIO_3$ and (b) 1 mmol of $NaIO_3$ and 16 mmol of NaI. Reproduced with permission from ref 11. Copyright 2011 The Chemical Society of Japan.

the time sequence of O_2 evolution on four different TiO_2 samples (A, anatase; R, rutile) in an aqueous $NaIO_3$ solution under UV light irradiation (λ > 300 nm). When the reaction took place in the presence of IO_3^-, both the rutile (R1 and R2) and anatase TiO_2 samples (A1 and A2) generated O_2. However, the rutile samples showed a higher rate of O_2 evolution than their anatase counterparts. The AQY on rutile TiO_2 was ~10% at 350 nm. Interestingly, O_2 evolution over rutile TiO_2 photocatalysts proceeded at an almost constant rate and continued until the total amount of O_2 reached 1.5 mmol

DOI: 10.1021/acs.chemrev.7b00286
Chem. Rev. 2018, 118, 5201−5241

in the absence of NaI (Figure 22a). This occurred even when a considerable amount of I^- was present (Figure 22b). An O_2 amount of 1.5 mmol was in line with the amount stoichiometrically anticipated from the IO_3^- (1 mmol) added to the solution before irradiation. The rate of O_2 evolution over anatase TiO_2 samples gradually decreased with time. This difference between anatase and rutile was observed more clearly when the reaction took place with excess I^-, where O_2 evolution was completely suppressed on both of the anatase TiO_2 samples as shown in Figure 22b. This phenomenon on rutile TiO_2 was very interesting because the thermodynamically less favorable water oxidation proceeds preferentially even in the presence of I^-. In contrast, such selective water oxidation did not take place on anatase TiO_2 samples.

The difference was due to adsorption characteristics regarding of IO_3^- and I^- anions on TiO_2 samples. IO_3^- ions could readily adsorb on the surfaces of rutile TiO_2 particles (Figure 23c,d), whereas I^- ions could not. Thus, one could

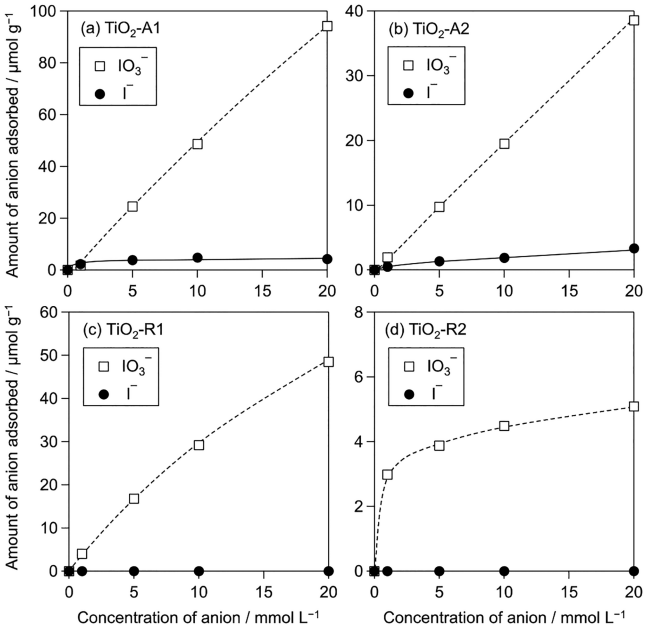

Figure 23. Adsorption properties of iodate (IO_3^-) and iodide (I^-) anions on various TiO_2 powders. Reproduced with permission from ref 11. Copyright 2011 The Chemical Society of Japan.

expect IO_3^- anions to readily adsorb onto rutile TiO_2 surfaces, even at low concentrations, thereby reacting efficiently with photoexcited electrons whereas the produced I^- could not be oxidized easily on rutile TiO_2 surface, leading to efficient water oxidation. In contrast, both IO_3^- and I^- ions relatively strongly adsorbed onto the surface of anatase TiO_2 (Figure 23a,b), enhancing the unexpected back reaction (i.e., oxidation of I^-).

Such interesting adsorption of IO_3^-/I^- couple and selective water oxidation were also observed on visible light-responsive WO_3 photocatalysts with PtO_x species as cocatalysts for IO_3^- reduction.[11,40,59,79,116] As shown in Figure 24, O_2 generation from $NaIO_3$ (aq) proceeded consistently on a PtO_x-loaded WO_3 sample under visible light irradiation until it reached stoichiometric value. Such steady, stoichiometric O_2 evolution was also observed even in the presence of a considerable amount of I^-, although it decreased the O_2 evolution rate appreciably. On the other hand, O_2 evolution from PtO_x-loaded $BiVO_4$, one of the best OEP, was completely suppressed by the

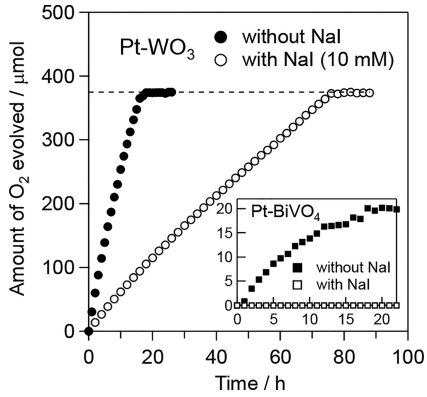

Figure 24. Time course of photocatalytic O_2 evolution over Pt (0.5 wt %)/WO_3 and Pt (0.5 wt %)/$BiVO_4$ (inset) suspended in aqueous solution (250 mL, pH 6.5 without adjustment) containing (a) 0.25 mmol of $NaIO_3$ and (b) 0.25 mmol of $NaIO_3$ and 10 mmol of NaI. Reproduced with permission from ref 11. Copyright 2011 The Chemical Society of Japan.

addition of I^- (see inset of Figure 24). Such difference could also be explained by the similarly selective adsorption of IO_3^-/I^- as observed on rutile and anatase TiO_2.[11]

4.1.4. IO_3^-/I^- Redox-Based Z-Scheme Water Splitting.

On the basis of the above findings on selective water oxidation, Z-scheme water splitting under UV light was achieved for the first time by using Pt-loaded anatase TiO_2 as the HEP alongside rutile TiO_2 as OEP in the presence of an IO_3^-/I^- redox mediator.[11,40,115] Simultaneous evolution of H_2 and O_2 in a stoichiometric ratio was observed when a combination of Pt/anatase TiO_2 and rutile TiO_2 was used but not observed on one of these photocatalysts or in other combinations, indicating that overall water splitting proceeded via a two-step photoexcitation mechanism combined with a redox cycle between anions IO_3^- and I^-. As proved in the Figure 23, different adsorption behavior of IO_3^- to I^- on rutile TiO_2 resulted in a very low IO_3^- concentration in solution, effectively suppressing the undesirable IO_3^- reduction (i.e., backward reaction) on the Pt/anatase TiO_2 catalyst, thus producing a higher H_2 evolution rate. Thus the key to achieve water splitting is that preferential oxidation of I^- to IO_3^- over the HEP and preferential oxidation of water to O_2 over the OEP must occur simultaneously.

In such IO_3^-/I^- redox based Z-scheme systems, the pH of the solution significantly affected the total efficiency.[11,40,115] Figure 25a shows, for example, the rates of gas evolution over a mixture of Pt/anarase-TiO_2 with bare rutile-TiO_2, suspended in 0.1 M NaI aqueous solutions with different pH values. The rates increased substantially as the pH increased from 3 to 9 and then decreased when the pH was above 11. The O_2 evolution was negligible at pH 3 because the main oxidation product produced on Pt/anatase-TiO_2 was I_3^-, which is not an efficient electron acceptor for O_2 evolution over bare rutile-TiO_2. Although O_2 evolution was observed after an induction period at pH 5 to 7, the quantity produced was less than stoichiometric amount with respect to H_2 evolved.[11] This was certainly due to the accumulation of I_3^- in the solution. The induction period suggested that some IO_3^- anions could be produced via the disproportional reaction of I_3^- in the aqueous solution during the photocatalytic reaction as mentioned in the section 4.1.1. The accumulation of I_3^- also caused loss of light because of strong light absorption by the anion. In basic solutions (pH ≥ 9), the stoichiometric evolution of H_2 and O_2

DOI: 10.1021/acs.chemrev.7b00286
Chem. Rev. 2018, 118, 5201−5241

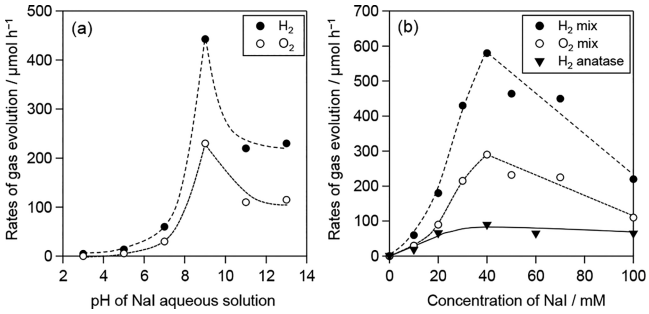

Figure 25. (a) Dependence of rates of gas evolution over a mixture of Pt-TiO_2-A1 and bare TiO_2-R2 photocatalysts upon the pH value of NaI solution (NaI: 0.1 M). (b) Dependence of rates of gas evolution over a mixture of Pt-TiO_2-A1 and bare TiO_2-R2 photocatalysts upon the concentration of NaI aqueous solution (pH 11). Reproduced with permission from ref 11. Copyright 2011 The Chemical Society of Japan.

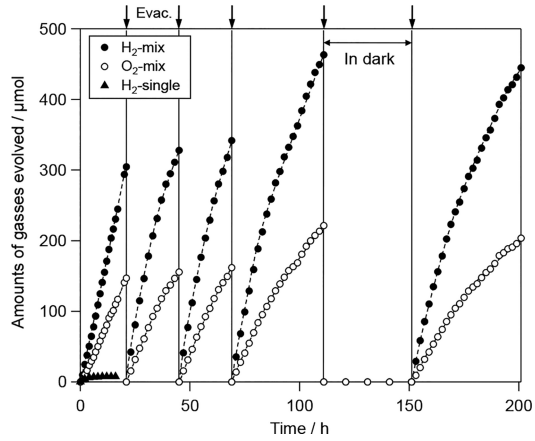

Figure 26. Time course of photocatalytic evolution of H_2 and O_2 using a mixture of Pt (0.3 wt %)/$SrTiO_3$ (Cr, Ta 4 mol % doped) and Pt (0.5 wt %)/WO_3 photocatalysts suspended in 5 mM of NaI aqueous solution (pH 6.5 without adjustment) under visible light irradiation (λ > 420 nm). Triangles indicate H_2 evolution using Pt/$SrTiO_3$:Cr/Ta alone. Reproduced with permission from ref 11. Copyright 2011 The Chemical Society of Japan.

was observed without induction period. Thus, conditions above pH of 9 resulted into high overall water splitting efficiencies due to efficient redox cycling between IO_3^- and I^- at these conditions. The concentration of the redox mediator also significantly affected the overall efficiency, mainly due to the occurrence of backward reactions on each photocatalyst.

Figure 25b shows, for example, the rates of gas evolution over the above mixture suspended in aqueous solutions with different NaI concentrations. The rates increased with increasing NaI concentration up to 40 mM, undoubtedly due to the enhanced reaction on HEP (Pt/anarase-TiO_2) with electron donor (I^-), as also supported by the increased rate of H_2 evolution on HEP in these concentrations (closed triangles). However, the higher concentration of I^- resulted in the decrease in the rate of O_2 evolution over OEP (rutile TiO_2) due to the increased rate of the competitive oxidation of I^-.

A visible light-driven water-splitting system was then constructed. $SrTiO_3$ co-doped with Cr and Ta ($SrTiO_3$:Cr/Ta) was found to be an active photocatalyst for both H_2 and IO_3^- production from an aqueous NaI solution under visible light irradiation (λ > 410 nm).[11,40,115] The photocatalyst was found to have a reasonably high activity for H_2 evolution from water under visible light irradiation in the presence of methanol as a sacrificial electron donor.[117] Although the rate of H_2 evolution over the Pt-loaded $SrTiO_3$:Cr/Ta photocatalyst decreased remarkably with irradiation time due to the backward reaction (reduction of IO_3^- to I^- by photoexcited electrons), using both Pt-loaded $SrTiO_3$:Cr/Ta and Pt-loaded WO_3 photocatalysts for the first time resulted in simultaneous evolution of H_2 and O_2 (initial H_2 rate, 16 μmol h^{-1}; initial O_2 rate, 8 μmol h^{-1}) from an aqueous NaI solution under visible light irradiation (λ > 410 nm), as shown in Figure 26. It represents one of the most important technical breakthroughs in the field of photocatalytic water splitting. Since this demonstration, various photocatalyst materials, including metal oxides, oxynitrides, nitrides, oxysulfides, and carbon nitrides, have been proved to form effective H_2-evolving photocatalyst couples with WO_3 for Z-scheme water splitting under visible light.

4.1.5. Issues and Future, Prospective IO_3^-/I^- Redox-Based Z-Scheme Systems. Although several IO_3^-/I^- redox-based Z-scheme systems have been demonstrated thus far, there are significant issues that should be addressed in order to improve total efficiency. The first is the rapid backward reduction of IO_3^- on a Pt cocatalyst loaded HEP, which significantly lowers the efficiency of H_2 evolution. The second is the requirement of a more efficient cocatalyst (e.g., Pt) for reduction of IO_3^- on an OEP due to the nature of six-electron reduction process. An in-depth understanding of the adsorptivity and reactivity of IO_3^-/I^- will provide clue to help control the selectivity of each step and developing new cocatalysts that exhibit high selectivity for forward reactions. The third issue is the limited choice of OEP that can function under visible light other than WO_3. Although some metal (oxy)nitirdes such as TaON and Ta_3N_5 can be used as OEP after appropriate surface modifications,[51] their long-term stabilities are insufficient due to the occurrence of self-oxidative deactivation. As shown above, the efficiencies of IO_3^-/I^- redox-based Z-scheme systems are significantly affected by the pH of the solution. Basic conditions (pH ~ 9) resulted in the highest efficiencies over a combination of Pt/anatase TiO_2 and rutile TiO_2 under UV light. This is due to the efficient IO_3^-/I^- redox cycle and absence of unfavorable intermediates such as I_3^-. Unfortunately, such conditions cannot be applied to visible light-responsive systems that use WO_3 as an OEP due to the instability of WO_3 particles in basic solutions. Therefore, the development of a visible light-driven photocatalyst with good durability in basic solutions and good selectivity for water oxidation is strongly desired in order to improve the overall efficiency of IO_3^-/I^- redox-based Z-scheme water splitting under visible light irradiation.

4.2. Fe (Fe^{3+}/Fe^{2+}) Redox System

4.2.1. Fundamental Properties of Fe^{3+}/Fe^{2+}. The redox cycle between trivalent and divalent Fe ions ($Fe^{3+} + e^- \rightarrow Fe^{2+}$; E° = +0.77 V) has been employed as a useful redox couple since the early stages of research on water splitting. In particular, the oxidant (Fe^{3+}) has been used as an effective electron acceptor for photocatalytic water oxidation (half reaction). The most advantageous characteristic of the Fe^{3+}/Fe^{2+} redox system, especially compared to the above IO_3^-/I^- redox system, is the facile reduction of Fe^{3+} to Fe^{2+} due to an one-electron transfer process, which eliminates the need for a

DOI: 10.1021/acs.chemrev.7b00286
Chem. Rev. 2018, 118, 5201−5241

cocatalyst (e.g., RuO_2, Pt, and PtO_x). Indeed, typical O_2-evolving photocatalysts such as WO_3 and $BiVO_4$ can efficiently generate O_2 from aqueous Fe^{3+} solutions, even without any cocatalysts.[2,19,60,90,118] The loading of an appropriate cocatalyst such as RuO_2 enhanced O_2 evolution in some cases.[19,119] Another advantage is the thermodynamic stability of the reduced Fe^{2+} due to the significantly negative potential of further Fe^{2+} reduction ($Fe^{2+} + 2e^- \rightarrow Fe$; $E^\circ = -0.44$ V). On the other hand, Fe^{3+}/Fe^{2+} redox has one disadvantage related to their chemical stability in high pH value solution. The Fe^{3+}/Fe^{2+} redox cycle is stable and reversible only at pH < 2.5, while the prompt precipitation of $Fe(OH)_3$ from Fe^{3+} cationic hydrolysis takes place at higher pH when water is used as solvent. This irreversibility of Fe^{3+}/Fe^{2+} redox consequently limits of the option to photocatalysts who have sufficient stability under highly acidic conditions.

With regard to photoabsorption of the Fe^{3+}/Fe^{2+} redox couple itself, careful attention must be paid to aqueous solutions containing Fe^{2+} species during UV light irradiation. As shown in Figure 27, aqueous solutions of $FeCl_2$ exhibit

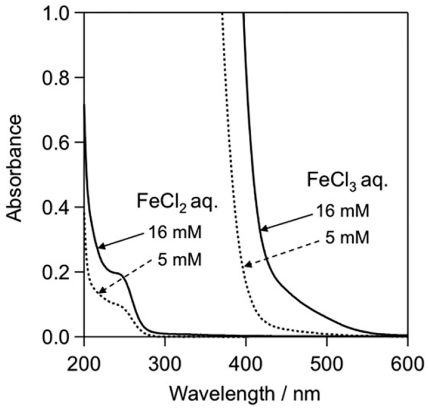

Figure 27. Absorption spectra of aqueous solutions containing Fe cation (precursor, $FeCl_3 \cdot 6H_2O$ or $FeCl_2 \cdot 4H_2O$, pH 2.1, adjusted by HCl).

obvious absorption of wavelengths shorter than ~280 nm. Aqueous $FeCl_3$ solutions exhibit stronger absorption across the UV spectrum and even in the visible light region up to ~550 nm. This is especially noticeable when the concentration is high (e.g., 16 mM). It has been reported that photochemical oxidation of Fe^{2+} to Fe^{3+} proceeded under irradiation with UV light with wavelengths <300 nm, accompanied by reduction of water to H_2 as indicated by the following equation

$$4H^+ + 4Fe^{2+} + h\nu(\lambda < 300\text{nm}) \rightarrow 2H_2 + 4Fe^{3+}$$

This photochemical reaction readily occurs if one uses a combination of high-pressure mercury (Hg) lamp and quartz water jacket,[120] leading to a misunderstanding that H_2 gas is generated on a HEP. To avoid this confusing photochemical reaction, it is suggested to use a Pyrex water jacket (or at least a Pyrex window) to block UV light with wavelengths shorter than 300 nm. In contrast, such photochemical reaction rarely occurs with Fe^{3+} in spite of its strong, broad photoabsorption up to the visible light region, while such strong absorption up to the visible light region will involve a significant light shielding effect, lowering the photocatalytic efficiency. Thus, the Fe^{3+}/Fe^{2+} redox concentration must be carefully optimized during development of a Z-scheme system, as is the case with IO_3^-/I^-.

4.2.2. Photocatalytic Water Oxidation Using Fe^{3+} as an Electron Acceptor. Nevertheless, the Fe^{3+}/Fe^{2+} redox system, especially with Fe^{3+} as an electron acceptor, has been employed extensively. This is most likely due to its easy handling, understood reaction mechanism and easy quantitative determination of product (i.e., Fe^{2+}) concentrations. In 1962, Krasnovskii et al. presented a brief description of water oxidation with a Fe^{3+} electron acceptor using WO_3 particles as a photocatalyst.[118,121] Unfortunately, this pioneering work attracted little attention for long time. In 1982, Dawent et al. reported a valuable study on photocatalytic O_2 evolution from aqueous $FeCl_3$ solutions using unmodified or cocatalyst-loaded WO_3 particles under visible light (λ > 400 nm).[119] In this detailed study, a reasonable correlation between the O_2 evolution rate and the WO_3 photoabsorption spectrum was confirmed using a high-radiance monochromator. The typical quantum yield of O_2 evolution was estimated to be ~0.3% at 405 nm. Furthermore, the significant influence of redox concentration was revealed. As shown in Figure 28, the rate

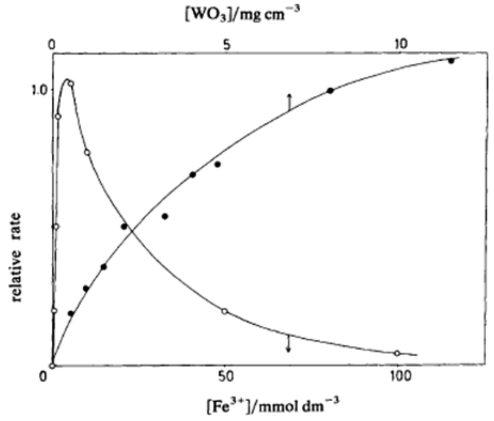

Figure 28. Initial rate of oxygen production as a function of the Fe^{3+} (open circles) and WO_3 (closed circles). All solutions were in 0.5 × 10^{-2} mol dm^{-3} H_2SO_4 for the variation of [Fe^{3+}], 7.5 mg cm^{-3} of WO_3 was used, and for the variation in [WO_3], 10^{-2} mol dm^{-3} of Fe^{3+} was present. Reproduced with permission from ref 119. Copyright 1982 The Royal Society of Chemistry.

of photocatalytic O_2 evolution on WO_3 increased dramatically with the initial Fe^{3+} concentration in aqueous solutions of up to 5 mM. This was attributed to the enhanced rate of consumption of photoexcited electrons by Fe^{3+}. The rate decreased significantly as the concentration increased beyond 5 mM. This decreased O_2 evolution could be justified via light shielding by Fe^{3+}, as explained above. However, the authors did not identify the origin at that time (they proposed several possibilities, including light shielding). On the other hand, increasing the Fe^{2+} concentration, even up to 1 mM as seen in Figure 29, significantly decreased the rate of O_2 evolution, most likely due to the preferential occurrence of backward oxidation of Fe^{2+} by photogenerated holes ($Fe^{2+} + h^+ \rightarrow Fe^{3+}$) in place of the oxidation of water. Such a significant backward reaction, i.e., reoxidation of Fe^{2+} by holes, was observed with WO_3 as well as with other visible light-responsive photocatalysts such as $BiVO_4$.[86] Therefore, it is one of the biggest issues that must be addressed to improve the overall efficiency of water splitting.

4.2.3. Unique Adsorption Properties of Fe^{3+}/Fe^{2+} that Enable Highly Selective Water Oxidation. Although recent progress on strategies for addressing backward reactions will be

DOI: 10.1021/acs.chemrev.7b00286
Chem. Rev. 2018, 118, 5201−5241

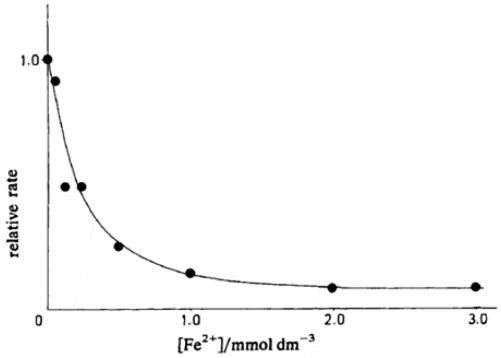

Figure 29. Effect of Fe^{2+} concentration on the initial rate of oxygen formation over WO_3 photocatalyst. Reproduced with permission from ref 119. Copyright 1982 The Royal Society of Chemistry.

reviewed in the next section (Section 5), Ohno et al. have performed a critical study that has shed light upon how to address this issue. Their study revealed the unique adsorption properties of the Fe^{3+}/Fe^{2+} redox system on specific photocatalysts such as rutile TiO_2. They demonstrated that the photocatalytic oxidation of water with a Fe^{3+} electron acceptor proceeded with reasonably good quantum yield (~9% at 365 nm) on rutile TiO_2 particles. More importantly, O_2 evolution continued until almost all of the Fe^{3+} ions in the solution were reduced into Fe^{2+} ions.[122,123] As seen in Figure 30, rutile TiO_2

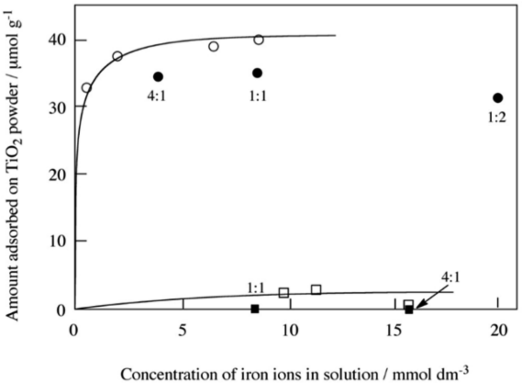

Figure 30. Adsorption isotherms of Fe^{3+} and Fe^{2+} ions on TiO_2 powder at 25 °C: for Fe^{3+} ions (open circles) and for Fe^{2+} ions (open squares). When both Fe^{2+} and Fe^{3+} ions were added to the solution, their adsorptivity was affected each other: for Fe^{3+} ions (closed circles) and for Fe^{2+} ions (closed squares). The molar ratio of Fe^{3+} ions: Fe^{2+} ions are described in the figure. Measurements were performed using TiO_2 (JCR TIO-5) powder. Reproduced with permission and addition of the correction in the horizontal axis from ref 122. Copyright 1997 American Chemical Society.

particles preferentially adsorb Fe^{3+} ions. Particularly, Fe^{3+} ions adsorb exclusively when both Fe^{3+} and Fe^{2+} ions are present. Thus, the photoexcited electrons generated on rutile TiO_2 particles could react efficiently with significant amounts of Fe^{3+} adsorbed on the surface. Simultaneously, photogenerated holes preferentially oxidized water to produce O_2 even in the presence of Fe^{2+}, in spite of a thermodynamic disadvantage, because of the negligible adsorption of Fe^{2+} ions on the rutile surface. Although such unique Fe^{3+}/Fe^{2+} redox couple adsorption properties were found only in a few specific photocatalysts, such as rutile TiO_2, this pioneering work provided better understanding of photocatalytic reactions with redox couples, as well as strong suggestion on how to address these backward reactions to improve total efficiency.

4.2.4. Half Z-Scheme Coupled with Photochemical or Electrochemical Reaction for Water Splitting. As described above, photocatalytic O_2 evolution using Fe^{3+} electron acceptor has been studied extensively since the 1980s and demonstrated on several photocatalysts, including some that were responsive to visible light such as WO_3. However, reliable overall water splitting (i.e., simultaneous generation of H_2 and O_2) through Fe^{3+}/Fe^{2+} redox-based Z-scheme photocatalysis was not achieved until 2004. This was undoubtedly due to the lack of effective H_2-evolving photocatalysts that could reduce water to H_2 during oxidation of Fe^{2+} ions to Fe^{3+}, even under UV light irradiation, despite extensive exploration of the subject.

Thus, several complex systems were developed to demonstrate overall water splitting with a Fe^{3+}/Fe^{2+} redox system. For example, Sayama et al. demonstrated a Z-scheme type water splitting system in 1997 by taking advantage of the above-mentioned "photochemical" H_2 evolution from aqueous Fe^{2+} ions (see Figure 31).[19] In this system, O_2 evolution proceeded

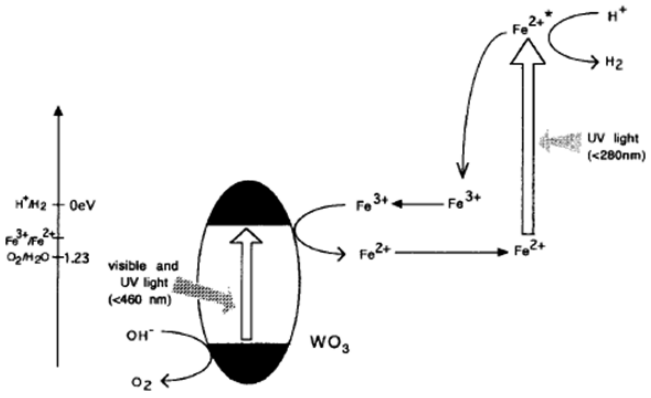

Figure 31. Presumed reaction mechanism of the photocatalytic decomposition of water using the Fe^{3+}/Fe^{2+} redox system. Reproduced with permission from ref 19. Copyright 1997 Elsevier.

"photocatalytically" on RuO_2-loaded WO_3 particles suspended in an aqueous solution containing a Fe^{3+} acceptor. This was accompanied by the generation of Fe^{2+}. H_2 evolution occurred "photochemically" via the absorption of photons by the aqueous Fe^{2+} ions with wavelengths shorter than 280 nm, resulting in the simultaneous, stoichiometric evolution of H_2 and O_2.[23] Although this system seems distant from artificial photosynthesis because the natural sunlight on Earth's surface contains little short-wavelength UV (λ < 280 nm), the authors demonstrated the interesting concept of achieving separate production of H_2 and O_2 by applying alternating photoirradiation, as shown in Figure 32. The first run was carried out via irradiation of $FeCl_2$ (aq) with short wavelength UV, without a photocatalyst, which generated only H_2. The second run was performed by using a Pyrex jacket to irradiate the system with UV wavelengths longer than 300 nm, in the presence of a WO_3 photocatalyst, resulting only in generation of O_2. Thus, alternating photoirradiation with different wavelengths of UV light through two different water jackets demonstrates alternating production of H_2 and O_2.

Another example of a complex Fe^{3+}/Fe^{2+} redox system was demonstrated by Ohno et al.[124] Two kinds of rutile TiO_2 photocatalysts were suspended in aqueous solution, and two

DOI: 10.1021/acs.chemrev.7b00286
Chem. Rev. 2018, 118, 5201−5241

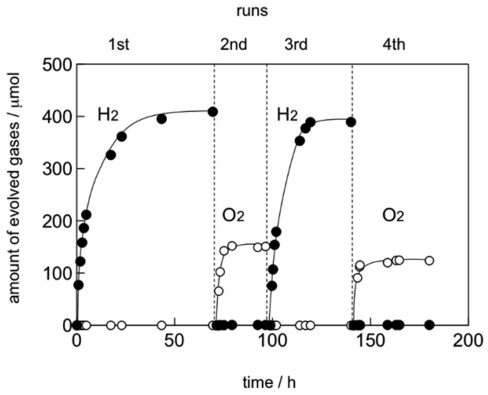

Figure 32. Alternative evolution of H_2 and O_2 gases using a RuO_2–WO_3 catalyst and Fe^{3+}/Fe^{2+} redox system. Run 1: mixture of $FeSO_4$ (1 mmol) and H_2SO_4 (10 mmol) and distilled water (350 mL) was irradiated through a quartz glass filter (λ > 200 nm). Run 2: RuO_2(1 wt %)–WO_3 catalyst (1 g) was added to the solution after run 1 and light was irradiated through a Pyrex glass filter (λ > 300 nm). Run 3: catalyst powder was filtered from the solution (or sedimented by stop stirring) after run 2, and then the solution was irradiated again through a quartz glass filter (λ > 200 nm). Run 4: same as run 2. Reproduced with permission from ref 19. Copyright 1997 Elsevier.

types of redox couples (Fe^{3+}/Fe^{2+} and Br_2/Br^-) in each solution were "electrochemically" coupled via two Pt electrodes and an external circuit (Figure 33a). In compartment I, a Pt-loaded TiO_2 photocatalyst reduces water (H^+) to H_2 and oxidizes Br^- to Br_2 (and/or probably Br_3^-) under UV light irradiation. Another bare TiO_2 photocatalyst is suspended in compartment II to reduce Fe^{3+} to Fe^{2+} and oxidize water to O_2 under UV light. Simultaneously, the Fe^{2+} ions accumulated at the electrodes in compartment II were "electrochemically" oxidized back to Fe^{3+} by the stronger oxidation potential of Br_2 (or Br_3^-), which was reduced back to Br^- (see the energy diagram shown in Figure 33b). Consequently, water could continuously split into H_2 and O_2 under photoirradiation. This was accompanied by the transportation of H^+ through a Nafion membrane. Although this system is more complicated than other Z-scheme systems consisting of suspension of two different photocatalysts and one redox couple in each single-compartment cell, conditions such as concentrations of reagents or quantities of photocatalyst powders could be independently optimized in each compartment and thus might allow us to improve the total water splitting efficiency in some cases.

4.2.5. Fe^{3+}/Fe^{2+} Redox-Based Z-Scheme Water Splitting. In 2004, a simple Z-scheme water splitting system consisting of two different photocatalysts and a Fe^{3+}/Fe^{2+} redox couple was demonstrated by Kudo et al. The system used $SrTiO_3$ doped with Rh cations ($SrTiO_3$:Rh) as the HEP.[36] Kudo et al. explored new class of visible light-responsive photocatalysts based on the doping of cations such as Cr^{3+} or Rh^{3+} into a conventional $SrTiO_3$ semiconductor and found that Pt-loaded $SrTiO_3$:Rh photocatalysts showed reasonable activity for H_2 evolution from water as well as simultaneous oxidation of Fe^{2+} ions via harvesting of visible light with wavelengths of up to ~550 nm.[16] They then combined the Pt/$SrTiO_3$:Rh with $BiVO_4$, an OEP that was also developed by the same group in the presence of a Fe^{3+}/Fe^{2+} redox system.[3,36,85,86,96,125−127] One important feature of this system is its unexpectedly high selectivity for H_2 evolution on the Pt/$SrTiO_3$:Rh photocatalyst, even in the presence of Fe^{3+} ions.

As shown in Figure 34a, excess O_2 was produced during the initial stage of the first run in 2 mM $FeCl_3$(aq); due to the more efficient reaction with the Fe^{3+} acceptor on $BiVO_4$, the rate of O_2 generation gradually decreased and became stoichiometric with H_2 evolution. H_2 and O_2 were produced in a stoichiometric ratio (2:1) from the start of the second run after evacuation of the gas phase. The reaction in 2 mM $FeCl_2$(aq) also exhibited nearly stoichiometric evolution of H_2 and O_2 at the end of the second run, while H_2 evolution predominated during the initial stage of the first run (see Figure 34b). This was attributed to a more efficient reaction on Pt/$SrTiO_3$:Rh with a higher concentration of the Fe^{2+} donor. In both cases, Fe^{3+} and Fe^{2+} ions reaching a steady state have

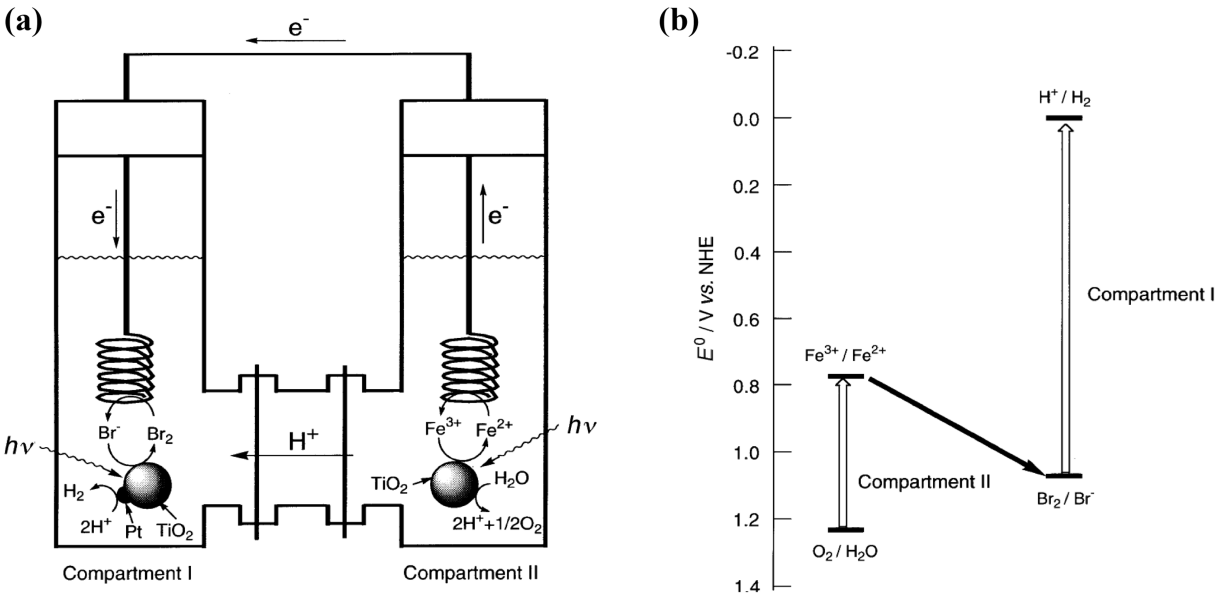

Figure 33. (a) Schematics of the photocatalytic reaction cell for splitting water and (b) energy diagram of splitting water by combined photocatalytic reactions. Reproduced with permission from ref 124. Copyright 1969 The Royal Society of Chemistry.

DOI: 10.1021/acs.chemrev.7b00286
Chem. Rev. 2018, 118, 5201−5241

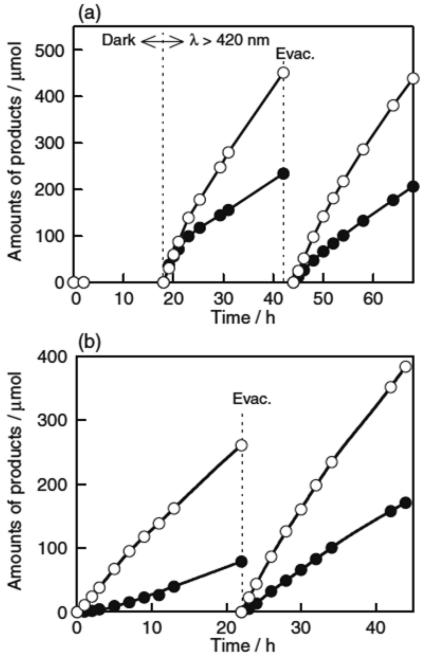

Figure 34. Photocatalytic overall water splitting using (Pt (0.5 wt %)/$SrTiO_3$:Rh (1%)−($BiVO_4$) system under visible light irradiation in an aqueous solution of (a) $FeCl_3$ (2 mmol L^{-1}) and (b) $FeCl_2$ (2 mmol L^{-1}). Open marks, H_2; closed marks, O_2. Catalyst, 0.1 g for each component; reactant solution, 120 mL, pH 2.4; light source, 300 W Xe-arc lamp with a cutoff filter (λ > 420 nm); cell, top irradiation cell with a Pyrex window. Reproduced with permission from ref 126. Copyright 2007 The Chemical Society of Japan.

concentrations of ∼1.5 and 0.5 mM, respectively, indicating that both H_2 and O_2 could evolve even in the copresence of relatively high concentrations of the reductant (Fe^{2+}) and the oxidant (Fe^{3+}).

Careful analysis of the two redox couples, one can find that H_2 production in IO_3^-/I^- redox system was significantly suppressed by the coexistence of a small amount of IO_3^- due to a preference for reduction of IO_3^- anions by photoexcited electrons,[11,40,116] whereas H_2 evolution in Fe^{3+}/Fe^{2+} redox system was enhanced by an increase in the Fe^{3+} concentration when concentration of $FeCl_2$ was fixed at 2 mM (see Table 2). Enhanced H_2 production with increased Fe^{3+} concentration is unusual in view of the electron acceptability of Fe^{3+}. However, the results of reactions in various aqueous solutions containing Fe^{3+} suggest that the adsorption of $[Fe(SO_4)(H_2O)_5]^+$ and/or $[Fe(OH)(H_2O)_5]^{2+}$ on the Pt surface efficiently suppresses both the undesirable backward reactions on the Pt surface, such as water formation from H_2 and O_2 and the reduction of Fe^{3+} by H_2 (see Figure 35). The authors did not mention the possibility of suppressing another key backward reaction, the photocatalytic reduction of Fe^{3+} by photoexcited electrons on Pt. However, the presence of highly selective H_2 evolution implies that this backward reaction is also suppressed. The rate of O_2 evolution over the $BiVO_4$ photocatalyst decreased as the Fe^{2+} concentration increased due to backward reactions, in a manner similar to that observed with WO_3. However, the $BiVO_4$ photocatalyst can generate O_2 even in the presence of a high (e.g., 5 mM) Fe^{2+} ion concentration (see Figure 36).

Because both the HEP and OEP possess sufficiently high selectivity, the combination of $SrTiO_3$:Rh and $BiVO_4$ resulted in efficient water splitting through the Fe^{3+}/Fe^{2+} redox cycle.

Table 2. Photocatalytic Activity of Pt/$SrTiO_3$:Rh for H_2 Evolution from an Aqueous Fe Chloride Solution under Visible Light Irradiation[a] (Reproduced with Permission from ref 126, Copyright 2007 The Chemical Society of Japan)

	concentration of iron chlorides/mmol L^{-1}		
run	$FeCl_2$	$FeCl_3$	rate of H_2 evolution/μmol h^{-1}
1	0	2	negligible
2	2	0	8.6
3	2	0.5	9.8
4	2	1	11.1
5	2	2	22.3
6	2	5	23.0
7	0.4	0.4	15.3
8	20	2	11.0

[a]Catalyst: 50 mg, reactant solution: 120 mL, pH was adjusted with H_2SO_4 to be 2.4, light source: 300W Xe lamp with a cutoff filter (λ > 420 nm).

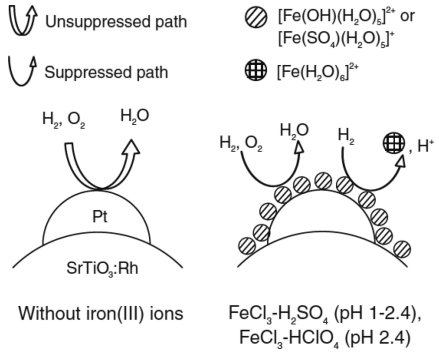

Figure 35. Suppression of backward reactions by Fe^{3+} ions. Reproduced with permission from ref 126. Copyright 2007 The Chemical Society of Japan.

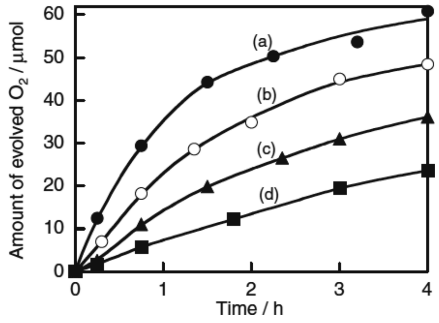

Figure 36. Photocatalytic O_2 evolution on the $BiVO_4$ photocatalyst under visible light irradiation in 2 mmol L^{-1} aqueous $FeCl_3$ solutions with (a) 0, (b) 1, (c) 2, and (d) 5 mmol L^{-1} of $FeCl_2$. Catalyst, 0.1 g; reactant solution, 120 mL, pH 2.4; light source, 300 W Xe-arc lamp with a cutoff filter (λ > 420 nm); cell, top-irradiation cell with a Pyrex window. Reproduced with permission from ref 126. Copyright 2007 The Chemical Society of Japan.

The unusually high selectivity of the Pt/$SrTiO_3$:Rh photocatalyst for both reduction of H^+ and oxidation of Fe^{2+} enabled the simultaneous, stoichiometric evolution of H_2 and O_2 under visible light via combination with various narrow-bandgap metal oxides such as WO_3 and $BiMoO_6$, which acted as O_2-evolving photocatalysts, even if their selectivity for water oxidation was not high. Not only such conventional metal oxides, but various

DOI: 10.1021/acs.chemrev.7b00286
Chem. Rev. 2018, 118, 5201−5241

Table 3. H_2 Evolution from Aqueous Solutions Containing $[Co(bpy)_3]^{2+}$, $[Co(phen)_3]^{2+}$, and Co^{2+} Ions on Various Photocatalysts[a] (Reproduced with Permission from ref 92, Copyright 2013 American Chemical Society)

entry	photocatalyst	electron donor	incident light (nm)	initial activity (μmol h^{-1})
1	Pt (0.3 wt %)/TiO_2-anatase	$[Co(bpy)_3]^{2+}$	>300	0
2	Pt (0.3 wt %)/TiO_2-anatase	$[Co(phen)_3]^{2+}$	>300	0.2
3	Pt (0.3 wt %)/$SrTiO_3$	$[Co(bpy)_3]^{2+}$	>300	0.02
4	Pt (0.3 wt %)/$SrTiO_3$	$[Co(phen)_3]^{2+}$	>300	0
5	Pt (0.3 wt %)/$SnNb_2O_6$	$[Co(bpy)_3]^{2+}$	>420	0
6	Pt (0.3 wt %)/$SnNb_2O_6$	$[Co(phen)_3]^{2+}$	>420	0
7	Pt (0.3 wt %)/ $SrTiO_3$:Rh	$[Co(bpy)_3]^{2+}$	>420	12
8	Pt (0.3 wt %)/$SrTiO_3$:Rh	$[Co(phen)_3]^{2+}$	>420	9.5
9	Pt (0.7 wt %)/$SrTiO_3$:Rh	$[Co(bpy)_3]^{2+}$	>420	16
10	Pt (0.7 wt %)/$SrTiO_3$:Rh	$[Co(phen)_3]^{2+}$	>420	12
11	Pt (0.7 wt %)/$SrTiO_3$:Rh	Co^{2+}	>420	0.5

[a]Conditions: catalyst, 0.1 g; starting reactant solutions, 120 mL of aqueous $[Co(bpy)_3]SO_4$ or $[Co(phen)_3]Cl_2$ solutions (0.5 mmol L^{-1}, initial pH ~ 7); light source, a 300-W Xe-arc lamp; cell, top-irradiation cell with a Pyrex glass window. $SrTiO_3$:Rh powder was prepared by calcination at 1273 K without Sr excess.

semiconductor materials such as tungstic acid (H_2WO_4) and metal oxyhalide (Bi_4NbO_8Cl), have also been demonstrated as effective OEP when coupled with $SrTiO_3$:Rh for Z-scheme overall water splitting under visible light.[56,88]

For long time after the first demonstration of Fe^{3+}/Fe^{2+} redox-based Z-scheme water splitting in 2004, there was only one available HEP ($SrTiO_3$:Rh) that worked with the system. In 2014, Tang et al. demonstrated that an organic semiconductor g-C_3N_4 could function as an effective HEP in Fe^{3+}/Fe^{2+} redox-based Z-scheme systems,[35] as described in the previous section.

4.2.6. Issues and Future, Prospective Fe^{3+}/Fe^{2+} Redox-Based Z-Scheme Systems. One of the biggest issues with the Fe^{3+}/Fe^{2+} redox system, along with the strict limitation on pH conditions below 2.5, is the limited choice of active HEP. Only $SrTiO_3$:Rh and g-C_3N_4 have been demonstrated so far. Thus, only wavelengths of up to ~550 nm can be used for H_2 evolution. Such a troublesome lack of photocatalyst materials is attributed to (1) high rate of reduction of Fe^{3+} on the cocatalyst or photocatalyst surface and (2) slow Fe^{2+} oxidation on the photocatalyst surface. The former is reasonable considering that Fe^{3+} cations work as efficient electron acceptors on various semiconductor photocatalysts even without any cocatalysts. Thus, it appears that a considerable fraction of photoexcited electrons readily react with Fe^{3+} cations adsorbed on the surfaces of conventional metal oxides before they reach the cocatalyst (e.g., Pt) where water reduction should occur. The development of effective oxidation sites for Fe^{2+} oxidation will be the key to addressing the latter cause (i.e., slow Fe^{2+} oxidation). Photocatalytic H_2 evolution on $SrTiO_3$:Rh photocatalysts proceeds via photoexcitation of electrons from the Rh^{3+} donor level to the conduction band under irradiation, generating oxidized Rh^{4+} species. It is thus reasonable to consider that the Rh^{4+} species work as effective and efficient oxidation sites for Fe^{2+} cations, especially when they are near the photocatalyst particle surface. The deeper understanding of the unique reactivity of Pt- (or Ru-loaded) $SrTiO_3$:Rh photocatalysts may provide clues which aid in the development of other active photocatalysts for H_2 production from aqueous Fe^{2+} solution. The activity of the g-C_3N_4 photocatalyst for this extremely difficult reaction also implies that surface properties which contrast with those of conventional metal oxides can be used for effective adsorption and reactivity in the Fe^{3+}/Fe^{2+} redox system. Further investigation and understanding of the surface properties of the newly developed g-C_3N_4 photocatalyst will also support the development of alternative photocatalysts that can harvest a wider range of visible light.

4.3. Metal Complex Redox System

Transition metal complexes have some advantages as redox mediator compared to simple ion couples, such as tunable redox potential by changing the ligands and good reversibility over a relatively wide pH range, and thus they can undoubtedly be alternative redox candidates in Z-scheme water splitting. In 2001, Grätzel et al. have proved that cobalt complexes could rival the conventional I_3^-/I^- redox couple for dye-sensitized solar cells (DSSCs) because of their favorable kinetic behaviors,[128,129] and then demonstrated highly efficient DSSCs with a light-to-electric power conversion efficiency of ~8% by using cobalt complexes such as $[Co(dbbip)_2](ClO_4)_2$ (dbbip = 2,6-bis(1′-butylbenzimidazol-2′-yl)pyridine) in organic solvents (e.g., a mixture of acetonitrile and ethylene carbonate).[128] In 2013, Spiccia et al. reported the first application of a cobalt tris(2,2′-bipyridine)-based aqueous electrolyte for the fabrication of highly efficient and stable DSSCs with a maximum energy conversion efficiency of ~5%,[130] suggesting that such complexes show high potential to applications to the Z-scheme water splitting. However, the greatest concern in such applications is the possibility of oxidative decomposition of the metal complexes with organic ligands, specifically on OEPs.

4.3.1. $[Co(bpy)_3]^{3+/2+}$ or $[Co(phen)_3]^{3+/2+}$ Redox-Based Z-Scheme Water Splitting. In 2013, Kudo et al. demonstrated a metal complex-redox-based Z-scheme water splitting using $[Co(bpy)_3]^{3+/2+}$ or $[Co(phen)_3]^{3+/2+}$ in aqueous solution under visible light irradiation.[92] One of the most important findings in this study was that the appropriate choice of photocatalyst materials, especially from the standpoint of oxidation power, is crucial in establishing such metal-complex-based Z-scheme water splitting. As seen in Table 3, only $SrTiO_3$:Rh photocatalysts (loaded with a Pt or Ru cocatalyst for water reduction) generate H_2 in the presence of reduced species of a Co complex (i.e., $[Co(bpy)_3]^{2+}$ or $[Co(phen)_3]^{2+}$) as the electron donor. On the other hand, conventional photocatalysts such as Pt/TiO_2 and $Pt/SrTiO_3$ exhibit no activity for H_2 evolution even under UV light irradiation. These findings indicated that the Rh species doped in $SrTiO_3$:Rh played a crucial role in oxidizing the Co complex based redox, as in the case described for the Fe^{3+}/Fe^{2+} redox

DOI: 10.1021/acs.chemrev.7b00286
Chem. Rev. 2018, 118, 5201−5241

system in the previous sections. Additionally, the negligible activity of nondoped materials such as $SrTiO_3$ implies that the oxidative decomposition occurred via the holes generated in the valence bands of such metal oxides, which possess a strong oxidation power. The choice of OEP is also crucial in achieving stable and stoichiometric water splitting using these complexes.

Table 4 summarizes the results of the overall water splitting by using combinations of Ru/$SrTiO_3$:Rh (HEP) and various

Table 4. Overall Water Splitting Using Ru/$SrTiO_3$:Rh OEP with $[Co(bpy)_3]^{3+/2+}$ and $[Co(phen)_3]^{3+/2+}$ Electron Mediators under Visible Light Irradiation[a] (Reproduced with Permission from ref 92, Copyright 2013 American Chemical Society)

			activity (μmol h^{-1})	
entry	O_2-evolving photocatalyst	starting reactant	H_2	O_2
1	WO_3	$[Co(bpy)_3]SO_4$	14	0.5
2	WO_3	$[Co(phen)_3]Cl_2$	15	0.4
3	TiO_2:Cr,Sb	$[Co(bpy)_3]SO_4$	3.0	0.8
4	TiO_2:Cr,Sb	$[Co(phen)_3]Cl_2$	1.3	0.7
5	$BiVO_4$	$[Co(bpy)_3]SO_4$	10	4.8
6	$BiVO_4$	$[Co(phen)_3]Cl_2$	7.9	3.5
7	$BiVO_4$	$CoSO_4$	1.0	0.2
8	$BiVO_4$	2,2′-bipyridine	3.2	0.6
9	$BiVO_4$	1,10-phenanthroline	5.5	0.5

[a]Conditions: catalyst, 0.1 g; starting reactant solutions, 120 mL of aqueous $[Co(bpy)_3]SO_4$ or $[Co(phen)_3]Cl_2$ solutions (0.5 mmol L^{-1}, initial pH ~ 7); light source, a 300-W Xe-arc lamp; cell, top-irradiation cell with a Pyrex glass window. $SrTiO_3$:Rh powder was prepared by calcinationat 1273 K without Sr excess.

OEPs in the presence of a Co complex redox, along with the results of comparative experiments (e.g., in the presence of Co^{2+} or ligands instead of the Co complex). The use of conventional WO_3 as an OEP resulted in the generation of a much smaller amount of O_2 gas than the stoichiometrically expected values. On the other hand, the use of $BiVO_4$ afforded stoichiometric generation of H_2 and O_2 with steady rates (see Figure 37 for the time courses of gas generation).

The use of TiO_2 co-doped with Cr and Sb cations also resulted in almost stoichiometric gas evolution. This can be

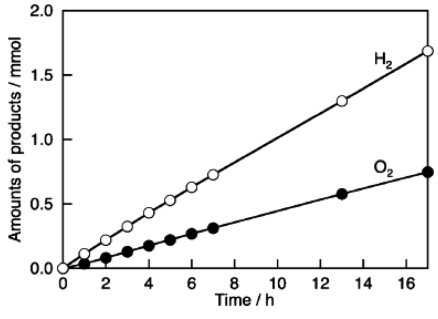

Figure 37. Overall water splitting by a (Ru/$SrTiO_3$:Rh)−($BiVO_4$)−($[Co(bpy)_3]^{3+/2+}$) system under visible light irradiation. Reaction conditions: catalyst, 0.1 g each; starting reactant solution, 120 mL of an aqueous $[Co(bpy)_3]SO_4$ solution (0.5 mmol L^{-1}, initial pH 3.8); light source, a 300 W Xe-arc lamp with a cutoff filter (λ > 420 nm); cell, top-irradiation type. $SrTiO_3$:Rh powder was prepared by calcination at 1373 K with Sr 3% excess. Reproduced with permission from ref 92. Copyright 2013 American Chemical Society.

explained by the oxidation potentials of photogenerated holes on each OEP. The oxidation power of conventional metal oxides such as TiO_2 and WO_3 is generally strong and sufficient for the decomposition of various organic molecules and metal complexes, attributed to their deeply positive levels of valence band maximum at around +3.0 V vs SHE formed by the O 2p orbitals. On the other hand, the valence band maximum of $BiVO_4$ with a monoclinic scheelite structure is located at a more negative potential (~2.5 V vs SHE) because of the significant contribution of the Bi 6s orbitals to the VBM. Thus, it appears that the undesirable oxidative decomposition of Co complexes is suppressed because of the moderate oxidation power of $BiVO_4$ and TiO_2:Cr,Sb photocatalysts.

The authors also found that the use of excess Sr in the preparation of $SrTiO_3$:Rh via a solid-state reaction, and the calcination temperature changes, significantly affected the activity for H_2 production using Co complex redox mediator. The $SrTiO_3$:Rh sample prepared at 1372 K with 3 mol % excess Sr afforded the highest rates (H_2, 100 μmol h^{-1}; O_2, 47 μmol h^{-1}) in the Z-scheme reaction combined with $BiVO_4$ under visible light (λ > 420 nm, from 300 W Xe lamp with cutoff filter). As seen in Figure 37, the water splitting reaction using such an optimized combination proceeds steadily for 17 h of irradiation, with a 2.1% quantum yield at 420 nm. The turnover number of reacted electrons with the $[Co(bpy)_3]^{3+/2+}$ redox was calculated to be 56, indicating sufficient stability of the metal complex as an electron mediator in the Z-scheme water splitting. The combination can also split water not only under a solar simulator (AM-1.5, 100 mW cm^{-2}) but also under natural sunlight, with about 0.06% solar energy conversion efficiency for H_2 production.

For the $[Co(bpy)_3]^{3+/2+}$ redox, its availability over a relatively wide pH range from 3.5 to 9 was confirmed, while almost neutral conditions (pH 6.9) shown the highest efficiency in water splitting with the (Ru/$SrTiO_3$:Rh)−($BiVO_4$) combination. The influence of pH on the total efficiency could be explained by the change in the driving forces of electron transfer between each photocatalyst and the $[Co(bpy)_3]^{3+/2+}$ redox, as illustrated in Figure 38. The band levels of metal oxide semiconductors generally shift with pH, which is attributed to surface protonation and deprotonation, whereas the redox potential of $[Co(bpy)_3]^{3+/2+}$ remains unchanged. Thus, the decreasing pH value increases the driving force of electron injection from $[Co(bpy)_3]^{2+}$ to HEP but simultaneously decreases the driving force from the OEP to $[Co(bpy)_3]^{3+}$. Consequently, the total efficiency for water splitting shows a volcano-type dependence on pH, resulting in the highest gas evolution rates at around neutral pH with this combination of HEP and OEP.

4.3.2. Separate Evolution of H_2 and O_2 by $[Co(bpy)_3]^{3+/2+}$ Redox-Based Z-Scheme. One of the advantages of a Z-scheme water splitting system compared to a conventional one-step system is its capability of separate evolution of H_2 and O_2 by employing a membrane that divides the HEP and OEP. Such a separate gas production is useful in practical applications to the storage of H_2 separately from O_2 (i.e., air) to avoid explosion. However, demonstration of such a separate production has likely been inhibited by the facile occurrence of backward reactions on each photocatalyst. Kudo et al. demonstrated for the first time such separate evolution by using the above-mentioned (Ru/$SrTiO_3$:Rh)−($BiVO_4$) combination with $[Co(bpy)_3]^{3+/2+}$ redox in a two-compartment reactor as shown in Figure 39. Such a successful demonstration

DOI: 10.1021/acs.chemrev.7b00286
Chem. Rev. 2018, 118, 5201−5241

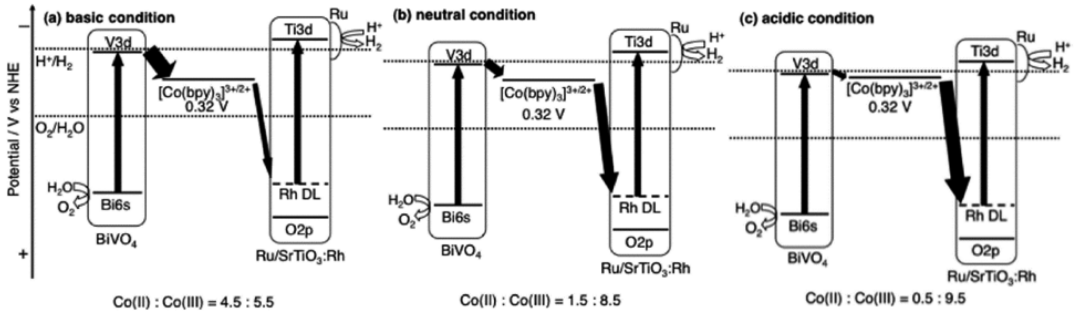

Figure 38. Energy diagrams of the Z-scheme photocatalyst system, $(Ru/SrTiO_3:Rh)-(BiVO_4)-([Co(bpy)_3]^{3+/2+})$, and the ratio of $[Co(bpy)_3]^{2+}$ ions to $[Co(bpy)_3]^{3+}$ ions during overall water splitting under basic, neutral, and acidic conditions. Reproduced with permission from ref 92. Copyright 2013 American Chemical Society.

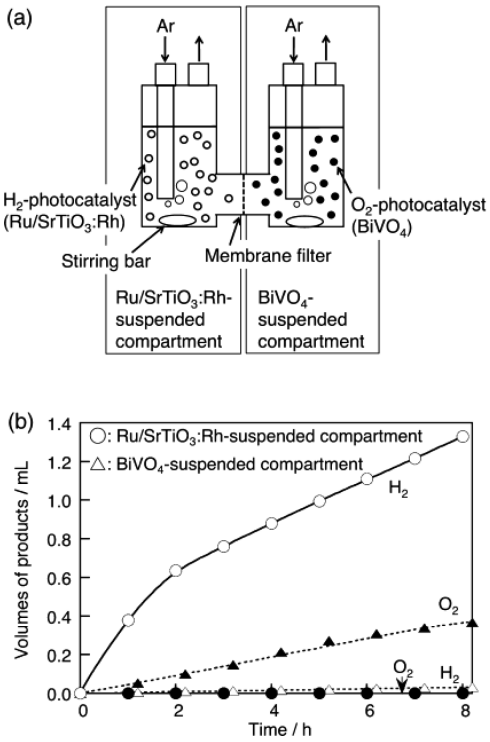

Figure 39. (a) Two-compartment-reactor for H_2 evolution separated from O_2 evolution. (b) H_2 evolution separated from O_2 evolution for overall water splitting by a $(Ru/SrTiO_3:Rh)-(BiVO_4)-([Co(bpy)_3]^{3+/2+})$ system. Catalyst, 0.1 g $(Ru/SrTiO_3:Rh)$, 0.3 g $(BiVO_4)$; starting reactant solution, 0.5 mmol L^{-1} of an aqueous $[Co(bpy)_3]SO_4$ solution, 300 mL; initial pH adjusted to 3.8; light source, two 300 W Xe-arc lamps with cutoff filters ($\lambda > 420$ nm). $SrTiO_3$:Rh powder was prepared by calcination at 1373 K with Sr 3% excess. Open and close marks indicate H_2 and O_2, respectively. Reproduced with permission from ref 92. Copyright 2013 American Chemical Society.

is undoubtedly attributed to the high selectivity for forward reactions (H_2 and O_2 evolution) in these Co complex redox systems. It was revealed that the rate of H_2 evolution on the $Ru/SrTiO_3$:Rh photocatalyst with $[Co(bpy)_3]^{2+}$ was rarely suppressed by the addition of $[Co(bpy)_3]^{3+}$, indicating that the rate of backward reaction, i.e., the reduction of $[Co(bpy)_3]^{3+}$ in place of water, is negligibly low in the present system. Although the authors did not show the results of the adsorption of these Co complexes on each photocatalyst, the high selectivity for water reduction may imply their unique adsorption properties. On the other hand, the rate of O_2 evolution on $BiVO_4$ was obviously suppressed by the increased concentration of $[Co(bpy)_3]^{2+}$, undoubtedly because of the occurrence of backward oxidation of $[Co(bpy)_3]^{2+}$ instead of water, the same as in the case of the Fe^{3+}/Fe^{2+} redox (see section 4.2.5). However, the $BiVO_4$ photocatalyst could generate O_2 even in the presence of a relatively high concentration of $[Co(bpy)_3]^{2+}$ (e.g., 0.25 mM), thus affording the successful separate production of H_2 and O_2 in the two-compartment reactor equipped with a simple membrane. It should also be noted that the mass transport resistance of redox couples across a membrane would limit the Z-scheme water splitting activity in such design, and thus engineering an adequate membrane should be on a case-by-case basis. A significant challenge would be the overall design of a two-compartment reactor as well, however, that is an engineering-based problem and would have to be addressed separately.

4.3.3. Application of Metal Sulfide Semiconductor with $[Co(terpy)_3]^{3+/2+}$ Redox Couple. Various metal sulfides have been extensively studied as photocatalysts for visible-light-induced H_2 production because many sulfides possess the narrow bandgaps required for visible light absorption and the appropriate band levels for water reduction. Another fascinating feature of such metal sulfides is the potential for band tuning via the formation of solid solutions, as demonstrated in binary $CuGaS_2-ZnS$ (i.e., $(CuGa)_{1-x}Zn_{2x}S_2$) and ternary $ZnS-CuInS_2-AgInS_2$ (i.e., $(CuAg)_xIn_{2x}Zn_{2(1-2x)}S_2$) systems. However, the biggest drawback of such metal sulfide photocatalysts is their instability, which is attributed to the occurrence of self-oxidative deactivation (e.g., $CdS + 2h^+ \rightarrow Cd^{2+} + S$). Thus, one of the most reasonable and attractive strategies to achieve overall water splitting using such metal sulfides under visible light involves a Z-scheme water splitting system.

In 2015, Kudo et al. demonstrated metal sulfide based Z-scheme water splitting with a $[Co(terpy)_3]^{3+/2+}$ redox.[77] The combination of Ru (0.5 wt %)-loaded $(CuGa)_{0.8}Zn_{0.4}S_2$ as HEP and $BiVO_4$ with $[Co(terpy)_3]^{3+/2+}$ redox resulted in stable generation of H_2 and O_2 with a stoichiometric ratio under visible light irradiation ($\lambda > 420$ nm), as well as under a solar simulator, without any reduced activity. The turnover number of the reacted electrons to the number of S atoms at the surface of $(CuGa)_{0.8}Zn_{0.4}S_2$ exceeded 70 after 17 h of irradiation, indicating that this sulfide semiconductor could function stably as a HEP with a $[Co(terpy)_3]^{3+/2+}$ redox with negligible photocorrosion. The VBM of the $(CuGa)_{0.8}Zn_{0.4}S_2$ was confirmed to predominantly consist of the Cu 3d orbital at a potential higher than that of the S 3p orbital. It is therefore speculated that the possibility of photocorrosion was decreased in this material compared to that in other conventional metal

DOI: 10.1021/acs.chemrev.7b00286
Chem. Rev. 2018, 118, 5201−5241

sulfides such as CdS or ZnS in which the VBMs are mainly formed by S 3p orbitals. Although such a successful combination of metal sulfides and Co complex redox is limited to this combination at present, the results may provide a new and promising strategy to achieve efficient water splitting under visible light using metal sulfide photocatalysts.

4.4. Polyoxometalate Redox System

Although some Co complexes have been employed as electron mediators in Z-scheme water splitting as descried above, the available OEP is still limited to $BiVO_4$ that possess moderate oxidation potential than conventional metal oxides. This is probably associated with oxidative decomposition of organic ligands in such metal complexes by photogenerated holes. It has been reported that many transition metal-incorporating polyoxometalates (POMs), which basically contain no organic components, exhibit reversible redox behavior derived from valence differences in the incorporated transition metals and/or in the constituent elements of the framework. Additionally, most POMs are stable in mildly acidic conditions, while the available ranges of pH are depended on their structure and constituent elements. Thus, such POMs will be alternative redox candidates with high stability in Z-scheme water splitting.

In 2016, Abe et al. demonstrated for the first time such POM based Z-scheme water splitting by using a redox couple of manganese-substituted Keggin-type silicotungstate $[SiW_{11}O_{39}Mn^{III}(H_2O)]^{5-}/[SiW_{11}O_{39}Mn^{II}(H_2O)]^{6-}$ (hereafter denoted $SiW_{11}Mn^{III}/SiW_{11}Mn^{II}$).[93] The cyclic voltammograms (Figure 40) of $K_6[SiW_{11}O_{39}Mn^{II}(H_2O)]\cdot 6H_2O$ in 0.5 M

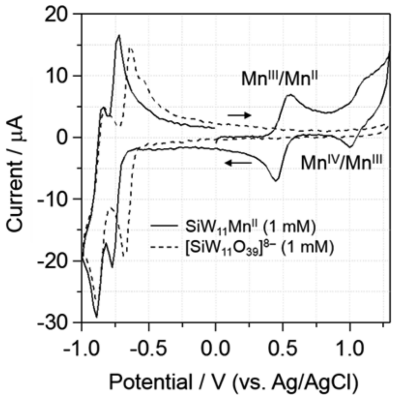

Figure 40. Cyclic voltammograms of 1 mM of $K_6[SiW_{11}O_{39}Mn^{II}(H_2O)]\cdot 6H_2O$ and $K_8[SiW_{11}O_{39}]\cdot 13H_2O$ in an aqueous solution containing KH_2PO_4 (0.5 M) as a supporting electrolyte (scan rate, 50 mV s^{-1}; initial potential, 0 V (vs Ag/AgCl); initial scan direction, toward more positive potential; working electrode, glassy carbon; reference electrode, Ag/AgCl; counter electrode, Pt coil). Reproduced with permission from ref 93. Copyright 2016 Wiley-VCH Verlag GmbH & Co. KGaA, Weinheim.

KH_2PO_4 solutions showed two reversible peaks assignable to the redox cycles of Mn species (Mn^{III}/Mn^{II}; $E_{1/2}$ at +0.51 V, Mn^{IV}/Mn^{III} $E_{1/2}$ at +1.08 V vs Ag/AgCl). Assuming pH = 4, at which most POMs are stable, the redox potentials of Mn^{III}/Mn^{II} and Mn^{IV}/Mn^{III} are determined to be ca. +0.70 and +1.06 V (vs SHE at pH = 4), respectively; that of Mn^{III}/Mn^{II} is close to the redox potential of Fe^{3+}/Fe^{2+} (+0.77 V vs SHE).

The reduced $SiW_{11}Mn^{II}$ was demonstrated to function as effective electron donor for H_2 evolution on $Ru/SrTiO_3$:Rh under visible light (see Figure 41). Interestingly, the initial rates were almost independent of the initial concentration of

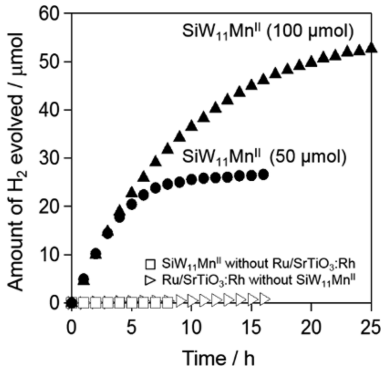

Figure 41. Time courses of H_2 evolution over $Ru/SrTiO_3$:Rh from a phosphate solution (0.5 M) containing $[SiW_{11}O_{39}Mn^{II}(H_2O)]^{6-}$ (photocatalyst, 0.1 g; the amount of water, 50 mL). Reproduced with permission from ref 93. Copyright 2016 Wiley-VCH Verlag GmbH & Co. KGaA, Weinheim.

$SiW_{11}Mn^{II}$ (50 or 100 μmol). Although the rate of H_2 evolution gradually decreased with irradiation time, finally reached the stoichiometric values expected from the amount of $SiW_{11}Mn^{II}$ present in the initial solutions. This behavior can be explained by the adsorption property of $SiW_{11}Mn^{III}/SiW_{11}Mn^{II}$ on the photocatalyst. As shown in Figure 42, the adsorption of

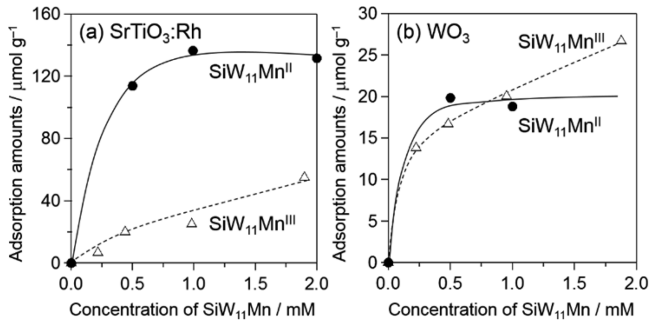

Figure 42. Adsorption amounts of $SiW_{11}Mn$ on (a) $SrTiO_3$:Rh and (b) WO_3 particles in 0.5 M phosphate solution (amount of photocatalyst, 15 mg; amount of Milli-Q water, 10 mL; stirring time, 15 h in dark; BET surface area, $SrTiO_3$:Rh 5.9 m^2 g^{-1}, WO_3 4.6 m^2 g^{-1}). Reproduced with permission from ref 93. Copyright 2016 Wiley-VCH Verlag GmbH & Co. KGaA, Weinheim.

$SiW_{11}Mn^{II}$ on the $SrTiO_3$:Rh was almost saturated at around 1 mM (corresponding to 50 μmol in the present reaction solutions). Thus, the rate of electron injection from $SiW_{11}Mn^{II}$ was certainly limited even when the reaction was started with higher amount. More importantly, $SiW_{11}Mn^{II}$ preferentially adsorbed on the surface of $SrTiO_3$:Rh over $SiW_{11}Mn^{III}$; the adsorption amount of $SiW_{11}Mn^{III}$ is much less than that of $SiW_{11}Mn^{II}$ when compared at a same concentration (e.g., 1 mM). It is thus reasonable to consider that the rate of undesirable backward reaction (reduction of $SiW_{11}Mn^{III}$) is low even if the concentration of $SiW_{11}Mn^{III}$ increases with the progress of reactions, resulting in relatively steady rate of H_2 evolution in the present system.

The oxidized $SiW_{11}Mn^{III}$ was also proven to function as an electron acceptor on PtO_x/WO_3 photocatalyst for O_2 evolution (see Figure 43). When the reaction was initiated with ca. 96 μmol of $SiW_{11}Mn^{III}$, O_2 evolution was observed at almost steady rates saturating at about 23 μmol, which was very close to the stoichiometrically expected value (24 μmol). When the

DOI: 10.1021/acs.chemrev.7b00286
Chem. Rev. 2018, 118, 5201−5241

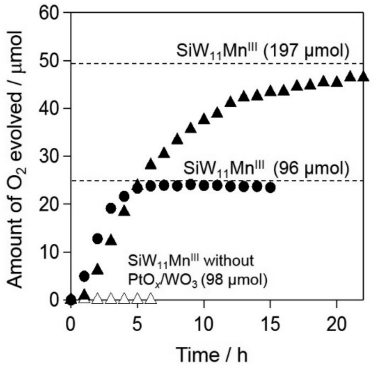

Figure 43. Time courses of O_2 evolution over PtO_x/WO_3 from an aqueous solution containing $[SiW_{11}O_{39}Mn^{III}(H_2O)]^{5-}$. Dotted lines indicate the theoretical amount of O_2 calculated from added $[SiW_{11}O_{39}Mn^{III}(H_2O)]^{5-}$ (photocatalyst, 0.1 g; the amount of water, 100 mL). Reproduced with permission from ref 93. Copyright 2016 Wiley-VCH Verlag GmbH & Co. KGaA, Weinheim.

reaction was initiated with a larger amount of $SiW_{11}Mn^{III}$ (197 μmol), the rate of O_2 evolution gradually decreased with irradiation time, undoubtedly due to the occurrence of backward reaction to some extent. Then, the combination of $Ru/SrTiO_3$:Rh and PtO_x/WO_3 with $SiW_{11}Mn^{III}/SiW_{11}Mn^{II}$ redox at pH = 4.5 resulted in stable generation of H_2 and O_2 with a stoichiometric ratio under visible light irradiation (λ > 420 nm).

Although the present $SiW_{11}Mn^{III/II}$ POM redox possesses an advantage over conventional Fe^{3+}/Fe^{2+} redox, i.e., the availability in mildly acidic conditions (e.g., pH = 4.5), it has some disadvantages. One is the necessity of effective cocatalyst on an OEP, even though this redox cycle takes place via one-electron transfer similar to Fe^{3+}/Fe^{2+}. Although bare WO_3 could generate O_2 in the presence of $SiW_{11}Mn^{III}$, the loading of PtO_x or Pt significantly enhanced the O_2 evolution, indicating that the reduction of $SiW_{11}Mn^{III}$ requires an appropriate cocatalyst. The second one is the light absorption in visible light region. Although the reduced $SiW_{11}Mn^{II}$ possesses absorption mainly at UV light region along with weaker one in visible region, the oxidized $SiW_{11}Mn^{III}$ shows strong and relatively broad absorption peak (at 500 nm) ranging from 450 to 600 nm. Thus, the accumulation of $SiW_{11}Mn^{III}$ undoubtedly causes a significant light shielding effect that decreases the number of photons absorbed by photocatalyst particles and consequently lowers the photocatalytic efficiency. Therefore, the searching and/or developing POMs with efficient redox cycle and good transparency to visible light is strongly desired for improving the total efficiency of POM-based Z-scheme water splitting.

4.5. Vanadate Redox System

A vanadate redox mediator has been reported to function in a Z-scheme system of $(Ru/SrTiO_3:Rh)-(VO_2^+/VO^{2+})-(Fe-H-Cs-WO_3)$ by Miseki et al.[109] The vanadate ion shuttle is expected to be redox active according to the following equation:

$$2VO^{2+} + 2H_2O + 2h^+ = 2VO_2^+ + 4H^+$$

$$2VO_2^+ + 4H^+ + 2e^- = 2VO^{2+} + 2H_2O$$

It should be noted that the V^{5+} structure varies with the pH of solution (i.e., pH 0–3 = VO^{2+}, pH 3–9 = H_2VO^{4-}, and pH 9–13 = HVO_4^{2-}),[131] and the redox potential of the V^{5+}/V^{4+} is also highly dependent on the complex structure (VO_2^+/VO^{2+} = 1.0 V and $H_2VO_4^-/HV_2O_5^-$ = 0.7 V, vs NHE, pH = 0).[109] Therefore, the authors carefully adjusted the pH of the system to 2.4, ensuring the desired pathway occurred, and the pH did not fluctuate. Prior to this, the authors measured the O_2 and H_2 half reactions in the presence of VO^{2+} and VO_2^+, respectively. The intermediate species were confirmed by UV–vis spectra as the VO^{2+} peak at 766 nm submerged in O_2 production and disappeared during H_2 production. Water is selectively oxidized due to H_3O^+ species on the surface of $Fe-H-Cs-WO_3$ and that the selective water oxidation may be much faster than unfavorable back-reactions. $Ru/SrTiO_3$:Rh as a HEP contains

Table 5. Summary of Different Types of Mediators in Visible Driven Z-Scheme Water Splitting

entry	mediators	working pH	advantages	disadvantages	benchmark activity	ref (year)
1	IO_3^-/I^-	4, 6–8, 11	wide pH range	side reactions occur in acidic media	AQY = 6.8% (420 nm)	83 (2015)
2	I_3^-/I^-	4.5	compatible with dye-sensitized systems	shields UV light from photocatalyst	H_2: 2.6 μmol h^{-1}, O_2: 1.3 μmol h^{-1}, 300 W Xe lamp (λ > 420 nm)	41 (2009)
3	Fe^{3+}/Fe^{2+}	2.1–3	can also be used as a H_2 producing catalyst (Fe^{2+})	low pH range only	AQY = 4.2% (420 nm)	86 (2013)
4	$Co^{3+/2+}$complex	3.8 and 7	homogenous; high turnover rate, good binding to surface/charge transfer	only work with specialized photocatalyst (e.g., TiO_2)	STH = 0.06%	92 (2013)
5	VO_2^+/VO^{2+}	2.4	good suppression of side reactions	only works with specialized photocatalysts (e.g., $SrTiO_3$:Rh)	STH = 0.06%	109 (2017)
6	polyoxometalate	4.5	versatile, nontoxic, easy to disperse on surfaces	shields UV light from photocatalyst	H_2: 1.7 μmol h^{-1}, O_2: 0.8 μmol h^{-1}, 300 W Xe lamp (λ > 400 nm) AQY = 0.24% (λ = 400 nm)	93 (2016)
7	metal	without control	expensive, only noble or PG metals	hard to disperse over every active site (clustering)	AQY = 33% (419 nm), STH = 1.1% (288 K, 5 KPa)	98 (2016)
8	RGO	3.5, 7, or without control	low cost	difficult to synthesize	AQY = 1.03% (420 nm)	99 (2011)
9	carbon	6.8	low cost; can work in pure water	difficult to synthesize	AQY = 26% (419 nm), STH = 1.0% (331 K, 91 KPa)	107 (2017)
10	none	mainly 3.5–3.9, 7	system is simpler and without disadvantages such as side-reactions	limited to a few photocatalysts	AQY = 1.7% (420 nm), STH = 0.12%	94 (2009)

DOI: 10.1021/acs.chemrev.7b00286
Chem. Rev. 2018, 118, 5201–5241

active VO^{2+} oxidation sites but no VO_2^+ reduction sites, thus suppressing the undesirable reactions and resulting in ideally selective performance. This work also demonstrated the context of separated stepwise Z-scheme H_2 and O_2 production. Briefly, a HEP was added at the beginning with VO^{2+} under visible irradiation. After the total H_2 reached a stable value, indicating the VO^{2+} were all converted to VO_2^+, the HEP was filtered, and OEP was added to perform the O_2 evolution consequently. The activity was reported to be H_2, 50 μmol h^{-1}, and O_2, 25 μmol h^{-1}, in one-pot reaction, and stepwise reaction was about 1.4 times higher. This might infer that the physical mixing of HEP and OEP caused negative interactions and a light scattering/shielding effect of $Ru/SrTiO_3$:Rh also influenced the activity to some extent.

To summarize, there are still some limitations for Z-scheme systems apart from advantages. For example, proper working conditions (e.g., pH) of different types of mediators and mediator-free Z-scheme for water splitting are very important for their performance. These are summarized in Table 5.

5. STRATEGIES FOR IMPROVING EFFICIENCY OF Z-SCHEME SYSTEMS

The previous sections detailed various Z-scheme systems with the appropriate redox couples. However, their efficiencies, except for the recently developed photocatalyst panels, are still moderate and must be further improved to demonstrate the feasibility of practical H_2 production. Various methods such as cocatalyst loading, surface modifications, morphology controls, and introduction of a heterojunction have been attempted to improve the efficiency of existing visible light responsive photocatalysts. This section will focus on the cocatalyst loading and the surface modifications, both of which have been proven as effective ways to improve the efficiency of Z-scheme systems.

5.1. Cocatalyst Loading

Cocatalyst loading onto photocatalyst particles has been widely studied as an effective way to improve the performance of semiconductor photocatalysts. The main role of such cocatalyst has been generally regarded as (1) enhancing the charge separation in the photocatalyst and (2) facilitating the surface chemical reactions by the carriers. For most photocatalysts used for conventional one-step water splitting, the cocatalysts that enhance water reduction but not catalyze the water formation from H_2 and O_2, (e.g., NiO_x, Cr_2O_3/Rh) are often employed to improve the efficiency of water splitting. Some recent studies also investigated coloading of an effective O_2-evolving cocatalyst (e.g., Mn_3O_4, IrO_2) with a H_2-evolving cocatalyst.[132] Cocatalyst loading also influences the efficiencies of Z-scheme water splitting systems significantly. In the Z-scheme systems with a dissolved redox couple, loading of the cocatalysts that facilitate reduction or oxidation of the redox mediator, rather than water, often dominates the total efficiency. For example, the reduction of IO_3^- to I^- via six electrons often becomes the rate-determining step in O_2 evolving part, thus the loading of effective cocatalysts (e.g., PtO_x, RuO_2) can drastically increase the rate of O_2 evolution and thereby improve the total efficiency of Z-scheme water splitting.

5.1.1. Cocatalysts for H_2 Evolution Photocatalysts with IO_3^-/I^- Redox Couple. Most semiconductor photocatalysts that have been developed for water splitting require suitable cocatalyst particles to promote H_2 production. Noble metals such as Pt that have low overpotentials for water reduction are often used as effective cocatalysts. However, it is well recognized that Pt-loaded photocatalysts such as Pt/TiO_2 cannot split pure water into H_2 and O_2 in a simple aqueous suspension system. This is basically attributed to backward reactions (i.e., catalytic H_2O formation from the evolved H_2 and O_2) on Pt surface before the produced gases escape from the suspension to gas phase.

On the other hand, many of the Z-scheme water splitting systems based on IO_3^-/I^- or Fe^{3+}/Fe^{2+} redox couple can generate H_2 and O_2 simultaneously even in the presence of Pt cocatalyst on HEP, as seen in Table 1. One can notice that most of the Z-scheme systems with IO_3^-/I^- (or I_3^-/I^-) redox employ Pt cocatalyst for the HEPs, with a few exceptions. The spontaneous formation of iodine layer on Pt surface is probably one of the reasons why H_2 and O_2 can generate stably even in the presence of Pt.[133] It has been reported that I^- anions in aqueous solution were spontaneously and oxidatively chemisorbed as zerovalent I atoms on Pt polycrystalline electrode and formed stable monolayer on the Pt surface.[134] As seen in Figure 44, a Pt/TiO_2 photocatalyst after photoreaction in an aqueous solution of NaI (1 mM) exhibits strong peaks at 618.5 and 630 eV in the I 3d XPS spectra, which indicate the presence of zerovalent iodine. These peaks were also observed over the same sample that was stirred in the NaI aqueous solution for 12 h in dark but not over the unloaded TiO_2 under the same conditions. As shown in Figure 45, the pressure of gas mixture of H_2 and O_2 rapidly decreased on a fresh Pt/TiO_2 sample due to the water formation from H_2 and O_2 on naked Pt surface. On the other hand, the pressure of the mixture decreased much more slowly on an I-adsorbed Pt/TiO_2 sample. These findings indicate that the iodine monolayers formed on Pt surface effectively suppress the backward reaction from H_2 and O_2. It was reported that electron transfer could occur through the iodine layer formed on the Pt surface and also that the iodine layers could be reductively eliminated from the surface either by exposure to electrochemically generated H_2 or by application of sufficiently negative potentials.[133] Therefore, the following two mechanisms can be proposed for the H_2 production over I-adsorbed Pt cocatalyst surfaces: (1) water reduction proceed directly on the iodine layer by photoexcited electrons migrated from semiconductor bulk via Pt, and (2) a part of the iodine layers is reductively eliminated by photogenerated electrons or

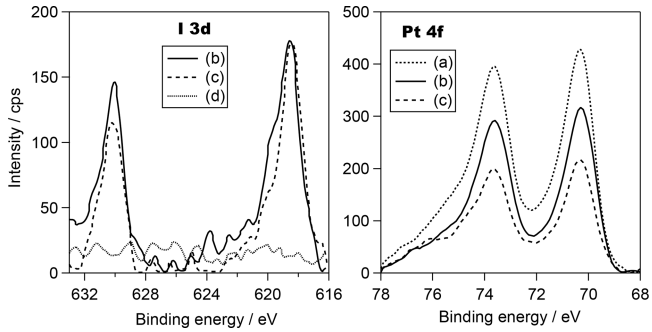

Figure 44. X-ray photoelectron spectra of I 3d and Pt 4f for Pt (3 wt %)−anatase TiO_2 powders; fresh sample (a), after stirring in an aqueous solution of NaI (1 mM) for 12 h in dark (b), after photoreaction in an aqueous solution of NaI (1 mM) for 20 h under UV light irradiation (c). X-ray photoelectron spectrum of I-3d for bare anatase TiO_2 powder after stirring in an aqueous solution of NaI (1 mM) for 12 h in the dark (d). Reproduced with permission from ref 133. Copyright 2003 Elsevier.

DOI: 10.1021/acs.chemrev.7b00286
Chem. Rev. 2018, 118, 5201−5241

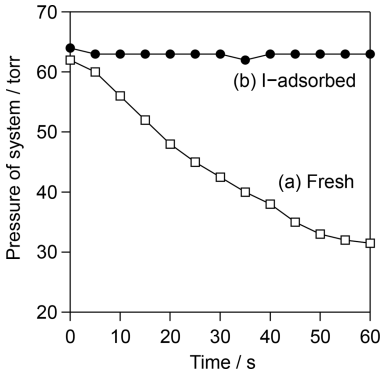

Figure 45. Water formation from H_2 and O_2 in gas phase reaction over (a) fresh and (b) I-adsorbed 3 wt % Pt−TiO_2 photocatalyst powders. A mixture of H_2 and O_2 (H_2:O_2 = 2:1) gases was introduced to a closed gas-circulating system with a Pyrex glass cell containing 10 mg of photocatalyst powder without water. Reproduced with permission from ref 133. Copyright 2003 Elsevier.

H_2 and then water reduction takes place on the exposed Pt surface.

5.1.2. Cocatalysts for H_2 Evolution Photocatalysts with Fe^{3+}/Fe^{2+} Redox Couple. In the primary Z-scheme systems with Fe^{3+}/Fe^{2+} redox couple, Pt cocatalyst was also utilized for HEP, as seen in Table 1. It was suggested that the adsorption of $[Fe(SO_4)(H_2O)_5]^+$ and/or $[Fe(OH)(H_2O)_5]^{2+}$ on the Pt surface efficiently suppresses undesirable backward reactions such as water formation from H_2 and O_2 (see section 4.2.5. for details).[126] On the other hand, Kudo et al. demonstrated that Ru cocatalyst exhibited better performance than Pt. As seen in Figure 46, the possible backward reactions (e.g., water formation from H_2 and O_2 and reduction of Fe^{3+} ions by H_2) are much more effectively suppressed on Ru cocatalyst.[85]

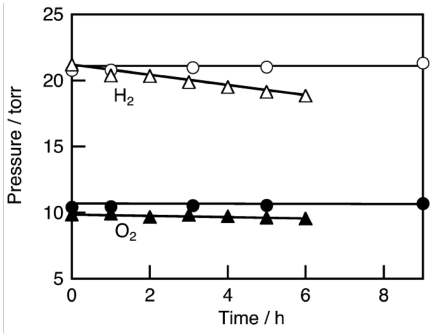

Figure 46. Consumptions of H_2 and O_2 due to back-reactions with 2 mmol L^{-1} aqueous $FeCl_3$ solution on the (Pt (0.3 wt %)/$SrTiO_3$:Rh)−($BiVO_4$) (triangles) and (Ru (0.7 wt %)/$SrTiO_3$:Rh)−($BiVO_4$) (circles) systems in the dark. Catalyst, 50 mg each; reactant solution, 120 mL, pH 2.4, adjusted by H_2SO_4. Reproduced with permission from ref 85. Copyright 2008 Elsevier.

Figure 47 shows time courses of photocatalytic overall water splitting for (Pt/$SrTiO_3$:Rh)−($BiVO_4$) and (Ru/$SrTiO_3$:Rh)−($BiVO_4$) systems with Fe^{3+}/Fe^{2+} redox under visible light irradiation.[85] The gas evolutions proceeded with almost steady rates on Ru cocatalyst-based system even at relatively high pressures, whereas the rate of gas evolution over the Pt cocatalyst-based system gradually decreased after 10 h of irradiation, undoubtedly due to the occurrence of backward

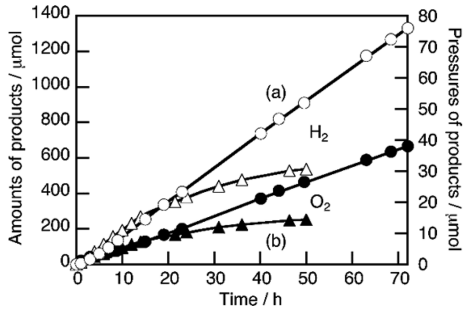

Figure 47. Photocatalytic overall water splitting on (a) the (Ru (0.7 wt %)/$SrTiO_3$:Rh)−($BiVO_4$) system and (b) the (Pt (0.1 wt %)/$SrTiO_3$:Rh)−($BiVO_4$) system. Catalyst, 50 mg each; reactant solution, 2 mmol L^{-1} of aqueous $FeCl_3$ solution, 120 mL, pH 2.4; light source, 300-W Xe-arc lamp (λ > 420 nm); cell, top-irradiation cell with a Pyrex glass window. Reproduced with permission from ref 85. Copyright 2008 Elsevier.

reactions accompanied by an increase in the pressures of evolved H_2 and O_2. It should be noted that the X-ray photoelectron spectroscopy (XPS) analysis on the samples revealed that the surface of Ru cocatalyst loaded by photodeposition is oxidized by air or water. Thus, it appears that the backward reactions are effectively suppressed by the presence of such thin oxide layer on the surface, which is different from what happened on Pt cocatalyst.

5.1.3. Nanostructured Cocatalysts for Selective H_2 Evolution. Suppressing backward reactions of redox couples is undoubtedly one of the most effective ways to improve the total efficiency of Z-scheme water splitting systems. For example, Pt nanoparticles that are selectively deposited in the interlayer space of layered semiconductor can work as selective reduction sites for H_2 production with I_3^-/I^- or IO_3^-/I^- redox couple.[62,135] As seen in Figure 48, H_2 evolution over dye-

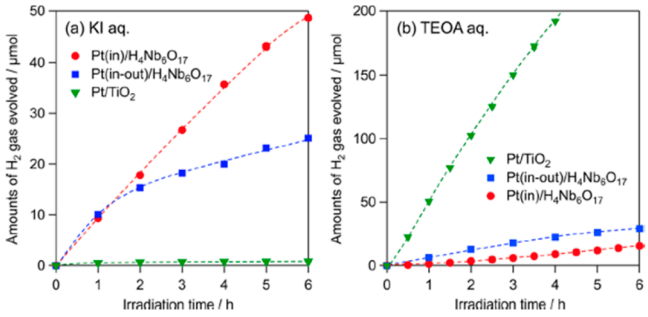

Figure 48. Time courses of photocatalytic H_2 evolution under visible light (λ > 410 nm) on NKX-2677 dye-adsorbed Pt(in)/$H_4Nb_6O_{17}$, Pt(in−out)/$H_4Nb_6O_{17}$, and Pt/TiO_2 photocatalysts suspended in (a) 0.1 M aqueous KI solution (pH ∼ 6.5, without adjustment) and (b) 0.1 M aqueous triethanolamine solution (pH ∼ 7, adjusted with HCl). Reproduced with permission from ref 62. Copyright 2013 American Chemical Society.

adsorbed Pt/TiO_2 photocatalyst with reversible I^- electron donor rapidly terminates with quite small amount of H_2 evolved, while it can generate H_2 stably from an aqueous triethanolamine solution. This is due to the significant backward reaction (reduction of I_3^- to I^-) on the Pt particles as illustrated in Figure 49a. On the other hand, H_2 evolution proceeded at a steady rate on the dye-adsorbed Pt(in)/$H_4Nb_6O_{17}$ sample, in which Pt nanoparticles were selectively loaded into the interlayer spaces of layered niobate. This is a

DOI: 10.1021/acs.chemrev.7b00286
Chem. Rev. 2018, 118, 5201−5241

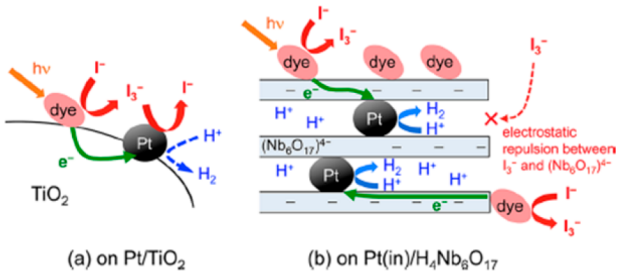

Figure 49. Conceptual schemes for suppression of backward reaction using nanostructured layered semiconductors. Reproduced with permission from ref 62. Copyright 2013 American Chemical Society.

result of the reduced backward reaction caused by I_3^- anions on Pt particles because of the electrostatic repulsion between I_3^- and the negatively charged niobate layers (see Figure 49b).

Suzuki et al. also demonstrated that the selective deposition of Pt cocatalyst into interlayer spaces of a nitrogen-doped tantalate ($H^+/RbLaTa_2O_{7-x}N_y$) was effective to achieve nonsacrificial and endergonic H_2 evolution from water using I^- as a reversible electron donor under visible light.[135]

5.1.4. Cocatalysts for O_2 Evolution Photocatalysts. The loading of cocatalyst, such as PtO_x or RuO_2, is indispensable for efficient O_2 evolution over OEPs such as WO_3 using the IO_3^- anion as an electron acceptor, because the reduction of IO_3^- to I^- via six-electrons often becomes the rate-determining step. On the other hand, even unmodified photocatalysts such as WO_3 and $BiVO_4$ can generate O_2 with Fe^{3+} electron acceptors. Suzuki et al. revealed a reasonable relation between the overpotential of each cocatalyst material for IO_3^- reduction and the rate of O_2 evolution on the cocatalyst-loaded photocatalyst with IO_3^- as electron acceptor.[136] As shown in Figure 50, the overpotentials of MO_x

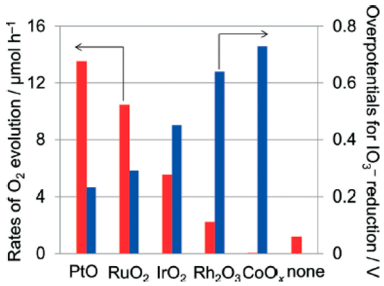

Figure 50. Rates of O_2 evolution over ex-$Ca_2Nb_3O_{10}/K^+$ loaded with 0.3 wt % of various metal oxides (PtO, RuO_2, IrO_2, Rh_2O_3, and CoO_x) in 5 mM $NaIO_3$ aqueous solution under UV light irradiation (λ > 300 nm, Xe lamp) and overpotentials for IO_3^- reduction on each catalyst. Reproduced with permission from ref 136. Copyright 2015 The Royal Society of Chemistry.

catalysts for IO_3^- reduction, which were determined by electrochemical measurements, decrease in the following order: CoO_x > Rh_2O_3 > IrO_2 > RuO_2 > PtO. Clearly, a good correlation was drawn that the rate of O_2 evolution on ex-$Ca_2Nb_3O_{10}/K^+$ samples (prepared via exfoliation and subsequent restacking of layered $KCa_2Nb_3O_{10}$ material) loaded with these MO_x cocatalysts increased with the decreased overpotentials for IO_3^- reduction on the MO_x.[136]

The surface chemical states also significantly influence the performance of cocatalysts. It was revealed that WO_3 photocatalysts loaded with platinum oxide (PtO) showed a much higher activity for O_2 evolution in the presence of the electron acceptor IO_3^- compared to those loaded with Pt metal.[59]

One can see in Figure 51 that an interesting dependence of the O_2 evolution rate from aqueous IO_3^- over the WO_3

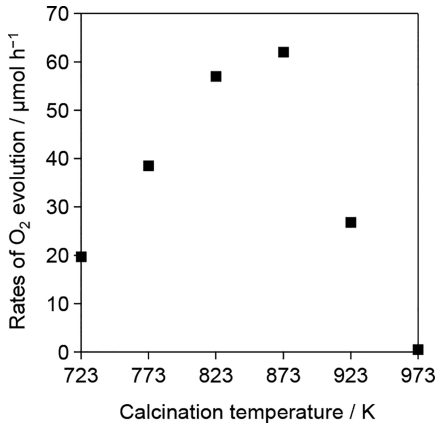

Figure 51. Dependence of rates of O_2 evolution over Pt(0.5 wt %)–WO_3 photocatalysts upon the calcination temperature after impregnation of H_2PtCl_6. The reaction was carried out in aqueous solution (250 mL) containing $NaIO_3$ (2 mM). Reproduced with permission from ref 59. Copyright 2011 Wiley-VCH Verlag GmbH & Co. KGaA, Weinheim.

photocatalyst loaded with Pt species upon calcination temperature after impregnation of H_2PtCl_6.[59] The rate increases significantly with increasing calcination temperature from 723 to 823 K, and then decreases drastically above 873 K. The XPS and STEM analysis revealed that the WO_3 samples loaded with Pt species at low temperatures (723–823 K) mainly contained highly dispersed PtO species, while that prepared at 873 K contained mixture of PtO and Pt species. On the other hand, the samples prepared at higher temperatures (>873 K) dominantly had relatively large particles of metallic Pt. Considering the fact that the photodeposited Pt/WO_3 samples, which were loaded with highly dispersed Pt metal particles, showed a much lower activity for O_2 evolution (ca. 5 μmol h^{-1}), it appears that PtO is a more favorable cocatalyst for O_2 evolution with IO_3^- acceptor than Pt metal. It is well-known that Pt nanoparticles act as highly efficient catalyst for O_2 reduction. Thus, one possible reason for the low activity of WO_3 samples loaded with a Pt metal cocatalyst is competitive reduction of O_2 molecules on the Pt metal surface alongside the reduction of IO_3^-. The increase in the O_2 evolution rate with temperature from 723 to 823 K is also due to the improved interface between WO_3 and PtO particles, which enables efficient electron transport from WO_3 to PtO.

The loading of the RuO_2 cocatalyst on TaON enhanced the O_2 evolution in the presence of IO_3^-, which enabled the RuO_2/TaON photocatalyst to be used as an OEP in combination with Pt/TaON. Structural analyses and (photo)electrochemical measurements revealed that the activity of RuO_2/TaON photocatalyst was strongly dependent on the generation of optimally dispersed RuO_2 nanoparticles, which simultaneously promote both the reduction of IO_3^- and oxidation of water.[33] It was recently revealed that the $Ru(OH)_xCl_y$ species obtained by the calcination of $RuCl_3 \cdot nH_2O$ at or below 200 °C showed a much higher activity for IO_3^- reduction than conventional RuO_2, while the $Ru(OH)_xCl_y$ species rarely catalyzed water

DOI: 10.1021/acs.chemrev.7b00286
Chem. Rev. 2018, 118, 5201–5241

oxidation.[137] Figure 52 shows current−potential curves for the TaON electrodes loaded with Ru species at various temperatures (x) in a Na_2SO_4 aqueous solution containing IO_3^- (1.0 mM) under dark conditions. XPS analysis indicated that the partially hydroxylated Ru species, e.g., $Ru(OH)_xCl_y$, were loaded onto TaON by the wet-impregnation process followed by calcination at relatively low temperatures (~200 °C), whereas the calcination at higher temperatures resulted in the formation of conventional RuO_2. Surprisingly, the onset potentials on the Ru-150 and Ru-200 electrodes, both of which mainly contain $Ru(OH)_xCl_y$ species, were observed around much more positive potentials of +0.1 V vs Ag/AgCl, along with astonishingly higher current densities. Co loading the $Ru(OH)_xCl_y$ and Co cation species (by simple impregnation of $Co(NO_3)_2$ at 100 °C) as water oxidation cocatalysts significantly improved O_2 evolution on the TaON photocatalyst by more than a factor of 2 compared to that loaded with only the conventional RuO_2 cocatalyst (see Figure 53). These findings strongly suggest that the coloading of two different cocatalysts independently optimized for reduction and oxidation can be an effective strategy to enhance the efficiency of OEPs (see Figure 54) in Z-scheme water splitting systems.

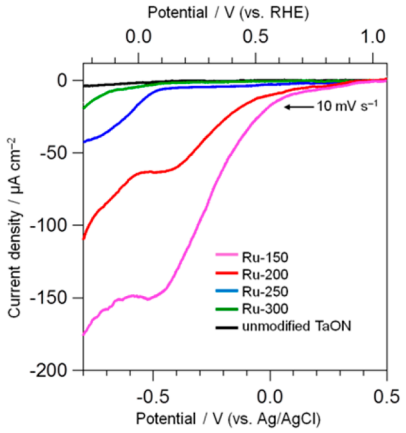

Figure 52. Current−potential curves of TaON electrodes loaded with Ru species and an unmodified TaON electrode in an aqueous Na_2SO_4 solution (0.1 M) containing $NaIO_3$ (1.0 mM) under dark conditions. Reproduced with permission from ref 137. Copyright 2017 The Royal Society of Chemistry.

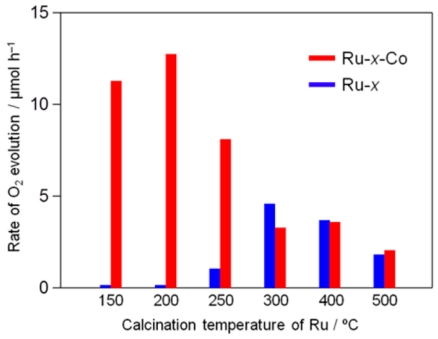

Figure 53. Initial rate of O_2 evolution on Ru-x and Ru-x-Co photocatalysts (50 mg) prepared at different temperatures in an aqueous solution (250 mL) containing $NaIO_3$ (1.0 mM) under visible light (λ > 400 nm). Reproduced with permission from ref 137. Copyright 2017 The Royal Society of Chemistry.

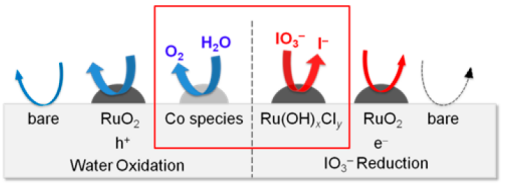

Figure 54. Summary of the speculated role and activities of the cocatalysts loaded onto TaON. Reproduced with permission from ref 137. Copyright 2017 The Royal Society of Chemistry.

5.2. Surface Modification

Sayama et al. demonstrated that the surface modification of WO_3 photocatalysts with Cs^+ species drastically improved the efficiency in O_2 evolution with Fe^{3+}/Fe^{2+} redox couple.[138] As seen in Table 6, the rate of O_2 evolution on WO_3 from aqueous $Fe_2(SO_4)_3$ solution is significantly increased after the hydrothermal reaction of WO_3 particles in aqueous Cs_2CO_3 solution at 393 K. The rate of O_2 evolution was further improved by the impregnation of aqueous Cs_2CO_3 solution followed by calcination in air at 773 K. Interestingly, the rate of O_2 evolution over the Cs-impregnated sample was much enhanced in the second run (196 μmol h^{-1}) compared to that in the first run (117 μmol h^{-1}).

Table 6. Photocatalytic O_2 Evolution on Cs-Modified WO_3 Photocatalyst Prepared by HT and IMP Methods with Cs_2CO_3 Aqueous Solution[a] (Reproduced with Permission from ref 138, Copyright 2010 American Chemical Society)

photocatalyst	surface modification condition	activity (μmol h^{-1})
WO_3 (as commercially available)		18
WO_3[b]	HT (393 K in H_2O)	63
Cs−WO_3[b]	HT (393 K in Cs_2CO_3 aq)	92
Cs−WO_3[b]	HT (393 K in H_2O) and then IMP (773 K with Cs_2CO_3 aq)	117
		196[c]

[a]Catalyst, 0.4 g; reactant solution, 2.1 mM $Fe_2(SO_4)_3$ 300 mL; light source, 300 Xe-arc lamp (λ > 420 nm); reaction cell, side irradiation cell. Initial pH of reactant solution was always adjusted to be pH 2.3 using sulfuric acid. [b]WO_3 was calcined at 973 K for 2 h in air as a pretreatment. [c]The activity at the second run.

As seen in Figure 55, the total amount of O_2 evolved on Cs-modified WO_3 reached 315 μmol, agreeing with the stoichiometric amount expected from the amount of Fe^{3+} (1260 μmol) in the initial solution. Such stoichiometric O_2 generation indicates high selectivity of Cs-modified WO_3 photocatalyst toward water oxidation by holes (i.e., low selectivity toward backward oxidation of Fe^{2+}). Results about material characterization on such Cs-modified WO_3 photocatalysts and photoanodes revealed that "ion-exchangeable sites" were formed on the WO_3 surface by incorporating Cs cations via hydrothermal or impregnation treatment with Cs_2CO_3. The Cs cations incorporated could be easily replaced by H^+ via acid-treatment as well as during the reaction in aqueous $Fe_2(SO_4)_3$ solution with low pH (~2). Then, the H^+-exchanged sites strongly absorbed water molecules as H_3O^+, which were more readily oxidized to O_2 by the photogenerated holes. It was also suggested that Fe^{2+} cations occupy a part of "ion-exchangeable sites", which enhances the electron transfer

DOI: 10.1021/acs.chemrev.7b00286
Chem. Rev. 2018, 118, 5201−5241

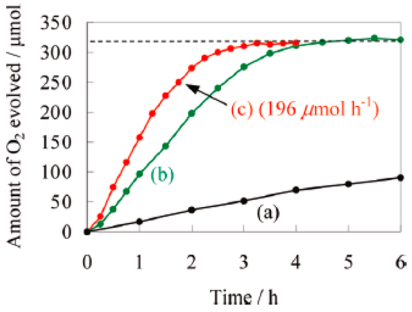

Figure 55. Photocatalytic O_2 evolution over (a) WO_3 without Cs-treatment, (b) Cs-WO_3 (first run) prepared by the IMP method, and (c) Cs-WO_3 (second run) under visible light irradiation. The dashed line shows the upper limit of O_2 evolution expected from the amount of Fe^{3+} (1260 μmol) added to the solutions. The second run reaction was performed by exchanging the reactant solution of the first run with fresh $Fe_2(SO_4)_3$ aqueous solution. Reproduced with permission from ref 138. Copyright 2010 American Chemical Society.

from WO_3 bulk to Fe^{3+} cations on the surface. Consequently, the rate of O_2 evolution on WO_3 photocatalysts with Fe^{3+}/Fe^{2+} redox couple is much enhanced, resulting in quite high quantum yield of 19% at 420 nm.[138]

Miseki et al. also demonstrated that such Cs-modified WO_3 photocatalysts could work as efficient OEPs with various redox couples such as IO_3^-/I^- and I_3^-/I^-, not only Fe^{3+}/Fe^{2+}.[80] As seen in Table 7, the rate of O_2 evolution on PtO_x-loaded WO_3

Table 7. Photocatalytic Water Oxidation over Various Treated WO_3 in IO_3^- Aqueous Solution[a] (Reproduced with Permission from ref 80, Copyright 2013 The Royal Society of Chemistry)

catalyst[b]	surface treatment	O_2 production rate (μmol h^{-1})
WO_3		0
PtO_x/WO_3		31
PtO_x/H−Cs−WO_3	done	126
PtO_x/H−Cs−WO_3[c]	done	50

[a]Catalyst, 0.4 g; reactant solution, 0.7 mM $NaIO_3$ aq soln (300 mL); light source, 300 W Xe-lamp (λ > 420 nm). Initial pH of reactant solutions were pH 6.8 without adjustment. [b]Amounts of PtOx and Cs^+ loaded are 0.5 wt % and 1.0 mol %, respectively. [c]PtO_x/H−Cs−WO_3 was calcined at 573 K for 30 min in air after H^+-exchange.

photocatalyst was much increased by Cs-modification. The activity of Cs-modified WO_3 was drastically lowered by the subsequent calcination in air at 573 K, implying that the ion-exchangeable sites formed via Cs modification absorb water molecules, similar to the case of Fe^{3+}/Fe^{2+} redox system, and facilitate water oxidation to O_2.

Interestingly, the Cs-modification enables the PtO_x/WO_3 photocatalyst to generate O_2 even in the presence of I_3^- electron acceptor. As seen in Figure 56, unmodified PtO_x/WO_3 photocatalyst shows negligibly low activity for O_2 evolution with I_3^- electron acceptor, as previously reported. Such low activity of conventional PtO_x/WO_3 photocatalyst with I_3^- is one of the biggest issues in Z-scheme water splitting with IO_3^-/I^- redox couple because I_3^- anions readily generate and accumulate under acidic (or even neutral) conditions. However, the Cs-modified WO_3 photocatalysts exhibit surprisingly high activity for O_2 evolution as seen in Figure 56; the O_2 evolution continues with an almost steady rate up to the expected amounts. Consequently, Z-scheme water splitting

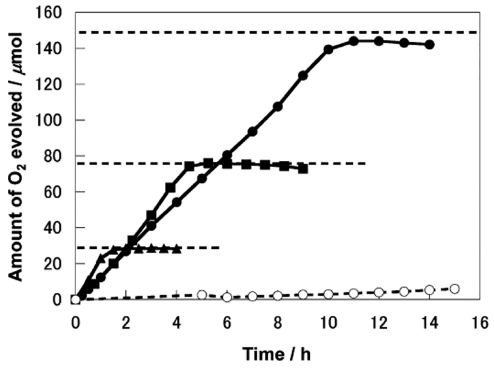

Figure 56. Time courses of the photocatalytic O_2 evolution over PtO_x/H−Cs−WO_3 (solid line) and PtO_x/WO_3 (dotted line) suspended in the solutions containing 10 mM NaI and different concentrations of I_3^- (circles, 1 mM; squares, 0.5 mM; triangles, 0.2 mM). Catalyst, 0.4 g; reactant solution, 300 mL; light source, 300 W Xe lamp attached with L-42 cutoff filter. The dashed lines (30, 75, and 150 μmol) show the upper limits of O_2 evolution (four-electron oxidation reaction) expected from the amount of I_2 (I_3^-) (reduced by two electrons) added to the solutions. Reproduced with permission from ref 80. Copyright 2013 The Royal Society of Chemistry.

proceeds steadily with much higher rates of gas evolution by employing such Cs-modified WO_3 as an OEP coupled with Pt/$SrTiO_3$:Cr,Ta as HEP in aqueous NaI solutions with wider range of pH, as seen in Figure 57 for example.

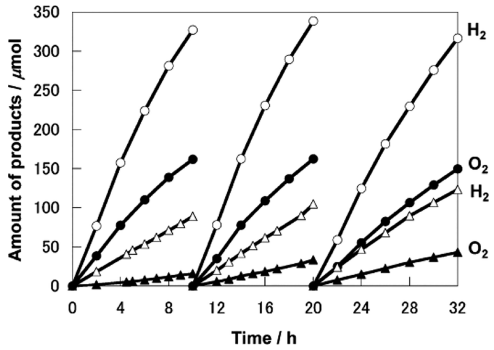

Figure 57. Time courses of photocatalytic evolution of H_2 and O_2 using a mixture of 0.2 g of Pt/$SrTiO_3$:Cr Ta as the H_2 evolution photocatalyst and 0.4 g of PtO_x/H−Cs−WO_3 (circle plots) or PtO_x/WO_3 (triangle plots) as the O_2 evolution photocatalyst suspended in 10 mM NaI aqueous solution (300 mL, pH 6.8). Light source: 300W Xe lamp attached with L42 cutoff filter. Reproduced with permission from ref 80. Copyright 2013 The Royal Society of Chemistry.

Developing adsorption-controlled photocatalyst particles will be another effective strategy for improving the efficiency of Z-scheme water splitting with dissolved redox couple. Tomita et al. recently demonstrated that the WO_3 particles with selectively exposed faces exhibited better selectivity for O_2 evolution with Fe^{3+}/Fe^{2+} redox couple.[91] As shown in Figure 58, the WO_3 particles prepared via hydrothermal reaction at greater than 255 °C (HT-255 and HT-315) have rectangular-like shapes with considerably flat surfaces. It was found that the HT-315 sample, which was prepared at 315 °C, exhibited favorable adsorption property to Fe^{3+}/Fe^{2+} redox couple compared to commercial samples (K-WO_3 and S-WO_3). For example, the HT-315 sample adsorbed much higher amount of Fe^{3+} (~7.0 μmol g^{-1}) than commercial WO_3 sample (e.g., ~1.1 μmol g^{-1} for K-WO_3) when compared at low concentrations of

DOI: 10.1021/acs.chemrev.7b00286
Chem. Rev. 2018, 118, 5201−5241

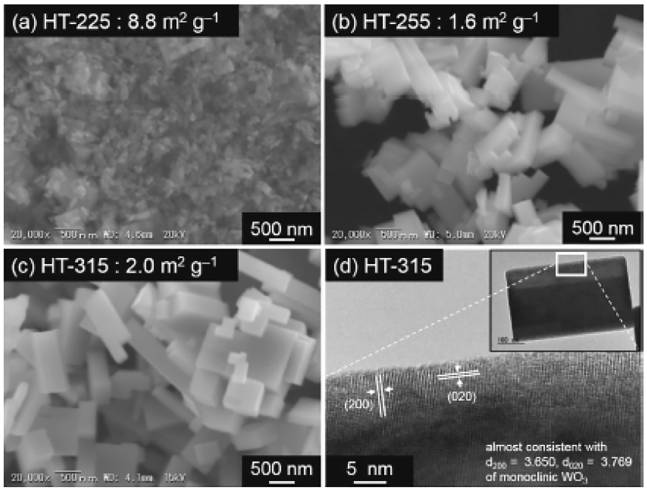

Figure 58. (a–c) SEM images of WO_3 samples prepared via hydrothermal reaction at different temperatures (reaction time, 4 h). (d) TEM image of HT-315. Reproduced with permission from ref 91. Copyright 2016 The Chemical Society of Japan.

Fe^{3+} (1.6 mM), in spite of the smaller specific surface area, as seen in Figure 59. On the other hand, the amount of Fe^{2+} adsorbed on the HT-315 sample was slightly but appreciably smaller than that on K-WO_3.

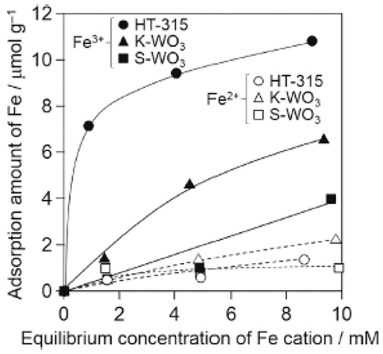

Figure 59. Adsorption isotherm (at 20 °C) of Fe cation on the surface of various WO_3 samples in aqueous solution with different concentration of $FeCl_3$ or $FeCl_2$ (amount of WO_3, 0.1 g; amount of solvent, 10 mL; time for mixing in dark under inert gas atmosphere, 15 h). Reproduced with permission from ref 91. Copyright 2016 The Chemical Society of Japan.

Consequently, the HT-315 showed higher rates and selectivity for O_2 evolution than commercial ones even with decreased Fe^{3+} and increased Fe^{2+} concentrations, as clearly seen in Figure 60. The efficiency of Z-scheme water splitting was indeed improved by employing this HT-315 sample as OEP couples with Ru/$SrTiO_3$:Rh as a HEP in the presence of Fe^{3+}/Fe^{2+} redox couple.[91]

5.3. Morphology Control and Heterojunctions

The morphology of photocatalysts also influences the properties, and generally a smaller particle size or higher crystallinity are believed to benefit the performance.[139] For example, the surface structure and particle size of $NaTaO_3$ can be tuned from 4 to 0.1 μm by doping with lanthanum and alkaline earth metal ions, resulting in an order of magnitude enhancement of water splitting activity.[140,141] A proper control of morphology also results in the enhancement of Z-scheme water splitting systems.

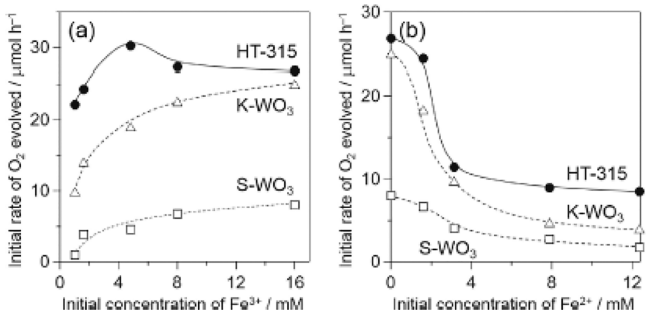

Figure 60. (a) Influence of Fe^{3+} concentration on the rate of O_2 evolution under light irradiation. (b) Initial rate of O_2 evolution on various WO_3 photocatalysts suspended in aqueous solutions containing Fe^{3+} (16 mM) and Fe^{2+} (0, 1.6, 3.1, 7.9, and 12.4 mM) under light irradiation (pH 2.1 adjusted with HCl). Reproduced with permission from ref 91. Copyright 2016 The Chemical Society of Japan.

One interesting example is the "nature-inspired" architecture CdS/Au/TiO_2 system.[142] Ding et al. investigated the black butterfly wing scale and realized that such a quasi-honeycomb (QH) morphology could promote a significant increase in light absorbance. The authors managed to synthesize TiO_2 with a QH structure using the wing of the black butterfly as an organic template, creating three different varieties of templates (wing, plate, and scale). CdS/Au/TiO_2 with wing architecture morphology exhibited a 230% increase in comparison to plate architecture based TiO_2, indicating that morphology control is of importance.

The construction of heterojunction is another commonly used strategies to control the properties of photocatalysts for superior performance including suppressed charge recombination.[29] An example is $(MgTa_2O_{6-x}N_y/TaON)-(IO_3^-/I^-)-(PtO_x/WO_3)$; a $MgTa_2O_{6-x}N_y$/TaON junction demonstrated 7 or 360 times higher activity than pure TaON and $MgTa_2O_{6-x}N_y$ in the presence of Pt.[83] Compared to the mechanically mixed powder of both, the heterojunction structure exhibited a 2-fold increase in activity due to a much more intimate interfacial contact. Both the mixed and junction samples were found to have a prolonged lifetime of charge carries according to time-resolved IR spectra, but the latter had a smaller defect density according to UV/vis spectra. SEM results also proved that the photodeposited Pt was on the surface of TaON, indicating the electron transfer from $MgTa_2O_{6-x}N_y$ to TaON enhanced charge separation. The advantages of such junctions compared to single HEP results in a benchmark AQY of 6.8% in Z-scheme water splitting in presence of liquid mediators.

6. CONCLUSIONS AND OUTLOOK

In this review article, following a short introduction of the conception of Z-scheme systems, we have thoroughly reviewed the recent progress on visible light-driven Z-scheme water splitting systems, with specific focuses on the recent developments of semiconductor materials, redox mediators, and the function of cocatalysts. Since the turn of the 21st century, various semiconductors, including metal oxides, (oxy)nitrides, (oxy)sulfides, oxyhalides, organic dyes, and carbon based nitrides, have been successfully incorporated into Z-scheme systems with a variety of different redox couples. The introduction of nonoxide semiconductors into Z-scheme water splitting systems has extended the available wavelengths

DOI: 10.1021/acs.chemrev.7b00286
Chem. Rev. 2018, 118, 5201–5241

up to 700 nm in comparison to conventional water splitting with one photocatalyst.

Among the three types of Z-scheme systems, the highest AQY in a liquid mediator system of 6.8% at 420 nm was achieved in a $MgTa_2O_{6-x}N_y$/TaON)−(IO_3^-/I^-)−(PtO_x/WO_3) system. An AQY of 1.7% at 420 nm was reported in the $BiVO_4$−Ru/$SrTiO_3$:Rh system without a need of shuttle mediator, resulting in an STH conversion efficiency of 0.12%. The most recent solid mediator system (Cr_2O_3/Ru-modified $SrTiO_3$:La,Rh/C/$BiVO_4$:Mo sheets) represented the record STH energy conversion efficiency of 1.2% at 331 K under 10 KPa. Although the three systems have individual advantages and disadvantages, they could be developed to meet the required solar to fuel conversion efficiency of 10% if all components could be optimized. Taking the recent solid mediator system ($SrTiO_3$:La,Rh/Au nanoparticle/$BiVO_4$:Mo sheets) as an example, one of its unsatisfactory is that the STH efficiency of 1.1% under 10 KPa dramatically declines as the pressure goes up due to back reactions, while later on the same group replaced Au layer by carbon film and maintained an STH of 1.0% under higher pressure of 90 KPa, showing the importance of a proper mediator to suppress the back reactions.[107] The solid shuttle mediator system at present represents the best efficiency to date and therefore should be further researched with impetus. To develop efficient OEPs and HEPs, new strategies for achieving efficient separation of electrons and holes in powdered semiconductor photocatalysts, such as p−n junctions or specifically exposed crystal facets, should be pursued continuously, along with developing new semiconductor materials with light absorption to longer wavelengths in the visible region. Polymer photocatalysts with readily tunable bandgaps and band positions could be another option to investigated, provided stability was on par with that of for example carbon nitride.

Although new redox couples such as metal complexes and polyoxometalates have been proven to work in the Z-scheme water splitting, most of these systems still require an IO_3^-/I^- or Fe^{3+}/Fe^{2+} redox couple. However, both redox couples possess intrinsic problems in improving the total efficiency of water splitting, for example, the requirement of an efficient cocatalyst (e.g., Pt, PtOx) for reduction of IO_3^- on O_2-evolving photocatalysts, attributed to the nature of the six-electron reduction. The limited choice of OEPs that can function with IO_3^-/I^- under visible light and proper pH range, other than WO_3, is also a problem. Although some metal (oxy)nitrides such as TaON and Ta_3N_5 can be used as OEPs after appropriate surface modifications, their long-term stabilities are insufficient because of the occurrence of self-oxidative deactivation. One of the most critical issues with the Fe^{3+}/Fe^{2+} redox system, along with a strict pH operation window (i.e., below 2.5), is the limited choice of active H_2-evolving photocatalysts. Only $SrTiO_3$:Rh and g-C_3N_4 have been demonstrated so far. Thus, only wavelengths of up to ∼550 nm can be used for H_2 evolution. Hence, the development of versatile and efficient redox couples will be a key step in achieving highly efficient water splitting. In such a development of redox couples, the control over reaction selectivity (forward or backward) by the intrinsic adsorption property of the redox couple, designing the surface properties of photocatalysts, and introducing reaction sites with high selectivity, will be other key issues. In parallel, solid mediators can be discovered by not only considering the electron conductivity but also their work functions to match with two separate photocatalysts. Clearly conductive and low cost carbon based materials such as graphene could be a good option.

So far, the charge transfer dynamics in the entire Z-scheme system has been less investigated although there are a few studies focusing on the so-called half Z-scheme. This poor understanding is one factor limiting the progress of the Z-scheme system for solar fuel synthesis, which should be put more efforts in future. Nevertheless, a Z-scheme promises a higher maximum solar to fuel conversion efficiency (∼40%) than a single photocatalyst system (∼30%),[22] which is a major driving force for development. Furthermore, such Z-scheme systems have the potential to spatially separate H_2 and O_2 if a suitable reactor design is conceived. However, the current solar to fuel conversion efficiency is still very moderate (e.g., only μmol/hour gas evolution rates) for a Z-scheme and a scale-up process could be considered when a very efficient system is developed. Thus, construction of tandem systems that enable the utilization of different wavelengths on each photocatalyst (e.g., short wavelength on OEP and longer wavelengths on HEP), as well as separate production of H_2 and O_2, will demonstrate a practical H_2 production system based on the mechanism of a double excitation Z-scheme.

AUTHOR INFORMATION

Corresponding Authors

*J.W.: E-mail, junwang.tang@ucl.ac.uk.
*R.A.: E-mail, ryu-abe@scl.kyoto-u.ac.jp.

ORCID

Yiou Wang: 0000-0001-8702-5304
Hajime Suzuki: 0000-0002-8891-2033
David James Martin: 0000-0002-3549-4202
Junwang Tang: 0000-0002-2323-5510

Notes

The authors declare no competing financial interest.

Biographies

Yiou Wang is currently in a doctorate program under the supervision of Prof. Junwang Tang at the Department of Chemical Engineering, UCL, after receiving his B.Sc. in Chemistry from Peking University, China, in 2014. Yiou's Ph.D. project focuses on the application of low-cost and tunable polymeric semiconductors for solar energy conversion such as overall water splitting and CO_2 conversion. Yiou's interests also include efficient microwave-assisted synthetic techniques and mechanism investigation via time-resolved spectroscopies.

Hajime Suzuki received B.Sc. (2013) and M.Sc. (2015) degrees from Kyoto University. He is currently in a doctorate course in Kyoto University under the supervision of Professor Ryu Abe. His current research focuses on the development of novel photocatalysts and cocatalysts for water splitting.

Jijia Xie received his B.Eng. degree from Sichuan University in 2014. After one-year of M.Sc. study at UCL, he became a Ph.D. research student in the Solar Energy and Advanced Materials Group at UCL Chemical Engineering in 2015. His current research focuses on the photocatalytic conversion of methane.

Osamu Tomita received his B.Sc. (2006) from Tokyo University of Science, and his M.Sc. (2009) and Ph.D. (2012) from Hokkaido University. He then worked as a postdoctoral fellow (2012−2016) at Kyoto University. He is currently an assistant professor (2017−present) at Kyoto University. His research interests are photocatalytic

DOI: 10.1021/acs.chemrev.7b00286
Chem. Rev. 2018, 118, 5201−5241

water splitting and photocatalytic selective oxidation of organic compounds.

David James Martin studied Physics at the University of Liverpool (M.Phys.), and then completed a Ph.D. at UCL under the supervision of Prof. Junwang Tang, focusing on developing new photocatalysts for water splitting. He then accepted a postdoctoral position under Prof. Andy Beale and used X-ray scattering and absorption techniques to study heterogeneous catalysts under operando conditions. He currently works as a senior researcher in the group of Prof. Moniek Tromp at the University of Amsterdam, applying X-ray absorption and emission techniques to study homogeneous and heterogeneous catalysts, for applications such as selective oligomerization of ethylene, partial oxidation of propene, the low temperature WGS reaction, and electrochemical water oxidation.

Masanobu Higashi received his B.Sc. (2003), M.Sc. (2005) from Tokyo University of Science, and Ph.D. (2008) from the University of Tokyo. He then worked as a postdoctoral fellow (2008−2012) at the Catalysis Research Center, Hokkaido University, and at Kyoto University (2012). After that, he worked as an assistant professor (2012−present) at Kyoto University. His current research focuses on the development of photocatalytic and photoelectrochemical water splitting.

Dan Kong is a Ph.D. student under supervision of Prof. Junwang Tang at the Department of Chemical Engineering, UCL, after receiving her master's degree (2014) in the Department of Material Science at Engineering, Zhejiang University. Her current research focuses on visible light driven water splitting by polymer photocatalysts and its reaction kinetics.

Prof. Ryu Abe received his B.Sc. (1996), M.Sc. (1998), and Ph.D. (2001) degrees from Tokyo Institute of Technology. He then worked as a postdoctoral fellow (2001−2002) and as a researcher (2002−2005) at the National Institute of Advanced Industrial Science and Technology (AIST), Japan. In 2005, his academic career as an associate professor began at the Catalysis Research Center, Hokkaido University. He was then promoted to a Professor at Graduate School of Engineering, Kyoto University, in 2012. His research is mainly focused on the development of new photocatalysts for water splitting and environmental purification.

Prof. Junwang Tang is the Director of UCL Materials Hub and Professor of Chemistry and Material Engineering in the Department of Chemical Engineering at UCL. He obtained his Ph.D. in Physical Chemistry in 2001. After that, he was appointed as a JSPS Fellow at NIMS, Japan, and a senior researcher in the Department of Chemistry at Imperial College London, working on solar fuels synthesis and mechanistic studies by time-resolved spectroscopies. After that, he took a faculty position at UCL. His current research interests lie in photocatalytic small molecules activation (e.g., CH_4, N_2, H_2O, CO_2) and mechanistic aspects of solar energy conversion and water treatment, alongside microwave intensified fluidic chemistry. He is also a Fellow of the RSC.

ACKNOWLEDGMENTS

Y.W. and D.K. thank the CSC for Ph.D. funding. J.T. acknowledges the financial support from EPSRC (EP/N009533/1), the Leverhulme Trust (RPG-2017-122), and Royal Society—Newton Advanced Fellowship grant (NA170422). R.A also acknowledges the supported by JSPS KAKENHI grant no. 17H06439 in Scientific Research on Innovative Areas "Innovations for Light-Energy Conversion (I^4LEC)".

REFERENCES

(1) Lewis, N. S.; Crabtree, G.; Basic Research Needs for Solar Energy Utilization: Report of the Basic Energy Sciences Workshop on Solar Energy Utilization, April 18−21, 2005, US Department of Energy, Office of Basic Energy Science: Washington DC, 2005.
(2) Hisatomi, T.; Kubota, J.; Domen, K. Recent advances in semiconductors for photocatalytic and photoelectrochemical water splitting. *Chem. Soc. Rev.* **2014**, *43* (22), 7520−7535.
(3) Kudo, A.; Miseki, Y. Heterogeneous photocatalyst materials for water splitting. *Chem. Soc. Rev.* **2009**, *38* (1), 253−278.
(4) Hess, G. Solar Energy Needs Major Push. *Chem. Eng. News* **2005**, *83*, 12.
(5) Maeda, K.; Domen, K. New Non-Oxide Photocatalysts Designed for Overall Water Splitting under Visible Light. *J. Phys. Chem. C* **2007**, *111* (22), 7851−7861.
(6) Wang, S.; Yun, J.-H.; Luo, B.; Butburee, T.; Peerakiatkhajohn, P.; Thaweesak, S.; Xiao, M.; Wang, L. Recent Progress on Visible Light Responsive Heterojunctions for Photocatalytic Applications. *J. Mater. Sci. Technol.* **2017**, *33* (1), 1−22.
(7) Baur, E.; Rebmann, A. Über Versuche zur Photolyse des Wassers. *Helv. Chim. Acta* **1921**, *4* (1), 256−262.
(8) Maeda, K.; Teramura, K.; Lu, D.; Takata, T.; Saito, N.; Inoue, Y.; Domen, K. Photocatalyst releasing hydrogen from water. *Nature* **2006**, *440* (7082), 295−295.
(9) Fujishima, A.; Honda, K. Electrochemical Photolysis of Water at a Semiconductor Electrode. *Nature* **1972**, *238* (5358), 37−38.
(10) Chen, C.; Ma, W.; Zhao, J. Semiconductor-mediated photodegradation of pollutants under visible-light irradiation. *Chem. Soc. Rev.* **2010**, *39* (11), 4206−4219.
(11) Abe, R. Development of a new system for photocatalytic water splitting into H_2 and O_2 under visible light irradiation. *Bull. Chem. Soc. Jpn.* **2011**, *84* (10), 1000−1030.
(12) Chen, D.; Ye, J. Photocatalytic H_2 evolution under visible light irradiation on $AgIn_5S_8$ photocatalyst. *J. Phys. Chem. Solids* **2007**, *68* (12), 2317−2320.
(13) Maeda, K.; Takata, T.; Hara, M.; Saito, N.; Inoue, Y.; Kobayashi, H.; Domen, K. GaN: ZnO solid solution as a photocatalyst for visible-light-driven overall water splitting. *J. Am. Chem. Soc.* **2005**, *127* (23), 8286−8287.
(14) Sato, J.; Saito, N.; Yamada, Y.; Maeda, K.; Takata, T.; Kondo, J. N.; Hara, M.; Kobayashi, H.; Domen, K.; Inoue, Y. RuO_2-Loaded β-Ge_3N_4 as a Non-Oxide Photocatalyst for Overall Water Splitting. *J. Am. Chem. Soc.* **2005**, *127* (12), 4150−4151.
(15) Zhang, G.; Lan, Z.-A.; Lin, L.; Lin, S.; Wang, X. Overall water splitting by Pt/g-C_3N_4 photocatalysts without using sacrificial agents. *Chem. Sci.* **2016**, *7* (5), 3062−3066.
(16) Konta, R.; Ishii, T.; Kato, H.; Kudo, A. Photocatalytic Activities of Noble Metal Ion Doped $SrTiO_3$ under Visible Light Irradiation. *J. Phys. Chem. B* **2004**, *108* (26), 8992−8995.
(17) Yang, M.; Huang, X.; Yan, S.; Li, Z.; Yu, T.; Zou, Z. Improved hydrogen evolution activities under visible light irradiation over $NaTaO_3$ codoped with lanthanum and chromium. *Mater. Chem. Phys.* **2010**, *121* (3), 506−510.
(18) Ferreira, K. N.; Iverson, T. M.; Maghlaoui, K.; Barber, J.; Iwata, S. Architecture of the Photosynthetic Oxygen-Evolving Center. *Science* **2004**, *303* (5665), 1831−1838.
(19) Sayama, K.; Yoshida, R.; Kusama, H.; Okabe, K.; Abe, Y.; Arakawa, H. Photocatalytic decomposition of water into H_2 and O_2 by a two-step photoexcitation reaction using a WO_3 suspension catalyst and an Fe^{3+}/Fe^{2+} redox system. *Chem. Phys. Lett.* **1997**, *277* (4), 387−391.
(20) Wang, X.; Liu, G.; Chen, Z.-G.; Li, F.; Wang, L.; Lu, G. Q.; Cheng, H.-M. Enhanced photocatalytic hydrogen evolution by prolonging the lifetime of carriers in ZnO/CdS heterostructures. *Chem. Commun.* **2009**, *23*, 3452−3454.
(21) Wang, X.; Liu, G.; Wang, L.; Chen, Z. G.; Lu, G. Q. M.; Cheng, H. M. ZnO−CdS@ Cd heterostructure for effective photocatalytic hydrogen generation. *Adv. Energy Mater.* **2012**, *2* (1), 42−46.

DOI: 10.1021/acs.chemrev.7b00286
Chem. Rev. 2018, 118, 5201−5241

(22) Hanna, M. C.; Nozik, A. J. Solar conversion efficiency of photovoltaic and photoelectrolysis cells with carrier multiplication absorbers. *J. Appl. Phys.* **2006**, *100* (7), 074510.
(23) Thilagam, A. Natural light harvesting systems: unraveling the quantum puzzles. *J. Math. Chem.* **2015**, *53* (2), 466−494.
(24) Andrews, D.; Scholes, G.; Wiederrecht, G. *Comprehensive Nanoscience and Technology*; Academic Press: New York, 2010.
(25) Jones, W.; Martin, D. J.; Caravaca, A.; Beale, A. M.; Bowker, M.; Maschmeyer, T.; Hartley, G.; Masters, A., A comparison of photocatalytic reforming reactions of methanol and triethanolamine with Pd supported on titania and graphitic carbon nitride. *Appl. Catal., B* **2017**, 10.1016/j.apcatb.2017.01.042.
(26) Wang, Y.; Bayazit, M. K.; Moniz, S. J. A.; Ruan, Q.; Lau, C. C.; Martsinovich, N.; Tang, J. Linker-controlled polymeric photocatalyst for highly efficient hydrogen evolution from water. *Energy Environ. Sci.* **2017**, *10* (7), 1643−1651.
(27) Turner, J. A. A Realizable Renewable Energy Future. *Science* **1999**, *285* (5428), 687−689.
(28) Tang, J.; Durrant, J. R.; Klug, D. R. Mechanism of Photocatalytic Water Splitting in TiO_2. Reaction of Water with Photoholes, Importance of Charge Carrier Dynamics, and Evidence for Four-Hole Chemistry. *J. Am. Chem. Soc.* **2008**, *130* (42), 13885−13891.
(29) Moniz, S. J. A.; Shevlin, S. A.; Martin, D. J.; Guo, Z.-X.; Tang, J. Visible-light driven heterojunction photocatalysts for water splitting − a critical review. *Energy Environ. Sci.* **2015**, *8* (3), 731−759.
(30) Kudo, A.; Omori, K.; Kato, H. A Novel Aqueous Process for Preparation of Crystal Form-Controlled and Highly Crystalline $BiVO_4$ Powder from Layered Vanadates at Room Temperature and Its Photocatalytic and Photophysical Properties. *J. Am. Chem. Soc.* **1999**, *121* (49), 11459−11467.
(31) Martin, D. J.; Umezawa, N.; Chen, X.; Ye, J.; Tang, J. Facet engineered Ag_3PO_4 for efficient water photooxidation. *Energy Environ. Sci.* **2013**, *6* (11), 3380−3386.
(32) Zheng, H.; Ou, J. Z.; Strano, M. S.; Kaner, R. B.; Mitchell, A.; Kalantar-zadeh, K. Nanostructured Tungsten Oxide − Properties, Synthesis, and Applications. *Adv. Funct. Mater.* **2011**, *21* (12), 2175−2196.
(33) Krishnan, C. V.; Brunschwig, B. S.; Creutz, C.; Sutin, N. Homogeneous catalysis of the photoreduction of water. 6. Mediation by polypyridine complexes of ruthenium(II) and cobalt(II) in alkaline media. *J. Am. Chem. Soc.* **1985**, *107* (7), 2005−2015.
(34) Browne, M. P.; Nolan, H.; Duesberg, G. S.; Colavita, P. E.; Lyons, M. E. G. Low-Overpotential High-Activity Mixed Manganese and Ruthenium Oxide Electrocatalysts for Oxygen Evolution Reaction in Alkaline Media. *ACS Catal.* **2016**, *6* (4), 2408−2415.
(35) Martin, D. J.; Reardon, P. J.; Moniz, S. J.; Tang, J. Visible light-driven pure water splitting by a nature-inspired organic semiconductor-based system. *J. Am. Chem. Soc.* **2014**, *136* (36), 12568−12571.
(36) Kato, H.; Hori, M.; Konta, R.; Shimodaira, Y.; Kudo, A. Construction of Z-scheme Type Heterogeneous Photocatalysis Systems for Water Splitting into H_2 and O_2 under Visible Light Irradiation. *Chem. Lett.* **2004**, *33* (10), 1348−1349.
(37) Sayama, K.; Mukasa, K.; Abe, R.; Abe, Y.; Arakawa, H. A new photocatalytic water splitting system under visible light irradiation mimicking a Z-scheme mechanism in photosynthesis. *J. Photochem. Photobiol., A* **2002**, *148* (1−3), 71−77.
(38) Sayama, K.; Mukasa, K.; Abe, R.; Abe, Y.; Arakawa, H. Stoichiometric water splitting into H_2 and O_2 using a mixture of two different photocatalysts and an IO_3^-/I^- shuttle redox mediator under visible light irradiation. *Chem. Commun.* **2001**, *23*, 2416−2417.
(39) Enesca, A.; Andronic, L.; Duta, A.; Manolache, S. Optical properties and chemical stability of WO_3 and TiO_2 thin films photocatalysts. *Rom. J. Inf. Sci. Technol.* **2007**, *10* (3), 269−277.
(40) Abe, R.; Sayama, K.; Sugihara, H. Development of New Photocatalytic Water Splitting into H_2 and O_2 using Two Different Semiconductor Photocatalysts and a Shuttle Redox Mediator IO_3^-/I^-. *J. Phys. Chem. B* **2005**, *109* (33), 16052−16061.
(41) Abe, R.; Shinmei, K.; Hara, K.; Ohtani, B. Robust dye-sensitized overall water splitting system with two-step photoexcitation of coumarin dyes and metal oxide semiconductors. *Chem. Commun.* **2009**, *24*, 3577−3579.
(42) Lim, A. R.; Choh, C.S. H.; Jang, M. S. Prominent ferroelastic domain walls in $BiVO_4$ crystal. *J. Phys.: Condens. Matter* **1995**, *7* (37), 7309−7323.
(43) Marschall, R. Semiconductor Composites: Strategies for Enhancing Charge Carrier Separation to Improve Photocatalytic Activity. *Adv. Funct. Mater.* **2014**, *24* (17), 2421−2440.
(44) Tokunaga, S.; Kato, H.; Kudo, A. Selective Preparation of Monoclinic and Tetragonal $BiVO_4$ with Scheelite Structure and Their Photocatalytic Properties. *Chem. Mater.* **2001**, *13* (12), 4624−4628.
(45) Maeda, K. Z-Scheme Water Splitting Using Two Different Semiconductor Photocatalysts. *ACS Catal.* **2013**, *3* (7), 1486−1503.
(46) Chun, W.-J.; Ishikawa, A.; Fujisawa, H.; Takata, T.; Kondo, J. N.; Hara, M.; Kawai, M.; Matsumoto, Y.; Domen, K. Conduction and Valence Band Positions of Ta_2O_5, TaON, and Ta_3N_5 by UPS and Electrochemical Methods. *J. Phys. Chem. B* **2003**, *107* (8), 1798−1803.
(47) Hitoki, G.; Takata, T.; Kondo, J. N.; Hara, M.; Kobayashi, H.; Domen, K. An oxynitride, TaON, as an efficient water oxidation photocatalyst under visible light irradiation ($\lambda \leq 500$ nm). *Chem. Commun.* **2002**, *16*, 1698−1699.
(48) Higashi, M.; Abe, R.; Ishikawa, A.; Takata, T.; Ohtani, B.; Domen, K. Z-scheme Overall Water Splitting on Modified-TaON Photocatalysts under Visible Light ($\lambda < 500$ nm). *Chem. Lett.* **2008**, *37* (2), 138−139.
(49) Martin, D. J. *Investigation into High Efficiency Visible Light Photocatalysts for Water Reduction and Oxidation*; Springer: New York, 2015.
(50) Maeda, K.; Abe, R.; Domen, K. Role and Function of Ruthenium Species as Promoters with TaON-Based Photocatalysts for Oxygen Evolution in Two-Step Water Splitting under Visible Light. *J. Phys. Chem. C* **2011**, *115* (7), 3057−3064.
(51) Tabata, M.; Maeda, K.; Higashi, M.; Lu, D.; Takata, T.; Abe, R.; Domen, K. Modified Ta_3N_5 Powder as a Photocatalyst for O_2 Evolution in a Two-Step Water Splitting System with an Iodate/Iodide Shuttle Redox Mediator under Visible Light. *Langmuir* **2010**, *26* (12), 9161−9165.
(52) Hitoki, G.; Ishikawa, A.; Takata, T.; Kondo, J. N.; Hara, M.; Domen, K. Ta_3N_5 as a Novel Visible Light-Driven Photocatalyst ($\lambda <$ 600 nm). *Chem. Lett.* **2002**, *31* (7), 736−737.
(53) Takata, T.; Hitoki, G.; Kondo, J. N.; Hara, M.; Kobayashi, H.; Domen, K. Visible-light-driven photocatalytic behavior of tantalum-oxynitride and nitride. *Res. Chem. Intermed.* **2007**, *33*, 13−25.
(54) Higashi, M.; Domen, K.; Abe, R. Highly Stable Water Splitting on Oxynitride TaON Photoanode System under Visible Light Irradiation. *J. Am. Chem. Soc.* **2012**, *134* (16), 6968−6971.
(55) Suzuki, H.; Tomita, O.; Higashi, M.; Abe, R. Tungstic acids H_2WO_4 and H_4WO_5 as stable photocatalysts for water oxidation under visible light. *J. Mater. Chem. A* **2017**, *5* (21), 10280−10288.
(56) Fujito, H.; Kunioku, H.; Kato, D.; Suzuki, H.; Higashi, M.; Kageyama, H.; Abe, R. Layered Perovskite Oxychloride Bi_4NbO_8Cl: A Stable Visible Light Responsive Photocatalyst for Water Splitting. *J. Am. Chem. Soc.* **2016**, *138* (7), 2082−2085.
(57) Abe, R.; Takata, T.; Sugihara, H.; Domen, K. Photocatalytic overall water splitting under visible light by TaON and WO_3 with an IO_3^-/I^- shuttle redox mediator. *Chem. Commun.* **2005**, *30*, 3829−3831.
(58) Nakamura, R.; Tanaka, T.; Nakato, Y. Oxygen photoevolution on a tantalum oxynitride photocatalyst under visible-light irradiation: How does water photooxidation proceed on a metal-oxynitride surface? *J. Phys. Chem. B* **2005**, *109* (18), 8920−8927.
(59) Abe, R.; Higashi, M.; Domen, K. Overall Water Splitting under Visible Light through a Two-Step Photoexcitation between TaON and WO_3 in the Presence of an Iodate−Iodide Shuttle Redox Mediator. *ChemSusChem* **2011**, *4* (2), 228−237.
(60) Higashi, M.; Abe, R.; Teramura, K.; Takata, T.; Ohtani, B.; Domen, K. Two step water splitting into H_2 and O_2 under visible light

DOI: 10.1021/acs.chemrev.7b00286
Chem. Rev. 2018, 118, 5201−5241

by $ATaO_2N$ (A = Ca, Sr, Ba) and WO_3 with shuttle redox mediator. *Chem. Phys. Lett.* **2008**, *452* (1−3), 120−123.
(61) Higashi, M.; Abe, R.; Takata, T.; Domen, K. Photocatalytic Overall Water Splitting under Visible Light Using $ATaO_2N$ (A = Ca, Sr, Ba) and WO_3 in a IO_3^-/I^- Shuttle Redox Mediated System. *Chem. Mater.* **2009**, *21* (8), 1543−1549.
(62) Abe, R.; Shinmei, K.; Koumura, N.; Hara, K.; Ohtani, B. Visible-light-induced water splitting based on two-step photoexcitation between dye-sensitized layered niobate and tungsten oxide photocatalysts in the presence of a triiodide/iodide shuttle redox mediator. *J. Am. Chem. Soc.* **2013**, *135* (45), 16872−16884.
(63) Wang, X.; Maeda, K.; Thomas, A.; Takanabe, K.; Xin, G.; Carlsson, J. M.; Domen, K.; Antonietti, M. A metal-free polymeric photocatalyst for hydrogen production from water under visible light. *Nat. Mater.* **2009**, *8* (1), 76−80.
(64) Martin, D. J.; Qiu, K.; Shevlin, S. A.; Handoko, A. D.; Chen, X.; Guo, Z.; Tang, J. Highly Efficient Photocatalytic H_2 Evolution from Water using Visible Light and Structure-Controlled Graphitic Carbon Nitride. *Angew. Chem., Int. Ed.* **2014**, *53* (35), 9240−9245.
(65) Ruan, Q.; Luo, W.; Xie, J.; Wang, Y.; Liu, X.; Bai, Z.; Carmalt, C. J.; Tang, J. A Nanojunction Polymer Photoelectrode for Efficient Charge Transport and Separation. *Angew. Chem., Int. Ed.* **2017**, *56* (28), 8221−8225.
(66) Zhang, G.; Zhang, M.; Ye, X.; Qiu, X.; Lin, S.; Wang, X. Iodine Modified Carbon Nitride Semiconductors as Visible Light Photocatalysts for Hydrogen Evolution. *Adv. Mater.* **2014**, *26* (5), 805−809.
(67) Zhang, J.; Zhang, M.; Sun, R. Q.; Wang, X. A facile band alignment of polymeric carbon nitride semiconductors to construct isotype heterojunctions. *Angew. Chem.* **2012**, *124* (40), 10292−10296.
(68) Zhang, J.; Sun, J.; Maeda, K.; Domen, K.; Liu, P.; Antonietti, M.; Fu, X.; Wang, X. Sulfur-mediated synthesis of carbon nitride: Band-gap engineering and improved functions for photocatalysis. *Energy Environ. Sci.* **2011**, *4* (3), 675−678.
(69) Zhang, Y.; Mori, T.; Ye, J.; Antonietti, M. Phosphorus-Doped Carbon Nitride Solid: Enhanced Electrical Conductivity and Photocurrent Generation. *J. Am. Chem. Soc.* **2010**, *132* (18), 6294−6295.
(70) Wang, Y.; Zhang, J.; Wang, X.; Antonietti, M.; Li, H. Boron- and Fluorine-Containing Mesoporous Carbon Nitride Polymers: Metal-Free Catalysts for Cyclohexane Oxidation. *Angew. Chem., Int. Ed.* **2010**, *49* (19), 3356−3359.
(71) Liu, G.; Niu, P.; Sun, C.; Smith, S. C.; Chen, Z.; Lu, G. Q.; Cheng, H.-M. Unique Electronic Structure Induced High Photoreactivity of Sulfur-Doped Graphitic C_3N_4. *J. Am. Chem. Soc.* **2010**, *132* (33), 11642−11648.
(72) Chen, X.; Zhang, J.; Fu, X.; Antonietti, M.; Wang, X. Fe-g-C_3N_4-Catalyzed Oxidation of Benzene to Phenol Using Hydrogen Peroxide and Visible Light. *J. Am. Chem. Soc.* **2009**, *131* (33), 11658−11659.
(73) Zhang, Y.; Thomas, A.; Antonietti, M.; Wang, X. Activation of Carbon Nitride Solids by Protonation: Morphology Changes, Enhanced Ionic Conductivity, and Photoconduction Experiments. *J. Am. Chem. Soc.* **2009**, *131* (1), 50−51.
(74) Niu, P.; Zhang, L. L.; Liu, G.; Cheng, H. M. Graphene-Like Carbon Nitride Nanosheets for Improved Photocatalytic Activities. *Adv. Funct. Mater.* **2012**, *22* (22), 4763−4770.
(75) Liu, J. H.; Zhang, T. K.; Wang, Z. C.; Dawson, G.; Chen, W. Simple pyrolysis of urea into graphitic carbon nitride with recyclable adsorption and photocatalytic activity. *J. Mater. Chem.* **2011**, *21* (38), 14398−14401.
(76) Zhao, W.; Maeda, K.; Zhang, F. X.; Hisatomi, T.; Domen, K. Effect of post-treatments on the photocatalytic activity of $Sm_2Ti_2S_2O_5$ for the hydrogen evolution reaction. *Phys. Chem. Chem. Phys.* **2014**, *16* (24), 12051−12056.
(77) Kato, T.; Hakari, Y.; Ikeda, S.; Jia, Q.; Iwase, A.; Kudo, A. Utilization of Metal Sulfide Material of $(CuGa)_{1-x}Zn_{2x}S_2$ Solid Solution with Visible Light Response in Photocatalytic and Photoelectrochemical Solar Water Splitting Systems. *J. Phys. Chem. Lett.* **2015**, *6* (6), 1042−1047.
(78) Maeda, K.; Higashi, M.; Lu, D. L.; Abe, R.; Domen, K. Efficient Nonsacrificial Water Splitting through Two-Step Photoexcitation by Visible Light using a Modified Oxynitride as a Hydrogen Evolution Photocatalyst. *J. Am. Chem. Soc.* **2010**, *132* (16), 5858−5868.
(79) Maeda, K.; Lu, D.; Domen, K. Solar-Driven Z-scheme Water Splitting Using Modified $BaZrO_3$−$BaTaO_2N$ Solid Solutions as Photocatalysts. *ACS Catal.* **2013**, *3* (5), 1026−1033.
(80) Miseki, Y.; Fujiyoshi, S.; Gunji, T.; Sayama, K. Photocatalytic water splitting under visible light utilizing I^{3-}/I^- and IO_3^-/I^- redox mediators by Z-scheme system using surface treated PtO_x/WO_3 as O_2 evolution photocatalyst. *Catal. Sci. Technol.* **2013**, *3* (7), 1750−1756.
(81) Hara, S.; Yoshimizu, M.; Tanigawa, S.; Ni, L.; Ohtani, B.; Irie, H. Hydrogen and Oxygen Evolution Photocatalysts Synthesized from Strontium Titanate by Controlled Doping and Their Performance in Two-Step Overall Water Splitting under Visible Light. *J. Phys. Chem. C* **2012**, *116* (33), 17458−17463.
(82) Tanigawa, S.; Irie, H. Visible-light-sensitive two-step overall water-splitting based on band structure control of titanium dioxide. *Appl. Catal., B* **2016**, *180*, 1−5.
(83) Chen, S.; Qi, Y.; Hisatomi, T.; Ding, Q.; Asai, T.; Li, Z.; Ma, S. S. K.; Zhang, F.; Domen, K.; Li, C. Efficient Visible-Light-Driven Z-Scheme Overall Water Splitting Using a $MgTa_2O_{6-x}N_y$/TaON Heterostructure Photocatalyst for H_2 Evolution. *Angew. Chem., Int. Ed.* **2015**, *54* (29), 8498−8501.
(84) Nakada, A.; Nishioka, S.; Vequizo, J. J. M.; Muraoka, K.; Kanazawa, T.; Yamakata, A.; Nozawa, S.; Kumagai, H.; Adachi, S.-i.; Ishitani, O.; Maeda, K. Solar-driven Z-scheme water splitting using tantalum/nitrogen co-doped rutile titania nanorod as an oxygen evolution photocatalyst. *J. Mater. Chem. A* **2017**, *5* (23), 11710−11719.
(85) Sasaki, Y.; Iwase, A.; Kato, H.; Kudo, A. The effect of co-catalyst for Z-scheme photocatalysis systems with an Fe^{3+}/Fe^{2+} electron mediator on overall water splitting under visible light irradiation. *J. Catal.* **2008**, *259* (1), 133−137.
(86) Kato, H.; Sasaki, Y.; Shirakura, N.; Kudo, A. Synthesis of highly active rhodium-doped $SrTiO_3$ powders in Z-scheme systems for visible-light-driven photocatalytic overall water splitting. *J. Mater. Chem. A* **2013**, *1* (39), 12327−12333.
(87) Niishiro, R.; Tanaka, S.; Kudo, A. Hydrothermal-synthesized $SrTiO_3$ photocatalyst codoped with rhodium and antimony with visible-light response for sacrificial H_2 and O_2 evolution and application to overall water splitting. *Appl. Catal., B* **2014**, *150-151*, 187−196.
(88) Suzuki, H.; Tomita, O.; Higashi, M.; Abe, R. Z-scheme water splitting into H_2 and O_2 using tungstic acid as oxygen-evolving photocatalyst under visible light irradiation. *Chem. Lett.* **2015**, *44* (8), 1134−1136.
(89) Kunioku, H.; Higashi, M.; Tassel, C.; Kato, D.; Tomita, O.; Kageyama, H.; Abe, R. Sillén−Aurivillius-related Oxychloride $Bi_6NbWO_{14}Cl$ as a Stable O_2-evolving Photocatalyst in Z-scheme Water Splitting under Visible Light. *Chem. Lett.* **2017**, *46* (4), 583−586.
(90) Horie, H.; Iwase, A.; Kudo, A. Photocatalytic Properties of Layered Metal Oxides Substituted with Silver by a Molten $AgNO_3$ Treatment. *ACS Appl. Mater. Interfaces* **2015**, *7* (27), 14638−14643.
(91) Tomita, O.; Nitta, S.; Matsuta, Y.; Hosokawa, S.; Higashi, M.; Abe, R. Improved Photocatalytic Water Oxidation with Fe^{3+}/Fe^{2+} Redox on Rectangular-shaped WO_3 Particles with Specifically Exposed Crystal Faces via Hydrothermal Synthesis. *Chem. Lett.* **2017**, *46* (2), 221−224.
(92) Sasaki, Y.; Kato, H.; Kudo, A. $[Co(bpy)_3]^{3+/2+}$ and $[Co(phen)_3]^{3+/2+}$ Electron Mediators for Overall Water Splitting under Sunlight Irradiation Using Z-Scheme Photocatalyst System. *J. Am. Chem. Soc.* **2013**, *135* (14), 5441−5449.
(93) Tsuji, K.; Tomita, O.; Higashi, M.; Abe, R. Manganese-Substituted polyoxometalate as an Effective Shuttle Redox Mediator in Z-scheme Water Splitting into H_2 and O_2 under Visible Light. *ChemSusChem* **2016**, *9*, 2201−2208.
(94) Sasaki, Y.; Nemoto, H.; Saito, K.; Kudo, A. Solar Water Splitting Using Powdered Photocatalysts Driven by Z-Schematic Interparticle

DOI: 10.1021/acs.chemrev.7b00286
Chem. Rev. 2018, 118, 5201−5241

Electron Transfer without an Electron Mediator. *J. Phys. Chem. C* **2009**, *113* (40), 17536−17542.
(95) Jia, Q. X.; Iwase, A.; Kudo, A. $BiVO_4$-Ru/$SrTiO_3$: Rh composite Z-scheme photocatalyst for solar water splitting. *Chem. Sci.* **2014**, *5* (4), 1513−1519.
(96) Kudo, A. Z-scheme photocatalyst systems for water splitting under visible light irradiation. *MRS Bull.* **2011**, *36* (01), 32−38.
(97) Ma, S. S. K.; Maeda, K.; Hisatomi, T.; Tabata, M.; Kudo, A.; Domen, K. A Redox-Mediator-Free Solar-Driven Z-Scheme Water-Splitting System Consisting of Modified Ta_3N_5 as an Oxygen-Evolution Photocatalyst. *Chem. - Eur. J.* **2013**, *19* (23), 7480−7486.
(98) Wang, Q.; Hisatomi, T.; Jia, Q.; Tokudome, H.; Zhong, M.; Wang, C.; Pan, Z.; Takata, T.; Nakabayashi, M.; Shibata, N.; Li, Y.; Sharp, I. D.; Kudo, A.; Yamada, T.; Domen, K. Scalable water splitting on particulate photocatalyst sheets with a solar-to-hydrogen energy conversion efficiency exceeding 1%. *Nat. Mater.* **2016**, *15* (6), 611−615.
(99) Iwase, A.; Ng, Y. H.; Ishiguro, Y.; Kudo, A.; Amal, R. Reduced Graphene Oxide as a Solid-State Electron Mediator in Z-Scheme Photocatalytic Water Splitting under Visible Light. *J. Am. Chem. Soc.* **2011**, *133* (29), 11054−11057.
(100) Iwashina, K.; Iwase, A.; Ng, Y. H.; Amal, R.; Kudo, A. Z-Schematic Water Splitting into H_2 and O_2 Using Metal Sulfide as a Hydrogen-Evolving Photocatalyst and Reduced Graphene Oxide as a Solid-State Electron Mediator. *J. Am. Chem. Soc.* **2015**, *137* (2), 604−607.
(101) Iwase, A.; Yoshino, S.; Takayama, T.; Ng, Y. H.; Amal, R.; Kudo, A. Water Splitting and CO_2 Reduction under Visible Light Irradiation Using Z-Scheme Systems Consisting of Metal Sulfides, CoOx-Loaded $BiVO_4$, and a Reduced Graphene Oxide Electron Mediator. *J. Am. Chem. Soc.* **2016**, *138*, 10260−10264.
(102) Suzuki, T. M.; Iwase, A.; Tanaka, H.; Sato, S.; Kudo, A.; Morikawa, T. Z-scheme water splitting under visible light irradiation over powdered metal-complex/semiconductor hybrid photocatalysts mediated by reduced graphene oxide. *J. Mater. Chem. A* **2015**, *3* (25), 13283−13290.
(103) Zhao, G. X.; Huang, X. B.; Fina, F.; Zhang, G.; Irvine, J. T. S. Facile structure design based on C_3N_4 for mediator-free Z-scheme water splitting under visible light. *Catal. Sci. Technol.* **2015**, *5* (6), 3416−3422.
(104) Iwashina, K.; Iwase, A.; Nozawa, S.; Adachi, S.; Kudo, A. Visible-Light-Responsive $CuLi_{1/3}Ti_{2/3}O_2$ Powders Prepared by a Molten CuCl Treatment of Li_2TiO_3 for Photocatalytic H_2 Evolution and Z-Schematic Water Splitting. *Chem. Mater.* **2016**, *28* (13), 4677−4685.
(105) Pan, Z. H.; Hisatomi, T.; Wang, Q.; Nakabayashi, M.; Shibata, N.; Pan, C. S.; Takata, T.; Domen, K. Application of $LaMg_{1/3}Ta_{2/3}O_2N$ as a hydrogen evolution photocatalyst of a photocatalyst sheet for Z-scheme water splitting. *Appl. Catal., A* **2016**, *521*, 26−33.
(106) Pan, Z. H.; Hisatomi, T.; Wang, Q.; Chen, S. S.; Iwase, A.; Nakabayashi, M.; Shibata, N.; Takata, T.; Katayama, M.; Minegishi, T.; Kudo, A.; Domen, K. Photoreduced Graphene Oxide as a Conductive Binder to Improve the Water Splitting Activity of Photocatalyst Sheets. *Adv. Funct. Mater.* **2016**, *26* (38), 7011−7019.
(107) Wang, Q.; Hisatomi, T.; Suzuki, Y.; Pan, Z.; Seo, J.; Katayama, M.; Minegishi, T.; Nishiyama, H.; Takata, T.; Seki, K.; Kudo, A.; Yamada, T.; Domen, K. Particulate Photocatalyst Sheets Based on Carbon Conductor Layer for Efficient Z-Scheme Pure-Water Splitting at Ambient Pressure. *J. Am. Chem. Soc.* **2017**, *139* (4), 1675−1683.
(108) Kobayashi, R.; Tanigawa, S.; Takashima, T.; Ohtani, B.; Irie, H. Silver-Inserted Heterojunction Photocatalysts for Z-Scheme Overall Pure-Water Splitting under Visible-Light Irradiation. *J. Phys. Chem. C* **2014**, *118* (39), 22450−22456.
(109) Miseki, Y.; Fujiyoshi, S.; Gunji, T.; Sayama, K. Photocatalytic Z-Scheme Water Splitting for Independent H_2/O_2 Production via a Stepwise Operation Employing a Vanadate Redox Mediator under Visible Light. *J. Phys. Chem. C* **2017**, *121* (18), 9691−9697.
(110) Tada, H.; Mitsui, T.; Kiyonaga, T.; Akita, T.; Tanaka, K. All-solid-state Z-scheme in CdS-Au-TiO_2 three-component nanojunction system. *Nat. Mater.* **2006**, *5* (10), 782−786.
(111) Zhou, P.; Yu, J. G.; Jaroniec, M. All-Solid-State Z-Scheme Photocatalytic Systems. *Adv. Mater.* **2014**, *26* (29), 4920−4935.
(112) Pan, Z. H. T.; Hisatomi, T.; Wang, Q.; Chen, S.; Nakabayashi, M.; Shibata, N.; Pan, C.; Takata, T.; Katayama, M.; Minegishi, T.; Kudo, A.; Domen, K. Photocatalyst Sheets Composed of Particulate $LaMg_{1/3}Ta_{2/3}O_2N$ and Mo-Doped $BiVO_4$ for Z-Scheme Water Splitting under Visible Light. *ACS Catal.* **2016**, *6*, 7188−7196.
(113) Yoshida, M.; Takanabe, K.; Maeda, K.; Ishikawa, A.; Kubota, J.; Sakata, Y.; Ikezawa, Y.; Domen, K. Role and Function of Noble-Metal/Cr-Layer Core/Shell Structure Cocatalysts for Photocatalytic Overall Water Splitting Studied by Model Electrodes. *J. Phys. Chem. C* **2009**, *113* (23), 10151−10157.
(114) Ohno, T.; Saito, S.; Fujihara, K.; Matsumura, M. Photocatalyzed production of hydrogen and iodine from aqueous solutions of iodide using platinum-loaded TiO_2 powder. *Bull. Chem. Soc. Jpn.* **1996**, *69* (11), 3059−3064.
(115) Abe, R.; Sayama, K.; Domen, K.; Arakawa, H. A new type of water splitting system composed of two different TiO_2 photocatalysts (anatase, rutile) and a IO_3^-/I^- shuttle redox mediator. *Chem. Phys. Lett.* **2001**, *344* (3), 339−344.
(116) Abe, R. Recent progress on photocatalytic and photoelectrochemical water splitting under visible light irradiation. *J. Photochem. Photobiol., C* **2010**, *11* (4), 179−209.
(117) Ishii, T.; Kato, H.; Kudo, A. H_2 evolution from an aqueous methanol solution on $SrTiO_3$ photocatalysts codoped with chromium and tantalum ions under visible light irradiation. *J. Photochem. Photobiol., A* **2004**, *163* (1−2), 181−186.
(118) Krasnovskii, A.; Brin, G. Inorganic Models of Hills Reaction. *Dokl. Akad. Nauk SSSR* **1962**, *147* (3), 656−659.
(119) Darwent, J. R.; Mills, A. Photo-oxidation of water sensitized by WO_3 powder. *J. Chem. Soc., Faraday Trans. 2* **1982**, *78* (2), 359−367.
(120) Heidt, L. J.; Mullin, M. G.; Martin, W. B., Jr; Beatty, A. M. J. Gross and Net Quantum Yields at 2537 Å. for Ferrous to Ferric in Aqueous Sulfuric Acid and the Accompanying Reduction of Water to Gaseous Hydrogen. *J. Phys. Chem.* **1962**, *66* (2), 336−341.
(121) Krasnovskii, A. A.; Fomin, G. V.; Brin, G. P.; Genkin, M. V.; Lyubimova, A. K.; Blyumenfel'd, L. A. *Dokl. Akad. Nauk SSSR* **1973**, 424−427.
(122) Ohno, T.; Haga, D.; Fujihara, K.; Kaizaki, K.; Matsumura, M. Unique effects of iron(III) ions on photocatalytic and photoelectrochemical properties of titanium dioxide (vol 101, pg 6416, 1997). *J. Phys. Chem. B* **1997**, *101* (49), 10605−10605.
(123) Ohno, T.; Tanigawa, F.; Fujihara, K.; Izumi, S.; Matsumura, M. Photocatalytic oxidation of water on TiO_2-coated WO_3 particles by visible light using Iron(III) ions as electron acceptor. *J. Photochem. Photobiol., A* **1998**, *118* (1), 41−44.
(124) Fujihara, B.; Ohno, T.; Matsumura, M. Splitting of water by electrochemical combination of two photocatalytic reactions on TiO_2 particles. *J. Chem. Soc., Faraday Trans.* **1998**, *94* (24), 3705−3709.
(125) Niishiro, R.; Tanaka, S.; Kudo, A. Hydrothermal-synthesized $SrTiO_3$ photocatalyst codoped with rhodium and antimony with visible-light response for sacrificial H_2 and O_2 evolution and application to overall water splitting. *Appl. Catal., B* **2014**, *150-151*, 187−196.
(126) Kato, H.; Sasaki, Y.; Iwase, A.; Kudo, A. Role of iron ion electron mediator on photocatalytic overall water splitting under visible light irradiation using Z-scheme systems. *Bull. Chem. Soc. Jpn.* **2007**, *80* (12), 2457−2464.
(127) Kudo, A.; Kato, H.; Tsuji, I. Strategies for the development of visible-light-driven photocatalysts for water splitting. *Chem. Lett.* **2004**, *33* (12), 1534−1539.
(128) Nusbaumer, H.; Zakeeruddin, S. M.; Moser, J. E.; Gratzel, M. An alternative efficient redox couple for the dye-sensitized solar cell system. *Chem. - Eur. J.* **2003**, *9* (16), 3756−3763.
(129) Nusbaumer, H.; Moser, J. E.; Zakeeruddin, S. M.; Nazeeruddin, M. K.; Gratzel, M. $Co^{II}(dbbiP)_2^{(2+)}$ complex rivals tri-

DOI: 10.1021/acs.chemrev.7b00286
Chem. Rev. 2018, 118, 5201−5241

iodide/iodide redox mediator in dye-sensitized photovoltaic cells. *J. Phys. Chem. B* **2001**, *105* (43), 10461−10464.
(130) Xiang, W. C.; Huang, F. Z.; Cheng, Y. B.; Bach, U.; Spiccia, L. Aqueous dye-sensitized solar cell electrolytes based on the cobalt(II)/(III) tris(bipyridine) redox couple. *Energy Environ. Sci.* **2013**, *6* (1), 121−127.
(131) Larson, J. W. Thermochemistry of vanadium (5+) in aqueous solutions. *J. Chem. Eng. Data* **1995**, *40* (6), 1276−1280.
(132) Xiong, A. K.; Yoshinaga, T.; Ikeda, T.; Takashima, M.; Hisatomi, T.; Maeda, K.; Setoyama, T.; Teranishi, T.; Domen, K. Effect of Hydrogen and Oxygen Evolution Cocatalysts on Photocatalytic Activity of GaN:ZnO. *Eur. J. Inorg. Chem.* **2014**, *2014*, 767−772.
(133) Abe, R.; Sayama, K.; Arakawa, H. Significant effect of iodide addition on water splitting into H_2 and O_2 over Pt-loaded TiO_2 photocatalyst: suppression of backward reaction. *Chem. Phys. Lett.* **2003**, *371* (3−4), 360−364.
(134) Berry, G. M.; Bothwell, M. E.; Bravo, B. G.; Cali, G. J.; Harris, J. E.; Mebrahtu, T.; Michelhaugh, S. L.; Rodriguez, J. F.; Soriaga, M. P. Spectroscopic and Electrochemical Studies of Iodine Coordinated to Noble-Metal Electrode Surfaces. *Langmuir* **1989**, *5* (3), 707−713.
(135) Suzuki, H.; Tomita, O.; Higashi, M.; Abe, R. Design of nitrogen-doped layered tantalates for non-sacrificial and selective hydrogen evolution from water under visible light. *J. Mater. Chem. A* **2016**, *4* (37), 14444−14452.
(136) Suzuki, H.; Tomita, O.; Higashi, M.; Abe, R. Two-step photocatalytic water splitting into H_2 and O_2 using layered metal oxide $KCa_2Nb_3O_{10}$ and its derivatives as O_2-evolving photocatalysts with IO_3^-/I^- or Fe^{3+}/Fe^{2+} redox mediator. *Catal. Sci. Technol.* **2015**, *5* (5), 2640−2648.
(137) Iwase, Y.; Tomita, O.; Higashi, M.; Abe, R. Enhanced Oxygen Evolution on Visible Light Responsive TaON Photocatalysts Co-loaded with Highly Active Ru Species for IO_3^- Reduction and Co Species for Water Oxidation. *Sustainable Energy Fuels* **2017**, *1*, 748−754.
(138) Miseki, Y.; Kusama, H.; Sugihara, H.; Sayama, K. Cs-Modified WO_3 Photocatalyst Showing Efficient Solar Energy Conversion for O_2 Production and Fe (III) Ion Reduction under Visible Light. *J. Phys. Chem. Lett.* **2010**, *1* (8), 1196−1200.
(139) Lianos, P.; Thomas, J. K. Cadmium sulfide of small dimensions produced in inverted micelles. *Chem. Phys. Lett.* **1986**, *125* (3), 299−302.
(140) Kudo, A.; Niishiro, R.; Iwase, A.; Kato, H. Effects of doping of metal cations on morphology, activity, and visible light response of photocatalysts. *Chem. Phys.* **2007**, *339* (1), 104−110.
(141) Shannon, R. D. Revised effective ionic radii and systematic studies of interatomic distances in halides and chalcogenides. *Acta Crystallogr., Sect. A: Cryst. Phys., Diffr., Theor. Gen. Crystallogr.* **1976**, *32* (5), 751−767.
(142) Ding, L.; Zhou, H.; Lou, S.; Ding, J.; Zhang, D.; Zhu, H.; Fan, T. Butterfly wing architecture assisted CdS/Au/TiO_2 Z-scheme type photocatalytic water splitting. *Int. J. Hydrogen Energy* **2013**, *38* (20), 8244−8253.

DOI: 10.1021/acs.chemrev.7b00286
Chem. Rev. 2018, 118, 5201−5241